INTERNATIONAL DOCTORAL
SCHOOL OF THE USC

Sara
Cloux González

PhD Thesis

Lagrangian transport of moisture in the atmosphere and floating plastic in the ocean

Santiago de Compostela, 2023

Doctoral Programme in Marine Science, Technology and Management

TESE DE DOUTORAMENTO

LAGRANGIAN TRANSPORT OF MOISTURE IN THE ATMOSPHERE AND FLOATING PLASTICS IN THE OCEAN

Sara Cloux González

ESCOLA DE DOUTORAMENTO INTERNACIONAL DA UNIVERSIDADE DE SANTIAGO DE COMPOSTELA

PROGRAMA DE DOUTORAMENTO EN CIENCIAS MARIÑAS, TECNOLOXÍAS E XESTIÓN

SANTIAGO DE COMPOSTELA

AÑO 2023

DECLARACIÓN DO AUTOR/A DA TESE

D./Dna. **Sara Cloux González**

Título da tese: **Lagrangian transport of moisture in the atmosphere and floating plastics in the ocean**

Presento a miña tese, seguindo o procedemento axeitado ao Regulamento, e declaro que:

1) A tese abarca os resultados da elaboración do meu traballo.
2) De ser o caso, na tese faise referencia ás colaboracións que tivo este traballo.
3) Confirmo que a tese non incorre en ningún tipo de plaxio doutros autores nin de traballos presentados por min para a obtención doutros títulos.
4) A tese é a versión definitiva presentada para a súa defensa e coincide a versión impresa coa presentada en formato electrónico

E comprométome a presentar o Compromiso Documental de Supervisión no caso de que o orixinal non estea na Escola.

En **Santiago de Compostela**, .

Sinatura electrónica

AUTORIZACIÓN DO DIRECTOR / TITOR DA TESE

LAGRANGIAN TRANSPORT OF MOISTURE IN THE ATMOSPHERE AND FLOATING PLASTICS IN THE OCEAN

Vicente Pérez Muñuzuri

INFORMA/N:

Que a presente tese, correspóndese co traballo realizado por Dna. Sara Cloux González, baixo a miña dirección/titorización, e autorizo a súa presentación, considerando que reúne os requisitos esixidos no Regulamento de Estudos de Doutoramento da USC, e que como director desta non incorre nas causas de abstención establecidas na Lei 40/2015.

De acordo co indicado no Regulamento de Estudos de Doutoramento, declara tamén que a presente tese de doutoramento é idónea para ser defendida en base á modalidade de Monográfica con reprodución de publicacións, nos que a participación da doutoranda foi decisiva para a súa elaboración e as publicacións se axustan ao Plan de Investigación.

En Santiago de Compostela, .

Fdo. Vicente Pérez Muñuzuri

A mis padres.

¿Pensaron alguna vez que si no fuera por todos nadie sería nada?

- Mafalda

Agradecimientos

El periodo de tesis es, sin lugar a dudas, una experiencia de aprendizaje y crecimiento personal. Durante esta etapa te enfrentas a retos que ponen a prueba tu perseverancia y habilidades de resolución de problemas. Recuerdo una conversación con un compañero en la que me dijo: ”El día que interioricé que la Tesis es un trabajo autónomo, y que el principal responsable soy yo, empecé a llevarlo mucho mejor”. Y es que para mí eso ha sido la Tesis, un ejercicio desafiante pero muy enriquecedor. Un desafío que, a pesar de ser autónomo, no hubiera logrado sin todas las personas que me han acompañado.

En primer lugar, quisiera expresar mi sincero agradecimiento a mi director de tesis, Vicente Pérez Muñuzuri, por su apoyo, respeto a mi trabajo y dedicación sobre todo estos últimos meses. Esta Tesis cumple años a la vez que su candidatura en la Vicerrectoría, y aunque ha sido duro compaginar ambas, quiero agradecer su esfuerzo. También a Dani, Dr. Garaboa, por ser mi guía académica y espiritual en los primeros años de esta Tesis. Sin sus consejos, quizá este trabajo hoy no vería la luz. En este sentido, quiero también dar las gracias a Damián por hacerse nuestro cómplice en la parte atmosférica de este trabajo y por su infinita curiosidad. Muchísimas gracias a ambos. Gracias también a Gonzalo Míguez Macho y a Alberto Pérez Muñuzuri por los consejos y la ayuda.

Gostaria de agradecer também ao professor Ramiro Neves, a quem tive a oportunidade de conhecer na etapa final desta tese e que me recordou a importância de ter presente a base fundamental que dá sentido ao problema que estamos estudando. E claro a Hilda, segunda guia academica e espiritual desta tese. Obrigada por me jogar um salva-vidas quando fez falta. Sem ela, esta tese não seria a mesma.

Muchísimas gracias a todos los que han compartido un poco de su tiempo en los estudios aquí presentados, para que fueran mucho más livianos. A Silvia, Pedro, Garbi y Patri, porque todos ellos son unos excelentes profesionales de los que he aprendido muchísimo y con los que espero volver a tener la oportunidad de trabajar.

Quisiera expresar también mi sincero agradecimiento a todos los compañeros del GFNL, a los que están y a los que estuvieron, con los que he podido compartir muchas experiencias. A Belén por ser el alma del GFNL actual, estar como una regadera y siempre dispuesta a escucharme. A Manuel por su pragmatismo, su modo de ver la vida y sus consejos. A Javi, el radiopatio del grupo, por los breaks para el café o para ver a la Panorama. A Alex por esas miradas de ánimo y por las charlas de despacho. A Santi, por ser la fuente de python-sabiduría y a Adri, por ser el primero en bajar al café. A Martín, Ismael, Martín, Alfredo, Arnau y Tito. Mucho ánimo a todos. Y no nos olvidemos de la *old-school*. A Miguel por darme de

los mejores (si no los mejores) consejos sobre la vida académica. También a Ana por ser mi compañera de despacho, compartir angustias y risas. Además, a Alberto, Martín, Charlie, David, Darío, Irma, Mariamo y Sabela por compartir algunos momentos de este período conmigo. E obrigado às pessoas do MARETEC pela agradável acolhida. Obrigado a Ana pela ajuda, os conselhos, as risadas e por me ensinar a facer bacalhau na brasa. Obrigado também a Lucian por seu carinho e sua ajuda.

Gracias a mis amigos por enseñarme tanto. A Samuel poles innumberables cañes y sidres, confesiones, rises y terapies. A Sheila, por ensinarme que o tesón ten recompensa e que as boas persoas de corazón existen. A Efrén, por demostrarnos que aunque no se haya planeado una ruta, perderse no es estar perdido. A Carlos, por estar siempre disponible y dispuesto a apoyarme y a Tonja y Dave, por ser un planazo de sábado noche.

Pero sobremanera, gracies a la mi familia, empezando poles mis güeles. Una que nos enseñó a toos qu'una muyer puede facer lo que se proponga, ensin importar lo que los demás digan. Y la otra, que la resilencia ye bien importante nesta vida. A mi madre por enseñame a defendeme y a luchar polo que quiero, y a mi padre por enseñame que los puentes crucense un dempués d'otru. A los mios tíos y primos, gracies pola paciencia y les sidres.

Esta tesis ha sido posible gracias al proyecto CleanAtlantic Interreg Project [1] y a la Xunta de Galicia [2].

[1] EAPA 46/2016
[2] Research Grant No. 2021-PG036-1

Contents

Summary

This thesis focuses on the study of Lagrangian transport, a field of physics that deals with the analysis of fluid transport. The aim of this work is to explore the interaction processes between particles and fluids on different areas of science, such as oceanography and meteorology. The practical applications of this area of study will be examined, such as the movement of plastics in the ocean and the transport of moisture in the atmosphere. To do so, the use of numerical models will be explored to validate results and test new hypotheses.

We begin this thesis with an introductory chapter on transport phenomena to provide context for the study of dynamic systems. Next, we will continue with two contextualization chapters on the problem of marine debris and extreme precipitation events.

Regarding the results, chapter 4 presents a study on the accumulation of marine debris in the Ría de Arousa. The objective is to evaluate the capability of a recently developed model to reproduce observational results and determine the zones of marine debris accumulation along the coast. Different time periods were simulated to compare with monitoring data at different time periods. The results show that the zones most exposed to oceanic action present the lowest rates of accumulation, and that wind direction has an influence on the distribution of accumulations. Considering the collection data, different retention scenarios can be represented by modifying the probability of stranding. In this study, simulations were carried out by varying the probability of stranding in three different scenarios: an 80% stranding factor reflecting areas of high retention, a 50% factor reflecting moderate retention, and a 20% factor reflecting areas of low retention, mainly rocky areas. The results of the comparison between simulated data and beach collection data show very similar trend behaviors for the vast majority of the beaches considered. Those cases that experience clear differences can be explained by the presence of structures that affect retention in the intertidal zone (presence of algae, port structures, etc.) or by the occurrence of meteorological phenomena such as storms that condition the collection data.

As a continuation of this study, a detailed statistical analysis is carried out in the fifth chapter that analyzes the dispersion of floating macroplastics on the Spanish Atlantic coast and offshore. The main objective of the study is to identify potential accumulation areas and estimate the contributions of different sources of emissions. Different types of emissions are considered, such as direct discharge into the sea from land, river discharges, and possible emissions from maritime traffic. To obtain statistically significant results, surface simulations are carried out for a period of 7 years. The highest concentrations are found near the peninsular coast, with three regions of particular interest being identified: the Bay of Biscay, the Gulf of Cadiz, and the Alboran Sea. High concentration cells are observed near the coast for

point sources. However, these concentrations are attenuated when considering sources located far from the coast. The relative dispersion in latitude and longitude is also estimated for point sources such as rivers and land sources. The results are grouped by emission regions, considering a retention factor of 50% to observe its influence on particle dispersion. In the first region (the Cantabrian coast), particles tend to accumulate near the emission points, while in the second region (the Gulf of Cadiz), particles do not disperse much in longitude, but do in middle latitudes. In the Canary Islands region, dispersion follows the circulation of the region and simulated Lagrangian particles are transported towards tropical and subtropical latitudes and towards the east coast of the Americas following the Canary Current. The relative cross-border contribution has finally been estimated in four regions of interest: the Bay of Biscay, the Strait of Gibraltar/Alboran Sea, the Gulf of Cadiz, and the Canary Islands. In the Bay of Biscay, French sources make the largest contribution, followed by Spanish sources, while Portuguese sources represent only 1% of the contribution. In the Gulf of Cadiz and the Alboran Sea regions, Spanish sources make the largest contribution, followed by Portuguese and French sources. In the region of the Canary Islands, the most significant contribution comes from Portuguese sources, followed by Spanish and French sources.

Moving to the atmospheric domain, chapter 6 presents a comparative study of two techniques for investigating the origin of moisture in the Western Mediterranean region during two extreme rainfall events in October and November of 1982. The Lagrangian FLEXPART-WRF and Eulerian WRF-WVTs models were compared to validate the performance of the former, considering the results of the latter as "truth". The potential sources considered were: 1) the Western Mediterranean; 2) the Central Mediterranean; 3) the North Atlantic Ocean; and 4) the tropical and subtropical Atlantic and tropical Africa. The results show that the Lagrangian method has acceptable ability to identify local sources (Western Mediterranean) and medium-distance sources (Central Mediterranean and North Atlantic). However, it underestimates remote moisture sources, such as tropical and subtropical areas. Particularly for the October event, the tropical and subtropical area reported a relative contribution six times lower than with WRF-WVTs. On the other hand, FLEXPART-WRF overestimates the contribution of some sources, especially North Africa. This indicates that the use of the Lagrangian model is limited for a quantitative study of moisture sources due to significant biases found compared to the WRF-WVTs model. Additionally, another recently developed Lagrangian tool was used to estimate the relative moisture sources. Although the results again show discrepancies for remote sources, the local sources present similar contributions. Therefore, we can confirm that the estimation of these sources can be established with some precision, while more distant sources must be studied with caution.

Resumen

Esta tesis se centra en el estudio del transporte lagrangiano, un campo de la física que se encarga del análisis del transporte en fluidos. El objetivo de este trabajo es explorar los procesos de interacción entre partículas y fluidos en distintas áreas de la ciencia, como la oceanografía y la meteorología. Se examinarán las aplicaciones prácticas de esta área de estudio, como el movimiento de plásticos en el océano y el transporte de humedad en la atmósfera. Para ello, se explorará el uso de modelos numéricos para validar resultados y probar nuevas hipótesis.

Comenzamos esta tesis con un capítulo introductorio sobre los fenómenos de transporte para dar contexto al estudio de los sistemas dinámicos. A continuación, seguiremos con dos capítulos de contextualización sobre el problema de la basura marina y los eventos de precipitación extrema.

En cuanto a resultados, el capítulo 4 presenta un estudio sobre la acumulación de plásticos en la Ría de Arousa. El objetivo es evaluar la capacidad de un modelo de transporte Lagrangiano para reproducir los resultados observados y determinar las zonas de acumulación a lo largo de la costa. Se simularon diferentes periodos de tiempo para comparar con los distintos datos de monitoreo. Los resultados muestran que las zonas más expuestas a la acción oceánica presentan las tasas más bajas de acumulación, y que la dirección del viento influye en la distribución de las acumulaciones. Considerando los datos de recogidas, se pueden representar diferentes escenarios de retención modificando la probabilidad de varamiento. En este estudio, se realizaron simulaciones variando la probabilidad de encallamiento en tres escenarios diferentes: un factor de encallamiento del 80% que refleja áreas de alta retención, un factor del 50% que refleja una retención media y un factor del 20% que refleja áreas de baja retención, principalmente rocosas. Los resultados de la comparación entre los datos simulados y los datos de recogida en playas muestran tendencias muy similares para la gran mayoría de las playas consideradas. Aquellos casos que experimentan diferencias claras pueden ser explicadas debido a la presencia de estructuras que afecten a la retención en la zona intermareal (presencia de algas, estructuras portuarias, etc) o, a la ocurrencia de fenómenos meteorológicos como borrascas y temporales que condicionaran los datos de recogida.

Como continuación a este estudio, en el quinto capitulo se realiza un estudio estadístico detallado que analiza la dispersión de macroplásticos flotantes en la costa española del Atlántico y en alta mar. El objetivo principal del estudio es identificar las zonas de acumulación potencial y estimar las contribuciones de diferentes emisiones de fuentes. Se consideran diferentes tipos de emisiones, como vertidos directos al mar desde tierra, las descargas de ríos y las posibles emisiones del tráfico marítimo. Para obtener resultados estadísticamente significativos se realizan simulaciones en superficie para un periodo de 7 años. Las concentraciones más

altas se encuentran cerca de la costa peninsular, identificándose tres regiones de particular interés: el Golfo de Vizcaya, el Golfo de Cádiz y el Mar de Alborán. Se observan zonas de alta concentración cerca de la costa para fuentes puntuales. Las concentraciones se atenúan al considerar fuentes ubicadas lejos de la costa. Los resultados se agrupan por regiones de emisión, considerando un factor de retención del 50% para observar su influencia en la dispersión de partículas. En la primera región (la cornisa cantábrica), las partículas tienden a acumularse cerca de los puntos de emisión mientras que en la segunda región (el Golfo de Cádiz), las partículas no se dispersan mucho en longitud, pero sí en latitudes medias. En la región de las Islas Canarias, la dispersión sigue la circulación de la región y las partículas lagrangianas simuladas se transportan hacia latitudes tropicales y subtropicales y hacia la costa este de las Américas siguiendo la Corriente de Canarias. Finalmente se ha estimado la contribución transfronteriza relativa en cuatro regiones de interés: la Bahía de Vizcaya, el Estrecho de Gibraltar/Mar de Alborán, el Golfo de Cádiz y las Islas Canarias. En la Bahía de Vizcaya, las fuentes francesas son las que más contribuyen, seguidas de las fuentes españolas, mientras que las fuentes portuguesas representan solo el 1% de la contribución. En el Golfo de Cádiz y las regiones del Mar de Alborán, las fuentes españolas suponen la mayor contribución, seguidas de las fuentes portuguesas y francesas. En la región de las Islas Canarias, la contribución más significativa proviene de fuentes portuguesas, seguidas de fuentes españolas y francesas.

Cambiando al ámbito atmosférico, el capítulo 6 presenta el estudio comparativo de dos técnicas para el estudio del origen de la humedad en la región del Mediterráneo Occidental en dos eventos extremos de lluvia en octubre y noviembre de 1982. Se compararon los modelos Lagrangiano FLEXPART-WRF y Euleriano WRF-WVTs para validar el rendimiento del primero, considerando los resultados del segundo como “ciertos”. Las potenciales fuentes consideradas son: 1) el Mediterráneo Occidental; 2) el Mediterráneo Central; 3) el océano Atlántico Norte y 4) el Atlántico tropical y subtropical y el África tropical. Los resultados muestran que este método Lagrangiano tiene una habilidad aceptable para identificar las fuentes locales (Mediterráneo Occidental) y de media distancia (Mediterráneo Central y Atlántico Norte). Sin embargo, subestima las fuentes de humedad remotas, como las áreas tropicales y subtropicales. Particularmente, para el evento de octubre, el área tropical y subtropical reportó una contribución relativa seis veces menor que con WRF-WVTs. Por el contrario, FLEXPART-WRF sobreestima la contribución de algunas fuentes, especialmente de África del Norte. Ello indica que el uso del modelo lagrangiano es limitado para un estudio cuantitativo de las fuentes de humedad debido a grandes sesgos encontrados en comparación con el modelo WRF-WVTs. Como complemento también se empleó otra herramienta Lagrangiana de reciente desarrollo para estimar las fuentes relativas de humedad. Aunque los resultados vuelven a mostrar discrepancias para las fuentes remotas, las fuentes locales presentan contribuciones similares. Por lo que podemos reafirmar que la estimación de estas fuentes se puede establecer con cierta precisión, mientras que las fuentes más alejadas han de ser estudiadas con precaución.

Resumo

Esta tese céntrase no estudo do transporte lagranxiano, un campo da física que se encarga da análise do transporte en fluídos. O obxectivo deste traballo é explorar os procesos de interacción entre partículas e fluídos en distintas áreas da ciencia, como a oceanografía e a meteoroloxía. Examinaranse as aplicacións prácticas desta área de estudo, como o movemento de plásticos no océano e o transporte de humidade na atmosfera. Co fin de profundar na comprensión do transporte de lixo mariño e as choivas intensas nas rexións costeiras do Mediterráneo, considerouse a exploración do uso de modelos numéricos que permitan validar resultados e probar novas hipóteses. Estes modelos permiten simular o comportamento do océano e a atmosfera e avaliar distintos escenarios en función das condicións océano-meteorolóxicas, o que pode contribuír significativamente á comprensión e prevención. En definitiva, o uso de modelos numéricos é unha ferramenta clave para abordar os desafíos que se expoñen nesta tese.

Ao describir o movemento dun fluído hai dous puntos de vista. Unha primeira forma de facelo é seguir cada partícula fluída no seu movemento, de xeito que buscaremos algunhas funcións que nos dean a posición, así como as propiedades da partícula fluída en cada instante. Esta é a descrición lagranxiana. Unha segunda forma é asignarlle a cada punto do espazo e en cada instante un valor para as propiedades ou magnitudes do fluído independentemente de que nese instante, a partícula do fluído ocupe ese volume diferencial. Esta é a descrición euleriana, que non está ligada ás partículas do fluído senón aos puntos do espazo ocupados polo fluído. Nesta descrición, o valor dunha propiedade nun punto e nun instante dado é o da partícula fluída que ocupa ese punto nese instante. O enfoque lagranxiano é máis axeitado para entender o movemento e a evolución dos obxectos ou propiedades transportados polo fluxo, mentres que o euleriano é máis adecuado para obter información detallada sobre as variacións de fluído en puntos espaciais. Así, a descrición lagranxiana proporciona unha visión completa das posibles traxectorias do fluxo dada unha condición inicial. Este mapa lagranxiano pode asimilarse co campo de velocidades, de modo que as traxectorias das partículas son obtidas integrando a velocidade. No caso das partículas inerciais dun tamaño e masa finitas, provocan cambios no fluído da súa contorna e poden provocar cambios na organización das partículas; agrupación, separación, etc. Por exemplo, os grandes obxectos flotantes cun longo tempo de axuste co fluído requiren formulacións máis completas, como a ecuación de Maxey-Riley, para modelar o seu movemento no océano. Con todo, os estudos presentados nesta tese restrínxense ao enfoque puramente lagranxiano.

Comezamos esta tese cun capítulo introdutorio sobre os fenómenos de transporte para dar contexto ao estudo dos sistemas dinámicos. O transporte de fluídos é un fenómeno ubicuo nas nosas vidas a todas as escalas, dende a atmosfera e o océano ata sistemas máis pequenos como

a circulación do zume nas plantas. Neste contexto, a propiedade escalar $C(r,t)$ transpórtase principalmente dun lugar a outro mediante a combinación de dous procesos: advección e/ou difusión. A advección é o método primario de transporte nun fluído que provoca a transferencia de material dunha área a outra debido ao propio movemento do fluído. Polo tanto, relaciónase directamente co campo de velocidades do fluído $v(r,t)$. Pola outra banda, a difusión é un proceso irreversible causado polo movemento aleatorio das moléculas que facilita o transporte desde zonas de alta concentración a áreas de baixa concentración ata lograr unha concentración uniforme. As escalas espazo-temporais definen o rango de magnitudes nun tempo e espazo determinados e poden afectar de maneira diferente os procesos de advección e difusión en función de distintas magnitudes como a velocidade, concentración, lonxitude e coeficiente de difusión. Neste estudo, conclúese que os termos difusivos non teñen impacto no contexto considerado.

Segundo o Programa das Nacións Unidas para o Medio Ambiente, o 95% do lixo mariño atopado nas costas, a superficie do mar e o fondo do océano consiste en plásticos. Nas últimas cinco décadas, a produción mundial de plástico aumentou exponencialmente, chegando a fabricar ao redor de 368 millóns de toneladas en 2019, e prevese que para o 2025 se produzan 600 millóns de toneladas. Ao redor do 40% do plástico producido é para embalaxe, o 20.4% para a industria da construción e aproximadamente o 10% utilízase no sector automotriz. Só o 6% é reciclado, mentres que o 55% xestiónase como residuo e o 10% incinérase. Estímase que entre 5 e 13 millóns de toneladas das 5 mil millóns de toneladas de plástico enviadas ás vertedoiro acabaron nos océanos, o que provoca graves consecuencias ambientais. É necesario desenvolver técnicas que faciliten a incorporación dos residuos plásticos, xa que só poden ser reciclados unha ou dúas veces e logo non se poden utilizar de novo de maneira similar. Aínda que algúns estudos suxiren que as fontes mariñas tamén contribúen significativamente, crese que a maioría dos residuos plásticos proveñen de fontes terrestres, especialmente de áreas poboadas. Con todo, hai unha gran discrepancia entre a cantidade estimada de residuos plásticos xerados en terra que chegan ás augas costeiras e a cantidade total de plástico observado no mar, o que indica que aínda non se comprende por completo a forma en que se move, as rutas e o destino do plástico no océano. Para abordar máis efectivamente o desafío da contaminación plástica, requírese unha comprensión máis profunda dos procesos físicos, químicos e biolóxicos que inflúen no transporte de plásticos na superficie do océano. Os plásticos no océano transpórtanse a través de procesos a gran escala en mar aberto baseados na dinámica xeofísica dos fluídos, como o transporte de Ekman, que crea zonas de converxencia e diverxencia na superficie. Os parches de lixo son grandes zonas de acumulación compostas por diminutos anacos de plástico que non son facilmente detectables polas imaxes de satélite nin polo ollo humano. Os remuíños, vórtices de mesoescala con diámetros de centos de quilómetros e profundidades duns centos de metros, poden transportar o que leven no seu centro de xiro ao longo de miles de quilómetros. A deriva de Stokes e a acción do vento en superficie son outros efectos que modifican a traxectoria dos obxectos plásticos a diferentes escalas. As achegas de auga doce, incluídas as plumas fluviais e a fusión e formación de xeo, tamén contribúen significativamente á acumulación de residuos plásticos. A distribución dos plásticos na columna de auga depende de varios factores distintos da flotabilidade, incluídos fenómenos como os procesos de submesoescala. Así, pode entenderse que o transporte de plástico no océano é un problema de amplas dimensións.

O capítulo 2 presenta a problemática dos residuos plásticos como contaminante, especialmente nos ecosistemas mariños. Nas últimas décadas, o interese pola difusión de plásticos na contorna mariña cobrou maior importancia. Atendendo ao seu tamaño, diferenciamos entre macro e micro plásticos, sendo macro aquelas fraccións cun diámetro por encima de 0.5-1cm, e micro aqueles fragmentos por baixo deste valor. A orixe destas diminutas partículas débese maioritariamente á descomposición dos macro-plásticos. Estes procesos de degradación aceléranse no ámbito mariño debido á fotodegradación pola acción do sol, a oxidación agravada pola salinidade e a abrasión mecánica da ondada e do vento. Estímase que desde os ríos chegan entre 1.15 e 2.4 millóns de toneladas de plástico ao océano aberto anualmente. As observacións realizadas en alta mar constatan unha maior abundancia de micro-plásticos. Dado que estes pequenos fragmentos atópanse na mesma escala que o plancto, nunha concentración seis veces maior en certas zonas do Pacífico, non é de estrañar a súa acusada aparición en diferentes especies mariñas e, polo tanto, na nosa propia especie. A acusada inxesta por parte das especies filtradoras fai que estas partículas atopen outro medio de difusión de maior impacto, a alimentación que consumimos día a día, chegando así ao noso organismo.

O capítulo 3 presenta o problema do transporte atmosférico. Entender a natureza e a evolución do ciclo hidrolóxico é, actualmente, un dos desafíos máis importantes dada a importancia do cambio climático global. A atmosfera, a pesar de conter unha pequena porción da auga do planeta, é esencial para conectar varias fontes de auga como océanos, lagos, chans, xeo tanto en terra como en mar, e ríos a través de procesos como o transporte de humidade, a evapotranspiración e a precipitación. O ciclo hidrolóxico pode ser descrito brevemente como o proceso polo cal a humidade se evapora dun lugar e eventualmente precipítase noutro, que se mantén mediante o transporte atmosférico, oceánico e hidrolóxico da auga. En rexións con presenza oceánica, a proporción de evaporación adoita superar a taxa de precipitación, sendo o océano a principal fonte de humidade que logo é transportada pola atmosfera cara ás masas terrestres. As masas terrestres representan unha fonte natural para a humidade atmosférica, xa que a precipitación é maior que a evapotranspiración. O excedente de auga superficial logo enche ríos, augas subterráneas e outros corpos de auga que eventualmente drenan no océano, completando así o ciclo. Cando a auga se evapora, a humidade tipicamente permanece na atmosfera durante uns 10 días antes de condensarse e volver á Terra como precipitación. Doutra banda os eventos de precipitación extrema e as inundacións asociadas, constitúen o principal risco meteorolóxico na rexión do Mediterráneo. As rexións costeiras son especialmente sensibles debido á alta actividade económica e densidade poboacional, o que provoca que as inundacións impliquen perdas de vidas humanas e custos económicos millonarios. En xeral, o principal mecanismo que xera estes episodios de choivas intensas é a forte inestabilidade creada pola diferenza entre a masa de aire cálido e húmido que se atopa sobre o mar Mediterráneo e o aire frío nas capas superiores da atmosfera, que adoita estar asociado comunmente a unha depresión illada en niveis altos (gota fría ou DANA) nas proximidades da rexión. En ocasións, a achega extrema de humidade doutras rexións non se ten en conta ou é subestimada. Con todo, existen numerosos estudos recentes sobre as fontes de humidade para a precipitación na rexión do Mediterráneo Occidental, que abordan tanto os valores climáticos como os casos extremos particulares.

Hai tres métodos principais para determinar as áreas fonte e sumidoiro da humidade

atmosférica: modelos analíticos ou de caixa, trazadores numéricos de vapor de auga e trazadores físicos de vapor de auga (isótopos). Os modelos analíticos utilizáronse historicamente para entender os cambios na hidroloxía superficial dunha rexión, e utilizáronse cumpridamente para calcular a taxa de reciclaxe. Estes modelos están baseados na ecuación do balance vertical integrado do vapor de auga. Un dos beneficios significativos destes modelos é a súa simplicidade e baixo custo computacional, con todo, a súa utilidade limítase por fortes suposicións, como a mestura completa do vapor de auga de todas as fontes dentro da columna atmosférica. Por tanto, a súa aplicabilidade está restrinxida e só poden proporcionar unha aproximación aproximada da taxa de reciclaxe.

Os "trazadores numéricos de vapor de auga" é unha técnica utilizada na investigación da hidroloxía e a meteoroloxía para estudar as fontes e destinos do vapor de auga na atmosfera. A técnica divídese en dous tipos de métodos: euleriano e lagranxiano. O método euleriano enfócase en lugares fixos no espazo e o movemento do fluído a través deles no tempo. Este método proporciona información sobre a precipitación reciclada, tendo en conta a orixe e o destino específico da humidade advectada. Os modelos eulerianos poden ser "offline" ou "online". Os modelos "offline" baséanse en variables integradas verticalmente, mentres que os modelos "online" están axustados cun modelo climático global ou rexional. Aínda que os modelos "online" son considerados os máis precisos, a súa precisión depende da calidade do modelo climático utilizado. Os modelos "offline" son unha alternativa aos modelos analíticos tradicionais. Son especialmente útiles para calcular os cocientes de reciclaxe de humidade continental a escala global. Con todo, a hipótese dunha atmosfera ben mesturada pode conducir a erros en rexións cunha forte cizalladura vertical. Nos últimos anos, algúns modelos "offline" melloraron ao agregar un nivel vertical adicional. Doutra banda, o método lagranxiano baséase no seguimento de partículas individuais de fluído a través do espazo e o tempo. Os modelos lagranxianos utilízanse para estudar as fontes e sumidoiros de humidade atmosférica. Hai dous tipos principais de modelos lagranxianos: as traxectorias de retroceso case-isentrópicas e a dispersión de partículas lagranxianas. Estes modelos teñen a vantaxe de ser computacionalmente eficientes e non precisan preseleccionar as rexións de orixe, xa que as partículas poden rastrexarse no tempo. Con todo, algúns modelos teñen limitacións na súa formulación que poden levar a erros nos resultados. Cada un destes métodos ten vantaxes e desvantaxes en termos de eficiencia computacional e precisión, e a súa elección dependerá da pregunta de investigación específica e da dispoñibilidade de datos e modelos adecuados. O uso de modelos numéricos e analíticos é importante para estudar o ciclo da auga, pero deben ser validados con datos físicos reais. Para iso, utilízanse isótopos estables de hidróxeno e osíxeno, como o deuterio e ^{18}O, que están presentes de forma natural na precipitación e o vapor de auga. Desde a década de 1960, recompiláronse e analizáronse múltiples veces datos sobre a composición isotópica na precipitación, e estes estudos demostraron consistentemente a influencia de factores como a temperatura, a latitude, a altitude e a cantidade na composición isotópica. Ademais, varios estudos utilizaron datos isotópicos para verificar modelos e explorar a reciclaxe atmosférica.

En canto aos resultados, o capítulo 4 presenta un estudo sobre a acumulación de residuos mariños na Ría de Arousa. O obxectivo é avaliar a capacidade de un novo modelo, de desenvolvemento recente, para reproducir os resultados observados e determinar as zonas de acumulación de residuos mariños ao longo da costa. Simuláronse diferentes períodos de

tempo para comparar coas observacións. Os resultados amosan que as zonas máis expostas á acción oceánica presentan as taxas máis baixas de acumulación, e que a dirección do vento ten influencia na distribución das acumulacións. Considerando os datos de recollida, pódense representar diferentes escenarios de retención modificando a probabilidade de encallamento. Neste estudo, realizáronse simulacións variando a probabilidade de encallamento en tres escenarios distintos: (i) 80% para áreas de alta retención, (ii) 50% para zonas de retención media e (iii) un factor do 20% que reflexa áreas de baixa retención, principalmente rochosas. Os resultados da comparación entre datos simulados e datos de recollida en praia amosan tendencias moi semellantes para a gran maioría das praias consideradas. Aqueles casos que experimentan diferenzas claras, poden ser explicadas debido á presenza de estruturas que afecten á retención na zona intermareal (presenza de algas, estruturas portuarias, etc) ou, á ocorrencia de fenómenos meteorolóxicos como borrascas e temporais que condicionasen os datos de recollida.

Como continuación a este estudo, no quinto capítulo realízase un estudo estatístico detallado que analiza a dispersión de macroplásticos flotantes na costa española do Atlántico e en alta mar. O obxectivo principal do estudo é identificar as zonas de acumulación potencial e estimar as contribucións de diferentes emisións de fontes. Considéranse diferentes tipos de emisións, como vertidos directos ao mar dende terra, as descargas de ríos e as posibles emisións de tráfico marítimo. Para obter resultados estatisticamente significativos realízanse simulacións de transporte superficial para un período de 7 anos. As concentracións máis elevadas atópanse preto da costa peninsular, identificando tres rexións de particular interese: o Golfo de Biscaia, o Golfo de Cádiz e o Mar de Alborán. Obsérvanse puntos da malla de alta concentración pegados á costa para fontes puntuais. Pero estas concentracións atenúanse ao considerar fontes localizadas lonxe da costa. Os resultados agrúpanse por rexións de emisión, considerando un factor de retención do 50% para observar a súa influencia na dispersión de partículas. Na primeira rexión (cornixa cantábrica), as partículas tenden a acumularse preto dos puntos de emisión mentres que na segunda rexión (o Golfo de Cádiz), as partículas non se dispersan moito en lonxitude, pero si en latitudes medias. Na rexión das Illas Canarias, a dispersión segue a circulación da rexión e as partículas lagranxianas simuladas transpórtanse cara latitudes tropicais e subtropicais e cara a costa este das Américas seguindo a Corrente das Canarias. Finalmente estimouse a contribución transfronteiriza relativa en catro rexións de interese: a Baía de Biscaia, o Estreito de Xibraltar/Mar de Alborán, o Golfo de Cádiz e as Illas Canarias. Na Baía de Biscaia, as fontes francesas fan a maior contribución, seguidas das fontes españolas, mentres que as fontes portuguesas representan unicamente o 1% da contribución. No Golfo de Cádiz e as rexións do Mar de Alborán, as fontes españolas fan a maior contribución, seguidas das fontes portuguesas e francesas. Na rexión das Illas Canarias, a contribución máis significativa provén de fontes portuguesas, seguida de fontes españolas e francesas.

Mudando ao ámbito atmosférico, o capítulo 6 presenta o estudo comparativo de dúas técnicas para o estudo da orixe da humidade na rexión do Mediterráneo Occidental en dous eventos extremos de choiva en outubro e novembro de 1982. Comparáronse os modelos lagranxiano FLEXPART-WRF e euleriano WRF-WVTs para validar o rendemento do primeiro, considerando os resultados do segundo como "verdade". As potenciais fontes consideradas son: 1) o Mediterráneo Occidental, 2) o Mediterráneo Central; 3) o Océano Atlántico

Norte e 4) o Atlántico tropical e subtropical e a África tropical. Os resultados amosan que este método lagranxiano ten unha habilidade aceptable para identificar as fontes locais (Mediterráneo Occidental) e de media distancia (Mediterráneo Central e Atlántico Norte). Sen embargo, subestima as fontes de humidade remotas, como as áreas tropicais e subtropicais. Particularmente, para o evento de outubro, a área tropical e subtropical reportou unha contribución relativa seis veces menor que con WRF-WVTs. Pola contra, FLEXPART-WRF sobreestima a contribución dalgunhas fontes, especialmente de África do Norte. Isto indica que o emprego do modelo lagranxiano é limitado para un estudo cuantitativo das fontes de humidade debido ás diferenzas atopadas en comparación co modelo WRF-WVTs. Como complemento tamén se empregou outra ferramenta lagranxiana de recente desenvolvemento para estimar as fontes relativas de humidade. Aínda que os resultados amosan de novo discrepancias para as fontes remotas, as fontes locais presentan contribucións similares. Polo que podemos reafirmar que a estimación destas fontes pode establecerse con certa precisión, mentres que as fontes máis remotas deben ser estudadas con precaución.

List of Figures

List of Tables

List of Publications

1. Cloux, S., Garaboa-Paz, D., Insua-Costa, D., Miguez-Macho, G., & Pérez-Muñuzuri, V. (2021). Extreme precipitation events in the Mediterranean area: contrasting two different models for moisture source identification. Hydrology and Earth System Sciences, 25(12), 6465-6477. DOI: `https://doi.org/10.5194/hess-25-6465-2021`
   Author contribution
   SC designed the experiment, performed the simulations and the data analysis, created the figures and wrote the first manuscript draft.
   Quality indexes
   Impact factor: 6.617
   CiteScore: 9.4
   Quantile: Q1

2. Cloux, S., Allen-Perkins, S., de Pablo, H., Garaboa-Paz, D., Montero, P., & Muñuzuri, V. P. (2022). Validation of a Lagrangian model for large-scale macroplastic tracer transport using mussel-peg in NW Spain (Ría de Arousa). Science of the Total Environment, 822, 153338. DOI: `https://doi.org/10.1016/j.scitotenv.2022.153338`
   Author contribution
   SC designed the experiment, performed the simulations and the data analysis, created the figures and wrote the first manuscript draft.
   Quality indexes
   Impact factor: 10.754
   CiteScore: 14.1
   Quantile: Q1

3. Cloux, S., Pérez, P., de Pablo, H., & Muñuzuri, V. P. (2023). A regional Lagrangian model to evaluate the dispersion of floating macroplastics in the North Atlantic Ocean from different types of sources in the Iberian Peninsula. Submitted to Science of Total Enviroment.
   Author contribution
   SC designed the experiment, performed the simulations and the data analysis, created the figures and wrote the first manuscript draft.
   Quality indexes
   Impact factor: 10.754
   CiteScore: 14.1
   Quantile: Q1

4. de Pablo, H., Sobrinho, J., Cloux, S., Neves, R. & Gaspar, M. (2022) Modelling chlorophyll a and nutrients fluxes within the adjacent coastal area of the Tagus estuary: the influence of the submarine outfall discharges. Submitted to Marine Pollution Bulletin.
   Author contribution
   SC participated in the writing of the first manuscript draft. the figures and wrote the first manuscript draft.
   Quality indexes
   Impact factor: 7.001
   CiteScore: 9.2
   Quantile: Q1

5. Coimbra, Maria Raquel Moura; Benevides, E., Farias, R., da Silva, B. C., Cloux, S., Pérez-Muñuzuri, V., Vera, M., & Torres, R. (2023) Restricted connectivity for cobia *Rachycentron canadum* (Perciformes: Rachycentridae) in the Western Atlantic Ocean. 1054-6006. Fisheries Oceanography. DOI: `http://doi.org/10.1111/fog.12642`

   Author contribution
   SC designed and performed the lagrangian simulations and the data analysis and participated in the writing of the first manuscript draft.
   Quality indexes
   Impact factor: 2.67
   CiteScore: –
   Quantile: Q3

Chapter 1

General Introduction

Lagrangian transport is a key concept in fluid dynamics, which is the study of how fluids move and react to forces. It is an important tool for understanding the behavior of fluids in many different settings, from the atmosphere to the ocean. Lagrangian transport helps us to understand how a fluid moves in response to an external force, how particles in the fluid interact with each other and how the fluid responds to changes in its environment. This insight enables us to make more accurate predictions and control the behavior of fluids in a variety of applications, such as predicting weather patterns, ocean circulation, and pollution. In particular, atmospheric transport refers to the movement of gases, particles and other substances through the Earth's atmosphere. This helps to determine the pathways that gases and particles follow as they are transported by wind and other atmospheric circulation patterns. For example, it can help to predict the dispersion of atmospheric pollutants, forecast the spread of forest fires, and track the movement of volcanic ashes and other hazardous substances. Lagrangian transport also plays a significant role in the movement of marine plastic debris. This type of transport is important because it helps to determine the pathways that marine plastic debris takes as it is carried by ocean currents and winds and the hotspots of accumulation where they can be found.

1.1 Motivation and Objectives

1.1.1 Motivation

Lagrangian transport is a method used to describe the motion of individual fluid particles in a flow field. It finds applications in diverse scientific fields such as physics, engineering, oceanography, and atmospheric sciences for the study of transport and mixing processes. The Lagrangian approach provides a unique perspective on the transport of fluids and tracers, enabling insights that are not possible with traditional Eulerian approaches. By following the path of individual particles described by their position, we can analyze complex systems with many interrelated processes and gain a more complete understanding of the entire system. Additionally, this method allows us to study the time evolution of various quantities such as temperature, velocity, and pressure. The Lagrangian method is widely used in various fields due to its ability to handle a large number of interacting processes, making it a versatile and robust tool.

In physics, the Lagrangian method finds applications in the study of turbulence and chaotic mixing processes, as well as in the understanding of the underlying mechanisms of fluid transport in complex flow fields. It is a powerful tool for analyzing compressible flows and provides a deeper understanding of flow dynamics. [1, 2, 3] have focused on the Lagrangian description of different systems, including plasmas, dilute gases, cosmology, and developments in the fields of plasma and nanotechnology. The evolution of Lagrangian coherent structures can be used to explain the large-scale structure of the universe, electron transport in diodes and triodes, and the behavior of current-driven two-component plasmas.

In engineering, Lagrangian methods are used to model complex systems related to phase change heat transfer. [4, 5, 6] have described different applications of Lagrangian methods in fluid dynamics simulations. Ryzhakov et al. [5] developed a multiscale Lagrangian simulation technique for investigating the flow dynamics of polymeric fluids. Murashima and Taniguchi [4] proposed a new Lagrangian particle method for solving Euler equations for compressible fluid or gas flows, with improvements in the approximation of differential operators, a second-order algorithm, and the resolution of entropy discontinuities. Takabatake et al. [6] focused on using the Moving Particle Semi-implicit method for simulating free surface fluid flows involving heat transfer and phase change, with a new heat flux model to overcome limitations of the existing method. Verification tests have shown the effectiveness of the heat transfer model in Lagrangian fluid dynamics simulations.

Lagrangian approaches are also used in other fields such as health. The study of Lagrangian coherent structures in cardiovascular flows is important for understanding blood transport and its barriers. Darwish et al. [7, 8] explore the use of Lagrangian descriptors, a recently developed and computationally efficient approach, for the first time in cardiovascular flows. Darwish et al. [8] considered two in vitro flow models, an abdominal aortic aneurysm, and a healthy left ventricle, and demonstrated the ability of Lagrangian descriptors to reveal Lagrangian coherent structures. Darwish et al. [7] performed experiments on fluid transport downstream of a bileaflet mechanical aortic valve under different malfunction scenarios and found an increase in particle residence time with the severity of malfunction. The time-evolution of Lagrangian coherent structures highlights the effect of valve dysfunction on the fluid transport and its barriers in the aorta, and a new technique is applied to evaluate the highest accumulated shear stresses.

In oceanography, ocean circulation and mixing processes can be described in terms of the Lagrangian transport [9, 10, 11, 12, 13], as well as to predict the spread of oceanic pollutants [14, 15, 16, 17, 18]. The interest in the transport of plastics in the marine environment has increased in recent decades. Marine litter is a global environmental problem of worldwide scope [19, 20, 21]. Marine plastic debris are emitted from rivers, land-based sources and marine traffic routes, and spreads across the ocean over long distances and periods of time due to poor waste management. This material eventually ends up in the sea and undergoes mechanical and chemical degradation processes [22, 23], transforming into microplastics (smaller than 5 mm in size). It is difficult to accurately estimate the extent and predict the behavior of these small items. There is growing concern about microplastics due to their presence in various biological organisms, including mollusks and humans, although the consequences for these organisms are not yet fully understood [24, 25, 26, 27]. It is known, however, that the effects can be

significant. Therefore, it is important to address this issue at the macro scale by identifying the sources of plastic waste entering the ocean and working to mitigate them on a global scale.

Lagrangian transport is used to study the dispersion of pollutants and track the transport of air masses. For example, Chalbot et al. [28] used trajectory regression analysis to determine the origin of PM2.5 particles in Athens, Greece, explaining the pathways of air masses prior to their arrival. Lagrangian-based approaches are also valuable for estimating infection risks, as demonstrated by Yan et al. [29] , who found that this method was more robust in estimating the risk of infectious disease transmission in commercial airliners than traditional methods. Lagrangian methods have also been applied to assess the potential impact of natural disasters, such as volcanic eruptions. Urlea et al. [30] used these methods to analyze the potential impact of a large eruption of Vesuvius volcano on the Romanian air space, finding that a long-wave trough and southwesterly flow would favor direct transport of the ash cloud to Romania, with the maximum values of average mass found at an altitude around 7 *km*. In addition to volcanic eruptions, Lagrangian transport is of special interest in the study of extreme natural events, such as Extreme Precipitation Events (EPE) and associated floods. These events are the main meteorological risk in the Mediterranean region, with coastal regions being particularly vulnerable due to high economic activity and high population density [31]. As a result, the consequences of floods can result in loss of human lives and billions of dollars in economic costs [32]. The main mechanism that generates these convective episodes is the strong instability created by the difference between the warm, moist air mass over the Mediterranean Sea and the cold air at high altitudes, which is often linked to an isolated depression at high levels (cut-off low or DANA) in the region. While the extreme contribution of moisture from other regions is often underestimated or not considered, there are numerous recent studies on moisture sources for precipitation in the Western Mediterranean region that address both climatic values and specific extreme cases [33, 30].

1.1.2 Objectives

Lagrangian analysis tools are essential for the study of various transport phenomena, particularly when dealing with dynamic flows like the atmosphere and the ocean. By treating the transported substance as a set of particles, it is possible to track their trajectories and observe how they change over time. The goal of this thesis will be to examine atmospheric and oceanic transport from a Lagrangian perspective. This work has been divided into sub-objectives that will help to understand the transport of quantities in different fluids such as the ocean and atmosphere. (1) Initially, a recently developed Lagrangian tool was validated at a local scale to allow for the simplest Lagrangian study of floating plastics tracking in the ocean. (2) This tool was then used to conduct a regional study to evaluate the impact of different types of sources on the Iberian Peninsula over the North Atlantic Ocean. (3) Finally, two atmospheric Lagrangian methodologies were used to determine the different sources of moisture involved in two extreme precipitation events in the Mediterranean region and to estimate their relative contribution.

1.2 Kinematics. Transport Phenomena

Kinematics is a branch of mechanics that focuses on studying quantities related to space and time. Fluid transport is an ubiquitous phenomenon in our lives at all scales, from the atmospheric and oceanic scale to smaller systems such as the circulation of sap in plants. One scalar property, $C(r,t)$, is primarily transported from one location to another based on the combination of two processes: advection and/or diffusion, at a specific position and time [34]. Advection is the primary method of transport in a fluid that moves, which causes the transfer of material from one area to another due to the fluid's motion. This process is strongly related to the velocity field of the fluid, $\mathbf{v}(r,t)$, and can be characterized by a concentration field, $C(\mathbf{r},t)$, describing the properties of the flow at a position $\mathbf{r}$ and time t. Diffusion is an irreversible process caused by the random walk motion of molecules. This process refers to the random transport from areas of high concentration to areas of low concentration until a uniform concentration is achieved. Thus, considering that the flow is described by an advective and a diffusive part (Fick's law) as:

$$\mathbf{J} = \mathbf{v}C - D_m \nabla C \tag{1.1}$$

D_m is the diffusive term which considers all the diffusion processes associated with the medium properties. The changes over time of $C(\mathbf{r},t)$ is governed by the conservation equation,

$$\frac{\partial C}{\partial t} + \nabla \cdot \mathbf{J} = S(\mathbf{r},t) + R(C,T) \tag{1.2}$$

where $S(\mathbf{r},t)$ accounts for source-sink terms and $R(C,T)$ is the rate of generation of species by chemical reaction, depending in general on the fluid temperature T [34]. Then,

$$\frac{\partial C}{\partial t} + \nabla \cdot (\mathbf{v}C - D_m \nabla C) = S(\mathbf{r},t) + R(C,T) \tag{1.3}$$

Considering an incompressible flow ($\nabla \cdot \mathbf{v} = 0$),

$$\frac{\partial C}{\partial t} + \mathbf{v}\nabla C - D_m \nabla^2 C = S(\mathbf{r},t) + R(C,T) \tag{1.4}$$

and assuming that there are no sources or sinks, nor there are any reactive forces,

$$\frac{\partial C}{\partial t} + \mathbf{v}\nabla C = D_m \nabla^2 C \tag{1.5}$$

1.3 Advection and Diffusion Scales

Fluid processes may not be equally influenced by advective and diffusive processes. Spatiotemporal scales define the range of magnitudes in a given time and space. The advective and diffusive terms that govern the fluid flow, represented by J, are determined by the magnitudes of velocity (U), concentration (C), length (L), and diffusion coefficient (D_m). By substituting these variables into each term of Eq. 1.5,

$$\mathbf{v} \cdot \nabla C \approx \frac{UC}{L} \qquad ; \qquad D_m \cdot \nabla^2 C \approx D_m \frac{C}{L} \tag{1.6}$$

Thus, comparing both processes

$$\frac{UC/L}{D_m C/L^2} = \frac{UL}{D_m} = Pe \tag{1.7}$$

the resulting dimensionless ratio is the Peclet number, and it relates the diffusion speed with the advection velocity. For transport processes with $Pe \gg 1$, advection is the dominant transport mechanism and the diffusion can be neglected. The processes under consideration in this study have the following scales: $D_m \in [10^{-5}, 10^{-1}]\ cm^2/s$; $U \in [0.1, 7.8]\ m/s$ and $L \in [10^{-6}, 10^{6}]\ m$. As a result, it can be inferred that diffusive terms have no impact in this context.

Taking the ocean as an example, we can see that in addition to Lagrangian particles, actual particles are subject to inertial forces that compete with the movement of water masses resulting from advection. As such, particles possess a unique time period (τ_p) during which they become coupled with fluid modifications. By incorporating this variable along with other flow characteristics (U, L), we obtain another dimensionless number: the Stokes number,

$$S_t = \frac{\tau_p U}{L} \tag{1.8}$$

The degree of coupling between the transported particle and the fluid is quantified by the Stokes number. If the value of the Stokes number is small, the particle's motion is significantly linked to the fluid motion, causing the particles to behave as Lagrangian particles. These particles are commonly used for quantitative flow measurements. However, if the Stokes number is larger than one, the particle's motion is less influenced by the flow, and its response time exceeds the flow's characteristic time, resulting in inertial domination of the particle's motion. This work examines problems covering a range of Stokes number regimes, examining transport processes resulting from inertial and Lagrangian motion.

1.4 Eulerian and Lagrangian Formalisms in Fluid Dynamics

In fluid dynamics, there are two formalisms for describing the movement of fluids: Eulerian and Lagrangian. The Eulerian formalism, developed by Leonard Euler (1707-1783), attempts to characterize the concentration statistics based on the statistical properties of fluid velocities measured at fixed points in the fluid. This approach is useful as the Eulerian statistics can be easily measured, and the mathematical expressions can be applied to situations involving chemical reactions. However, it leads to a mathematical challenge called the closure problem, which has yet to be fully resolved. In contrast, Lagrangian methods describe the concentration statistics based on the statistical properties of particle displacement groups released into the fluid. The mathematics of this approach is more manageable, as it does not encounter the closure problem. The advantage of Lagrangian analysis is in understanding the movement and evolution of objects, matter, or properties carried by the flow, as well as any property derived from the integrated fluid motion. From the Eulerian perspective, variations of the fluid at points in space are considered, so detailed information regarding variation cannot be obtained.

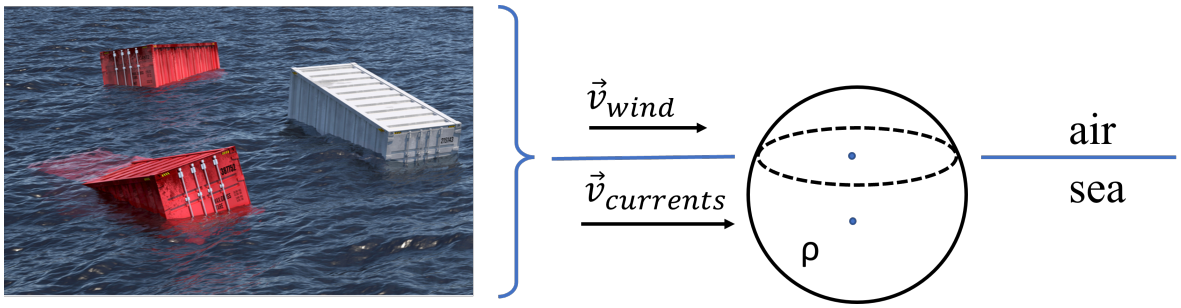

Figure 1.1: Parameterization of a partially submerged shipping container using the Maxey-Riley approximation.

1.5 Dynamical System Approach

Lagrangian particles ($S_t \ll 1$). The left-hand side of Eq. 1.5 represents the Lagrangian or material derivative of C, which defines the change in concentration along the path of a fluid element [1] [35]. As it was defined initially, $C \equiv C(\mathbf{r},t) \equiv C(\mathbf{r}(t),t)$, where $\mathbf{r}(t)$ is the path followed by the fluid element, and satisfies,

$$\dot{\mathbf{r}} = \mathbf{v}[\mathbf{r}(t),t] \tag{1.9}$$

This equation characterizes the movement of tiny particles that have minimal inertia and instantly assume the local velocity of the surrounding medium. Solving Eq.1.9 requires an initial condition $\mathbf{r_0}$. As the particle progresses, a series of states based on $\mathbf{r_0}$ describes its path. All the possible solutions corresponding to that initial position determine a mapping between initial and final positions at the t-instant of each fluid element.

$$\mathbf{r}(t) = \phi_{0,t}(\mathbf{r_0}) \tag{1.10}$$

The *flow map* ϕ, also called Lagrangian map, provides a complete description of the flow and corresponds to the Eulerian notion of velocity field $\mathbf{v}(r,t)$. Thus, the velocity field can be obtained by differentiating the Lagrangian map over time and therefore, the Lagrangian map can be recovered by integrating the velocity field. Then, the Lagrangian spatio-temporal evolution of the quantity $C(\mathbf{r}(t),t)$ can be described in terms of the trajectory on the flow map. In case no particular quantity evolution is involved, we can just obtain particle tracking. This way, the formal solution of Eq. 1.5, considering no diffusive terms, in terms of the inverse of the Lagrangian map ϕ^{-1} can be expressed as,

$$C(\mathbf{r},t) = C[\phi_{0,t}^{-1}(r),t=0] \tag{1.11}$$

This means that the concentration at any particular point is obtained as the sum of the initial concentration at the starting location of the fluid element with all the contributions as it moves along its path.

[1] By *fluid element*, we refer to a volume of fluid that is large compared to molecular dimensions but small enough to be considered a single point that moves precisely with the fluid.

Inertial particles ($S_t \gg 1$)**.** So far, we have focused on ideal tracers. Considering finite-sized particles, new forces will appear due to their finite size effects such as density and size. The motion of these particles is not conservative due to dissipative effects, causing the preservation of phase space volumes to be lost and resulting in contraction or expansion. These changes in the concentration, clustering, and preferential separation of particles, have significant impacts on natural phenomena [36]. The presence of a diverse range of items in plastic transport in the ocean significantly amplifies the complexity of the underlying dynamical system. The dynamics of inertial particles on the surface of the ocean is described in terms of the Maxey-Riley framework [37, 38, 39], since many heavy bodies with $S_t \gg 1$ can be described this way, as shown in Figure 1.1. A heavy half-sunken body such as a shipping lost container, under the Maxey-Riley consideration, can be viewed as a half-sunken sphere of radius r and density ρ. This framework can be adapted to account for the effects of the Earth's rotation and the non-uniform winds and ocean currents that exist above and below a small spherical particle floating at the air-sea interface. Four apparent forces affect the particle's horizontal movement: (1) the force exerted on the particle by the fluid, (2) the added mass force produced by the fluid moving with the particle, (3) the lift force created by the particle's rotation in a sheared flow, and (4) the drag force caused by fluid viscosity. To model the dynamics of these systems accurately, it is essential to add all these factors that influence the motion of the particles. Large containers or Abandoned Lost or Discarded Fishing Gear (ALDFG) are examples of drifting objects that have a long coupling time with the fluid and are subject to dissipative effects. Because of the additional forces involved, these large bodies cannot be adequately studied using Lagrangian assumptions alone. Instead, more comprehensive approaches such as the Maxey-Riley equation must be used to model their movement in the ocean.

1.6 Methodology

Lagrangian methods are often preferred over Eulerian methods when studying transported quantities in fluids. This is because Lagrangian methods follow individual particles within the fluid, allowing for a more detailed analysis of their behavior and interactions. In contrast, Eulerian methods analyze fluid properties at fixed points in space, which can miss important details about individual particle behavior. Therefore, this thesis will address the Lagrangian perspective to study transported quantities in fluids.

Lagrangian modeling will be used to study particle transport in the ocean. This recently developed transport tool will be validated in a high-resolution domain using data collected from beaches. The data will be based on the collection of mussel-pegs floating plastic items that are dumped into the sea during mussel farming. They form a purely Lagrangian transport problem, for which we know the emission origin and accumulation zones. The study will focus on the surface level, considering that the transport of fluid particles depends solely on surface ocean currents. Once the model is validated, it will be used to conduct a statistical study to determine the high accumulation zones in the North Atlantic open ocean. This will involve identifying various emission points along the Iberian Peninsula, as well as the Atlantic coastline of France and Portugal. The objective is to identify the impact of potential sources such as rivers, land-based points, or maritime traffic on the accumulation of marine debris in seas and oceans.

On the other hand, atmospheric simulations will be carried out to better understand moisture transport in the atmosphere. The WRF (Weather Research and Forecasting) computational model will be used to obtain the meteorological variables necessary for the study of two extreme events that occurred in the fall of 1982 in the Mediterranean region of Spain. Using the FLEXPART-WRF model, backward in time Lagrangian simulations will be carried out to determine the origin of the humidity involved in both events. To identify potential evaporation and precipitation zones, the $E - P$ representation will be used, while analytical methods will be used on the trajectory to obtain the proportion of evaporated moisture for a more accurate estimation. In addition, the recently developed U-Track atmospheric moisture model will be used as a second check to validate the results obtained by FLEXPART-WRF.

Chapter 2

Marine Plastic Pollution

2.1 Marine Plastic Debris

The prevalence and persistence of plastic waste as a pollutant, especially in marine ecosystems, have been increasing rapidly, attracting great interest around the world. According to the United Nations Environment Programme, 95% of the marine litter found on coastlines, sea surfaces, and the ocean floor consists of plastics. Over the past five decades, the global production of plastic has increased exponentially. Approximately 368 million tons of plastic were manufactured in 2019. And it is anticipated that the production of plastic will reach 600 million tons by 2025 (`https://www.plasticsoupfoundation.org/en/`). Around 40% of the plastic produced is intended for packaging, 20.4% for the construction industry, and approximately 10% is used in the automotive sector. From 1950 to 2017, the production of plastic reached 9.2 billion tons, and 55% of it was managed as waste, 29% still in use, 10% were incinerated, and only 6% were recycled. Of the 71% that are no longer in use, 40% were disposed of within the first month, making most of the plastic intended for disposable and single-use purposes. On average, each European citizen produces about 33 kg of plastic waste per year due to packaging. It is estimated that between 5 and 13 million tons of the 5 billion tons of plastic sent to landfills have ended up in the oceans, either through various rivers or direct dumping by fishermen. The buoyancy of plastic depends on its density compared to that of seawater, which determines whether it floats or sinks. This issue is expected to worsen by 2050, with projections indicating that 12.3 billion tons of plastic will be sent to landfill and another 12.3 billion tons will be incinerated, with only 8.5 billion tons recycled [40, 41]. The implications of plastic waste go beyond the lack of recycling, as each ton of plastic produced generates 2.5 tons of CO_2 emissions, and incineration produces 2.7 tons of CO_2 emissions per ton of plastic. Therefore, it is essential to develop techniques that facilitate the incorporation of plastic waste, as plastic can only be recycled once or twice and then cannot be used again in a similar application.

Although some studies suggest that marine sources also contribute significantly, it is commonly believed that the majority of plastic waste comes from land-based sources, particularly from densely populated inland areas. However, there is a significant discrepancy between the estimated amount of land-generated plastic waste entering coastal waters and the estimated total amount of plastic actually observed in the sea. This fact indicates that our comprehension of the movements, routes and fate of plastics is still incomplete. Part of this

inconsistency could be due to our incomplete knowledge of plastic transport mechanisms or the impossibility of knowing what happens and how much time elapses between the entry of plastic into the ocean and its arrival to areas where the majority of measurements are conducted [42]. Several physical mechanisms, such as stranding, sedimentation and fragmentation, which have not yet been carefully studied, may explain some of the differences found. Large debris has been observed to suffer variations in both size and composition in relation to proximity to major land-based sources [43]. In addition, biological processes, such as ingestion or sedimentation, can facilitate the transport of plastics within the oceans in both horizontal and vertical directions. To more effectively address the challenge of plastic pollution, a deeper understanding of the physical, chemical, and biological processes that influence the transport of plastics in the surface ocean is required. Van Sebille et al. [44] conducts a review of the various oceanic processes that can influence the trajectory of plastic, as it shown in Figure 2.1.

2.2 Oceanic Physical Processes and Other Mechanisms Affecting Plastic Movement

The main way to transport plastics through the ocean is via large-scale open ocean processes that are based on the geophysical dynamics of fluids. Surface winds, which cause Ekman drift at the sea surface, are the main drivers of the large-scale circulation. The resulting Ekman transport creates regions of convergence and divergence at the surface. Convergence zones are found in the five subtropical gyres, while divergence occurs in the subpolar gyres and parts of the Southern Ocean. These large-scale processes, especially the convergent processes, help us to identify the accumulation zones in the open ocean. The centers of the subtropical gyres have been identified as regions of high accumulation, also known as *hot-spots* [45]. However, the concept of garbage patches is often misunderstood. They are not compact islands of macroplastic traveling together through the ocean. Cozar et al. [46] redefined the term based on monitoring work in the subtropical gyre regions. Garbage patches are now defined as large accumulation zones (thousands of square kilometers in surface area) composed of tiny pieces of plastic (at the millimeter scale) that are not easily detectable by satellite images or the human eye [47]. Moreover, these gyres are not stationary structures, but vary in time and space [48]. Therefore, we can conclude that these convergence zones are a significant driver of marine debris on a large scale [49].

Another characteristic oceanic structures are the eddies. These mesoscale vortices are characterized by diameters of hundreds of kilometers and depths of a few hundred to thousands of meters. The coherence of these structures ranges from weeks to years. The interaction of these gyres with each other can lead to destabilization and rupture of the structures, resulting in smaller eddies (with diameters of 1-10 km and a coherence time ranging from days to weeks). They can be classified into two types: cyclonic and anticyclonic eddies. Similar to large-scale gyres, in the Northern Hemisphere, cyclonic eddies have an associated vertical current flowing toward the surface and away from the eddy. This phenomenon is responsible for phenomena such as upwelling. On the other hand, anticyclonic eddies correspond to a vertical flow towards the seafloor. At the surface, this movement leads to a radial motion towards the eddy center. This attractive motion could also be responsible for certain accumulations of debris at the turning centers [50]. Consequently, a cyclonic eddy would also lead to greater

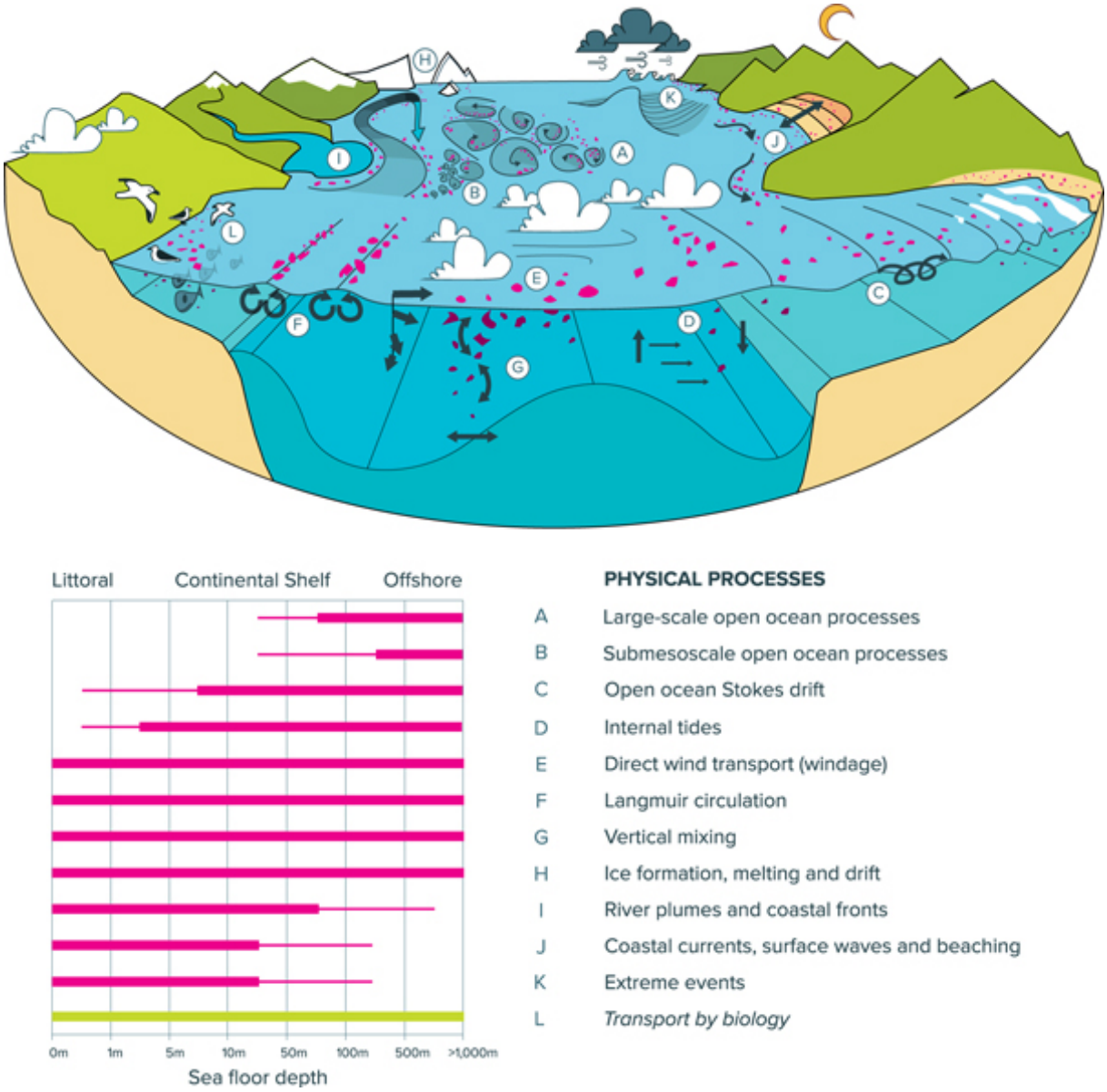

Figure 2.1: Oceanic physical processes (adapted with permission of IOP Publishing from ref. [44]).

dispersion of marine debris. These structures are not only important in terms of accumulation but can transport whatever they carry in their center of gyration for thousands of kilometers, as demonstrated in [51]. Below the 10 *km* scale, submesoscale processes appear and play a vital role locally in drift currents as an essential mixing force. However, it is more challenging to differentiate their structures in these ranges, and submesoscale processes are not typically resolved, even in "high-resolution" models.

Other effects modifying the trajectory of plastic items are the Stokes drift and windage, which operates on different scales. Stokes drift is an important phenomenon that relates to the movement of particles on the free surface of waves [52]. The net drift velocity experienced by a particle floating on the surface of a wave is in the direction of wave propagation because

the particle advances faster at the top of its orbit than it recedes at the bottom. Coastal waves are primarily caused by winds and they may be important for accumulation of plastics on the shore, and wave models can be used to predict Stokes drift accurately.

Windage refers to the impact of wind on objects that have a portion of their surface area above the water surface [53]. While the velocity of displacement due to wind can be directly proportional to the wind speed, it is important to note that windage is not the same as the surface current generated by the wind. Rather, it is the actual force of the wind drag that directly affects objects at the sea surface [54]. Another wind-related effect is the presence of coherent structures called Langmuir circulations in the mixed layer, which generate counter rotating vortices aligned parallel to the wind direction at the surface [55]. These circulations can be identified by their surface structure known as windrows, which are lines of surface debris and bubbles that align with the wind direction and indicate the convergence zones between the vortices.

Freshwater inputs also significantly contribute to the accumulation of plastic debris. River plumes occur where river water mixes with ocean water, creating fronts that can extend for tens or hundreds of kilometers into the open ocean [56, 57]. Floating objects, both natural and anthropogenic, tend to accumulate at these fronts due to the same factors that lead to the formation of submesoscale fronts, resulting in higher concentrations of debris along the outer edge of the river plume. Additionally, the melting and formation of ice also play a role in plastic transport. Sea ice is an important agent for sediment transport, as well as the accumulation of pollutants such as microplastics [58]. During its formation, plastic particles tend to concentrate in sea ice through a process called scavenging. The melting of sea ice occurs at the interface of the air and sea, which creates a “lifting” mechanism for plastic particles during freeze/thaw cycles, leading to their vertical movement. The distribution of plastics in the water column depends on various factors other than buoyancy, including phenomena such as large-scale pumping (Ekman), upwelling and downwelling, fronts, and turbulence-induced structures like convection cells and Langmuir circulations.

The transport of plastic particles in coastal zones is a complex phenomenon influenced by various factors. Coastal waters are characterized by high turbulence due to the movement of tides, making it difficult for plastic particles to move [59]. Moreover, the morphology of the coastline and its interaction with hydrodynamics also play a crucial role in determining the transport of plastic particles. The shallow depth of these waters makes the bathymetry particularly significant. Coastal regions are frequently characterized by the presence of river estuaries that exert a significant influence on the local dynamics, as well as anthropogenic elements such as dams that can modify the dynamics of the region. The phenomena of plastic particles stranded in sand, known as stranding or beaching, and the subsequent re-circulation of stranded particles, known as resuspension, are subject to significant influence from various external factors. Tidal patterns and physical impediments encountered by the particles, such as macro rocky intertidal zones or algae, are among the key factors impacting these phenomena. Additionally, wave breaking increases the mixing of the water column, which can cause resuspension of particles from the seabed.

Plastic items can also be transported and modified by biological organisms. Some birds incorporate plastic debris in their nests and burrows, while others become trapped in fishing gear, altering their trajectory [60]. Ingested plastics can be excreted in different locations, and biota can transport floating plastic from the sea surface to deeper depths, causing fragmentation through biting or shredding during digestion. Biofouling, the accretion of biological material around a plastic fragment, is another effect of biota on plastic debris [61]. The smaller scale biota that colonizes a fragment initiates a growth process, which alters its morphology.

A considerable proportion of plastic waste directly dumped into the ocean originates from lost or abandoned fishing gear used during fishing activities. The fishing gear employs various synthetic fibres, such as polyamide (PA), polyester (PES), polyethene (PE) and polypropylene (PP). Cigarette butts, a significant source of plastic pollution, are also commonly deposited in oceans, seas, rivers, and beaches, either directly or indirectly. Cigarette butts, which comprise 95% cellulose acetate fibres, a bioplastic, contain numerous toxic compounds, including formaldehyde, nicotine, arsenic, lead, copper, chromium, and a variety of polyaromatic hydrocarbons (PAHs).

Given the challenges associated with removing plastics from the environment and their well-documented resistance to degradation, it is also essential to investigate the degradation process of each type of plastic. Degradation occurs when the polymeric chains undergo a chemical reaction, leading to the separation of the chains. Various physical and chemical agents can trigger degradation and modify the properties of polymeric materials irreversibly. The degradation of plastics is contingent upon their type and the conditions to which they are exposed. These conditions encompass physical factors, including water, light, radiation, temperature, humidity, atmosphere, acidity, tides, and aerial exposure, water clarity, solar energy, tides, and waves that characterize the ocean environment. The role of microorganisms, such as bacteria and fungi, in assimilating plastics also merits consideration. Both degradation factors may operate simultaneously. But this phenomenon is out of the scope of this thesis.

Plastics may endure in the environment for extended periods, with ultraviolet radiation being one of the primary factors leading to plastic degradation. Plastics exposed to solar radiation undergo oxidative degradation, and as the plastic enters the advanced stages of degradation, it loses mechanical integrity, developing weaknesses. Mechanical forces resulting from waves, wind, and other macro particles may fragment plastics progressively, ultimately yielding micro- and nano-plastics. Plastics may also degrade when subjected to temperatures higher than those that polymeric chains can withstand, leading to chemical changes in the polymers. The temperature effect, combined with radiation and chemical attacks from the environment, causes the loss of properties, reaction with oxygen (oxidation), and the formation of oxidation products and carbon dioxide.

The influence of various physical processes on the transport of plastic marine debris that moves on the ocean remains uncertain, given the diverse shapes, densities, and sizes of the particles involved. The morphology of such particles renders the problem inertial, rather than purely Lagrangian, thereby subject to distinct impacts of the aforementioned phenomena, based on their individual configuration. For example, ALDFG is a growing problem that poses a wide range of negative impacts on marine ecosystems [62]. One of the most significant impacts is the

entanglement of marine animals, which can lead to injury or death. These structures can also damage or destroy habitats such as coral reefs, seagrass beds and rocky shores. The presence of ALDFG can also introduce foreign materials and species into marine ecosystems, disrupting natural food chains and potentially leading to the spread of invasive species. Moreover, they can also have economic impacts, as it can damage or destroy fishing gear, boats and infrastructure. Cleanup operations can be costly, and the presence of ALDFG can reduce the value of coastal tourism. The transport dynamics of these bodies can be complex, with pieces of gear moving at different rates and in different directions. This makes it difficult to predict where and when ALDFG will wash up on shore or become a hazard to shipping. Overall, the impacts of these structures highlight the need for effective management and prevention measures to reduce the amount of fishing gear lost or abandoned at sea.

In summary, the transport of objects in the ocean constitutes a multidisciplinary problem that relies on several factors that can be defined numerically in simulations. However, despite efforts to develop models that can account for such factors, there remains a significant number of cases that are beyond the scope of the existing numerical models.

2.3 Particle Tracking Model

Particle tracking methods are frequently employed in oceanography to simulate the movement and distribution of marine debris, pollutants, and other particles of interest. These methods are based on tracking the movement of virtual particles in a simulated fluid flow, whose motion is due to advection by surface ocean currents and diffusion. Lavers and Villarini [63] performed a global-scale particle tracking study using the hydrodynamic model HYCOM to predict the surface currents of the world's oceans. Then, virtual particles were introduced and forced only by the hydrodynamics. The model used a second-order accurate advection scheme, and horizontal diffusion was modeled as a random walk with separate longitudinal and lateral coefficients set to simulate random turbulence. Wind-driven currents were already expressed in the HYCOM hydrodynamic data, so no additional wind stress terms were applied to the motion of particles.

Similarly, Stuparu et al. [64] used the Delft3D model to simulate water flow and sediment transport in the North Sea at a local scale. They employed the PART module of Delft3D to simulate particle tracking. Lammerts [65] and Sousa et al. [66] also used the Delft3D model to simulate transport in the complex system of channels in the port of Rotterdam and in the Ria de Vigo, respectively. Carlson et al. [67] conducted a study of particle tracking to compare with field data in the Adriatic Sea, using the Particle Tracking and Analysis Toolbox (PaTATO) for Matlab. Turrell [68] used a simplified particle-tracking model with an idealized coastline to investigate the spatial operation of the interaction between variable winds and water level (VaWWL) along a coast. The model included a constant along-coast current, horizontal diffusion, onshore/offshore wind drift, beach/cliff combinations, and point/distributed litter sources. Here, we employ the recently developed Lagrangian tool, the MOHID-Lagrangian model.

2.3.1 MOHID-Lagrangian Model

This Lagrangian tool was developed from the MOHID hydrodynamic model for the dynamic study of marine transport [69]. The MOHID-Lagrangian model is a complete and high-resolution tracking model that can function both as a library for the MOHID Water modeling system and as a standalone program, making it versatile in working with diverse hydrodynamic models and producing studies of different scales. The model employs the concept of a tracer to monitor particles, where the position of the tracer (x,y,z) is accurately determined at each time step. The motion of the tracers is influenced by the velocity derived from the hydrodynamic module, the wind as determined by the surface module, and the velocity generated by the waves. The velocity field is obtained by interpolating the hydrodynamic Eulerian velocity field to the particle position. The position of a particle is determined by integrating the velocity field and a diffusive term, expressed as:

$$\frac{d\mathbf{r}_p}{dt} = \mathbf{v}_p(r(t),t) + D_i \tag{2.1}$$

where $\mathbf{v}_p$ is the velocity field at a t instant an D_i is the diffusion velocity. The diffusion term attempts to model the movement of marine litter due to unresolved scales of motion and it should gain relevance in regions where eddy activity and hence shear are more intense. In general, it is modelled by a random walk motion parametrized as,

$$D_i = R_n \cdot \sqrt{2K_h\Delta t} \tag{2.2}$$

R_n is a vector of zero mean with random numbers generated at each time step in each spatial direction, with a standard deviation equal to one. K_h is a horizontal dispersion tensor which, in most cases, is taken to be of diagonal form with given longitudinal and lateral eddy diffusivity. To ensure that diffusion primarily affects the motion of tracers when the resolution of the underlying current velocity field cannot capture motion on scales shorter than the model output, we constrain the update of D_i in relation to the model resolution $\Delta_{x,y}$,

$$D_i \cdot \Delta t < 2 \cdot \Delta_{x,y} \tag{2.3}$$

This way, a particle maintains the same stochastic diffusion velocity noise while it remains in a neighboring area with a size lesser than $2\Delta_{x,y}$. The noise is updated once the particle moves into a new region in the flow field with a size larger than $2\Delta_{x,y}$.

One of the most powerful features of this model is its beaching parameterization. The state variable $LI(t)$, or land interaction, for each particle is defined based on the type of cell it is in, in a set of particle trajectories $\mathbf{r_i}$. To do this, we need to consider the land interaction mask (LIM) obtained from the current field, which has values ranging from -1 to 2. Non-missing value cells are considered as water (w_c), while missing value cells are considered as land (l_c). Adjacent cells to missing cells above a set threshold height are considered as beach cells (b_c), and cells below the threshold are considered as seafloor cells (d_c). The threshold is set by the user in the simulation settings. Cell values are categorized as it is shown in Figure 2.2a).

Once the scalar Land-Interaction-Mask field (LIM) is obtained (see Figure 2.2a), the

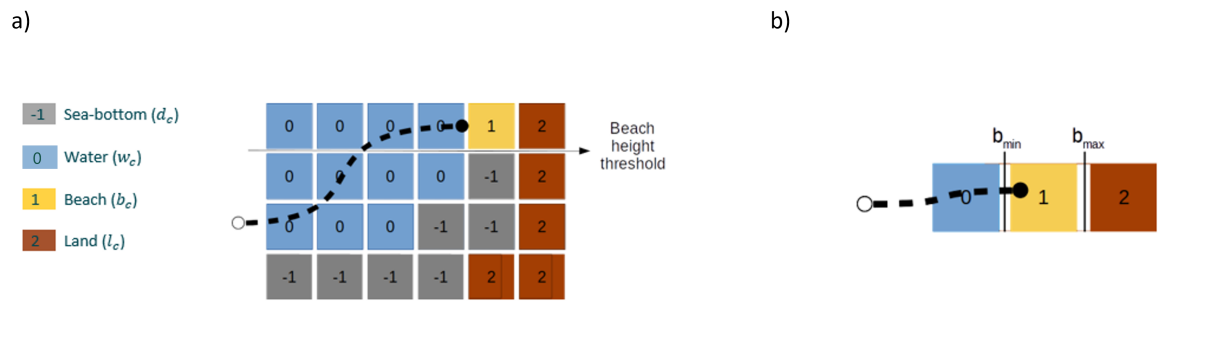

Figure 2.2: Beaching process implemented in MOHID-Lagrangian model. a) Assignment of the Land-Mask Interface values (LIM). b) Beaching scenario where a particle moves from water to beach.

Land-Interaction for each particle at each time instant is calculated as follows:

$$LI(t)_i = LIM(r(t)_i) \tag{2.4}$$

Considering a particle i with an associated LI value that causes it to become trapped on land, as shown in Figure 2.2b), the beaching process is computed based on a velocity reduction factor. When a particle is beached, its factor reduces its current speed to 0. The velocity reduction factor is obtained using the following equation:

$$f_v(LI) = b_{w(LI)} \cdot r_{W(RC)} \tag{2.5}$$

with b_w a beach quadratic weight in the range [0,1] that weights how deep a particle is in a beach cell.

$$b_W(LI) = 1 - \left(\frac{LI - b_{min}}{b_{max} - b_{min}} \right)^2 \tag{2.6}$$

and r_w is a threshold value that relates to the percentage probability of beaching to determine the particles that become beached. This way, it is possible to set a threshold depth value above which the particle becomes stranded, as well as a probability for particle beaching. The depth value establish the sea-bottom value (d_c). With these parameters, different accumulation scenarios can be modeled since depending on the morphology of the coastline to be simulated, the values that configure the retention vary.

Another feature of this model is the different types of set emission points, including points, lines, box, spheres, KMZ-polygons, XY-polygons, and position time series. There are different types of emissions used to model pollution scenarios. The simplest type is called “point emissions”, which are defined by a set of coordinates that include longitude, latitude, and depth. Line emissions are similar, but they extend one dimension. Emission boxes are defined by their lower left and upper right corners. In case a 3D below-surface emission is required, a sphere type emission will be used. Additionally, emissions can have different resolutions within KMZ or XY polygons, or vary in space and time to simulate a moving ship’s spill. Therefore, we can configure the emission type to match the scenario being modeled. Additionally, the MOHID-Lagrangian’s post-processing module offers considerable flexibility in presenting the obtained results. It provides a tool that enables the dissociation of emissions on the output grid, thus allowing for a separate evaluation of the impact of each emission source. The user has

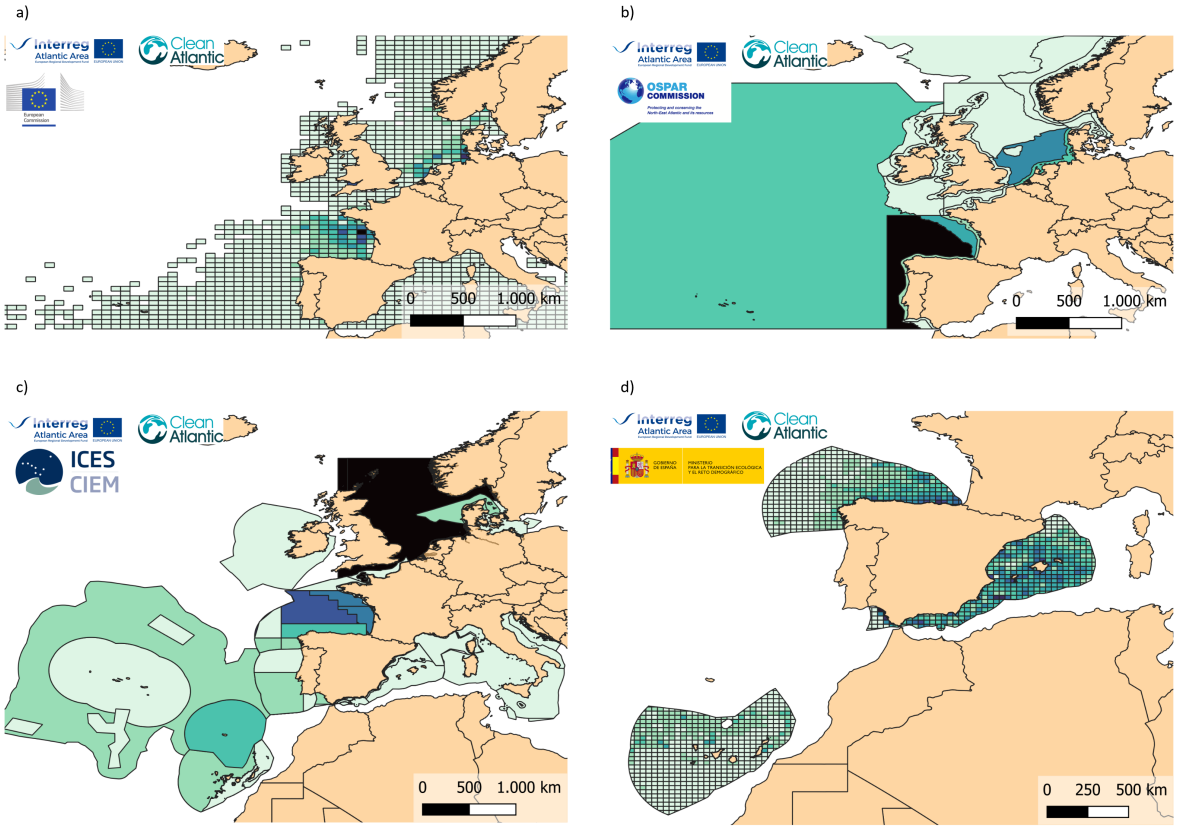

Figure 2.3: Different grid representation for the same MOHID-Lagrangian output. Surface distribution of Lagrangian particles originating from 61 European rivers during 4 years of simulation (2016-2019). Maps show the mean number of particles in (a) Marine Report Units (MRU), (b) OSPAR marine protected areas, (c) ICES divisions, and (d) Marine Spanish Demarcations.

the option to select and define the output grid. Figure 2.3 shows different grid representations for the same MOHID-Lagrangian simulation output. Here, the contribution of 61 European rivers during 4 years of simulation (2016-2019) are presented in four different demarcations of the European North Atlantic Area: (a) Marine Report Units (MRUs), (b) OSPAR marine protected areas, (c) ICES divisions, and (d) Marine Spanish Demarcations. Additionally, the tool provides the user with the choice to select the type of statistical data for the representation of the results, such as total accumulation, mean, median, or statistical deviation. Furthermore, the user can group the results based on their temporal frequency, including options such as total period, annual, monthly, weekly, seasonal, among others.

As part of the Interreg CleanAtlantic project, The MOHID-Lagrangian tool was developed to help achieve the project's goals of protecting biodiversity and ecosystem services in the Atlantic region. By improving capabilities for monitoring, preventing, and removing macro marine litter, CleanAtlantic aims to enhance awareness and shift attitudes among stakeholders, as well as improve management systems for marine litter. Therefore, our ocean studies using MOHID-Lagrangian, as presented here, fall within the scope of the Interreg CleanAtlantic project.

Chapter 3

Transport of Atmospheric Moisture

3.1 Heavy Precipitation Events

Heavy Precipitation Events (HPEs) are one of the most destructive weather phenomena. In 2019, this extreme rainfall and resulting floods took the lives of over 5,000 people, affected more than 30 million individuals, and caused economic losses exceeding USD 35 billion, according to the International Disaster Database (EMDAT.database, 2021 [70]). Such catastrophic events highlight the urgent need for improved prediction and anticipation. Studying extreme rainfall and floods can help us to better understand the underlying causes and contributing factors of these events. By analyzing meteorological data, we can identify patterns and trends that can serve as the basis for predictive models and early warning systems. This, in turn, can help authorities and communities to prepare for and to mitigate the impact of extreme weather events. Furthermore, the impact of extreme rainfall and floods can be studied to develop more resilient infrastructure and land-use policies. For instance, the effectiveness of current flood control measures can be analyzed, and areas that require additional protection can be identified. The effects of deforestation and urbanization on water drainage and runoff can also be studied to develop strategies to mitigate their impact. Studying extreme rainfall and floods can also provide insight into the social and economic impact of such events. By analyzing the response of communities and the effectiveness of relief efforts, areas that require improvement can be identified, and more effective disaster response plans can be developed. Additionally, the long-term economic impact of these events, including the cost of rebuilding and their effect on local economies, can be studied.

Precipitation is not evenly distributed across the planet, with some regions being more prone to heavy precipitation events that result in large amounts of rainfall over a short period of time. Conversely, other areas experience more moderate precipitation regimes. Floods are a common occurrence in the Western Mediterranean Region (WMR) due to the emergence of powerful convective situations that cause brief but severe periods of rainfall. The studies on humidity transport presented in this thesis take place in this region.

3.1.1 The Western Mediterranean Region

The Western Mediterranean Region is known to experience frequent extreme precipitation and flooding [71]. The susceptibility of this region to heavy rainfall can be attributed to several

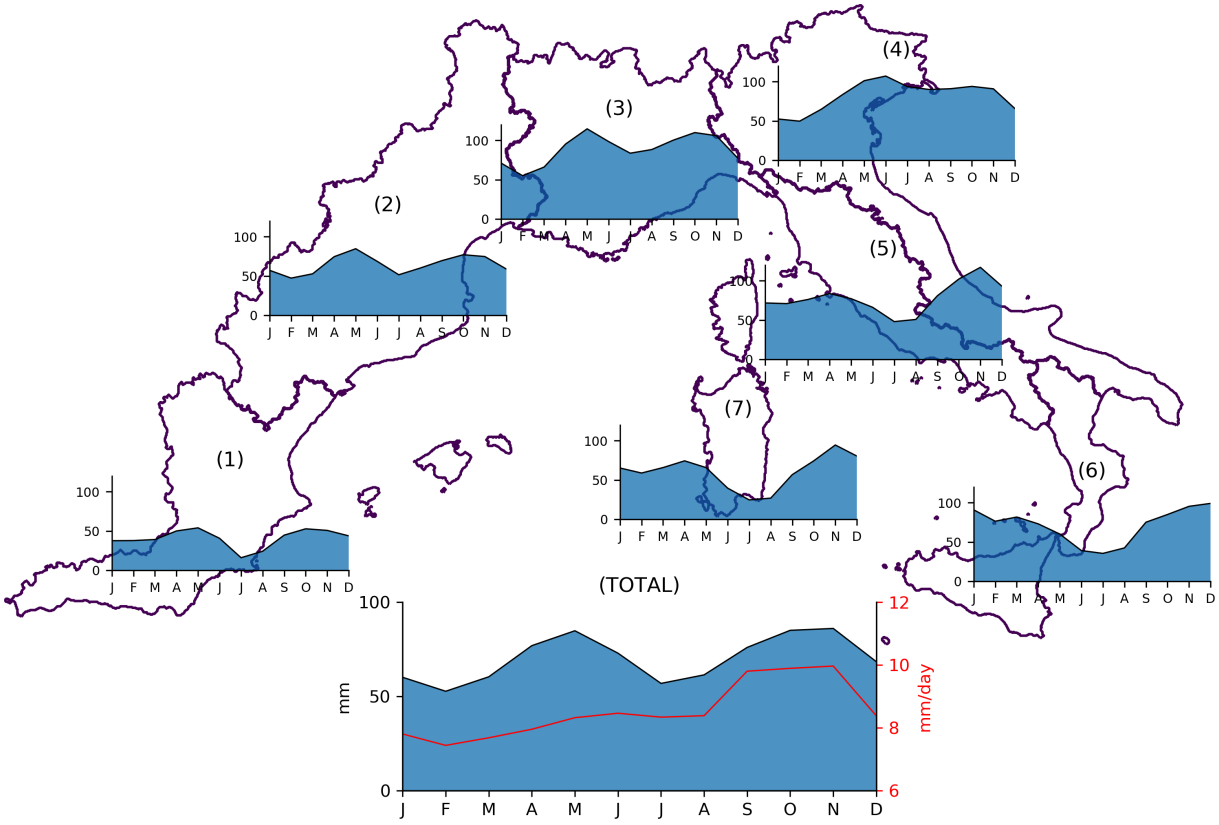

Figure 3.1: Monthly precipitation distribution for the WMR sub-regions, with the average daily precipitation on wet days represented by a red line. Data obtained from MESCAN analysis [77] and the monthly averages ranges between 1980-2015.(adapted with permission of the author from ref.[78]).

factors. Firstly, the Mediterranean Sea is a vast water body with relatively mild temperatures, which makes it a source of moisture for the surrounding landmass. Additionally, the area's complex topography, which consists of high mountains, valleys, and plateaus, makes it highly vulnerable to flooding. Furthermore, the region is located in a relatively northern latitude, which means that it is more prone to extreme weather events such as cyclones and Atlantic lows [72, 73, 74]. In Figure 3.1 the average monthly distribution for each of the regions comprising the WMR is shown. The central figure represents the average monthly distribution for the entire region. From this graph, it can be seen that both spring and autumn are the seasons with the highest occurrence of HPE. However, when observing the average daily precipitation on wet days (red line), it can be noticed that the events are much more intense in autumn [75]. This is because Atlantic lows or cutoff lows often interact with the warm Mediterranean Sea waters [76] during this period, resulting in strong convection that leads to heavy rainfall and flooding in the surrounding areas. Therefore, it is essential to understand the complex meteorological processes that occur in the Western Mediterranean Region to mitigate the risks associated with extreme precipitation and flooding.

In this regard, Insua-Costa et al. [31] used the high-resolution MESCAN dataset [77] for rainfall to identify recorded events, classify them by magnitude and weather type, and check for their association with flooding. To verify if the precipitation resulted in flooding, data from FLOODHYMEX [79] and EM-DAT (`http://www.wmdata.be/`) databases were used. All

this information was compiled into a single publicly available database. The analysis revealed that the Languedoc-Roussillon region in France and the Valencian Community in Spain have the highest number of events per year. The most severe events, which also caused more floods, occurred mostly in September, October, and November. The study also found that only four weather types are common during hazardous rainfall days in the Western Mediterranean. The most dangerous weather pattern is characterized by a low-pressure system across all levels of the troposphere in the eastern Atlantic, forming a block pattern with an anticyclonic ridge extending from the Central Mediterranean to Central Europe. This pattern was responsible for about 40% of the most severe cases. For instance, the notorious 1994 Piedmont episode in Italy, which ranked among the top 10, was due to this type of atmospheric configuration.

Although HPEs occur at specific regions, the source of moisture that feed them may not be local. Instead, it can originate from remote areas and be transported by various atmospheric mechanisms. Studies have shown that Atmospheric Rivers (ARs), which are narrow and elongated corridors of water vapor in the atmosphere, are an essential contributor to the total precipitation recorded in Europe and the United States. Additionally, ARs are also associated with extreme rainfall episodes. In the case of the WMR, recent studies suggest that remote sources of moisture, such as the North Atlantic or tropical and subtropical areas, could significantly contribute to the frequent torrential rains in the region. Winschall et al. [80] found that the WMR received a significant amount of moisture from the North Atlantic during an extreme precipitation event in October 2010. Similarly, Pinto et al. [81] and Krichak et al. [82] reported that the WMR was affected by moisture transported from the Sahel region of Africa and the Red Sea, respectively. Insua-Costa et al. [83] also suggested that tropical and subtropical areas could be a source of moisture for extreme precipitation events in the WMR.

Various techniques have been employed to identify the source of moisture, with Lagrangian models being the most commonly used methodology. This technique involves both backward and forward tracking of air parcels and analyzing the changes in their moisture content over time. Lagrangian models are efficient from a computational point of view as they are offline. In contrast, Eulerian methods are more computationally expensive but more accurate for moisture source studies. In a recent classification of different models used for moisture tracking, Dominguez et al. [84] categorized them based on their complexity. Although Lagrangian methods have been widely used in the western Mediterranean region [85, 86, 33, 87], Eulerian approaches have been less utilized due to their high computational demands. Winschall et al. [80] and Insua-Costa et al. [83] are among the few authors who have employed online Eulerian methods in the region.

3.2 Modeling of Precipitation Processes

3.2.1 The Water Cycle

Understanding the nature and evolution of the hydrological cycle is, currently, one of the most compelling challenges given the importance of global climate change. The atmosphere, despite holding a minor portion of the planet's water, is essential for linking various water sources such as oceans, lakes, soils, ice both on land and sea, and rivers through processes like moisture transportation, evapotranspiration, and precipitation. The hydrologic cycle can be

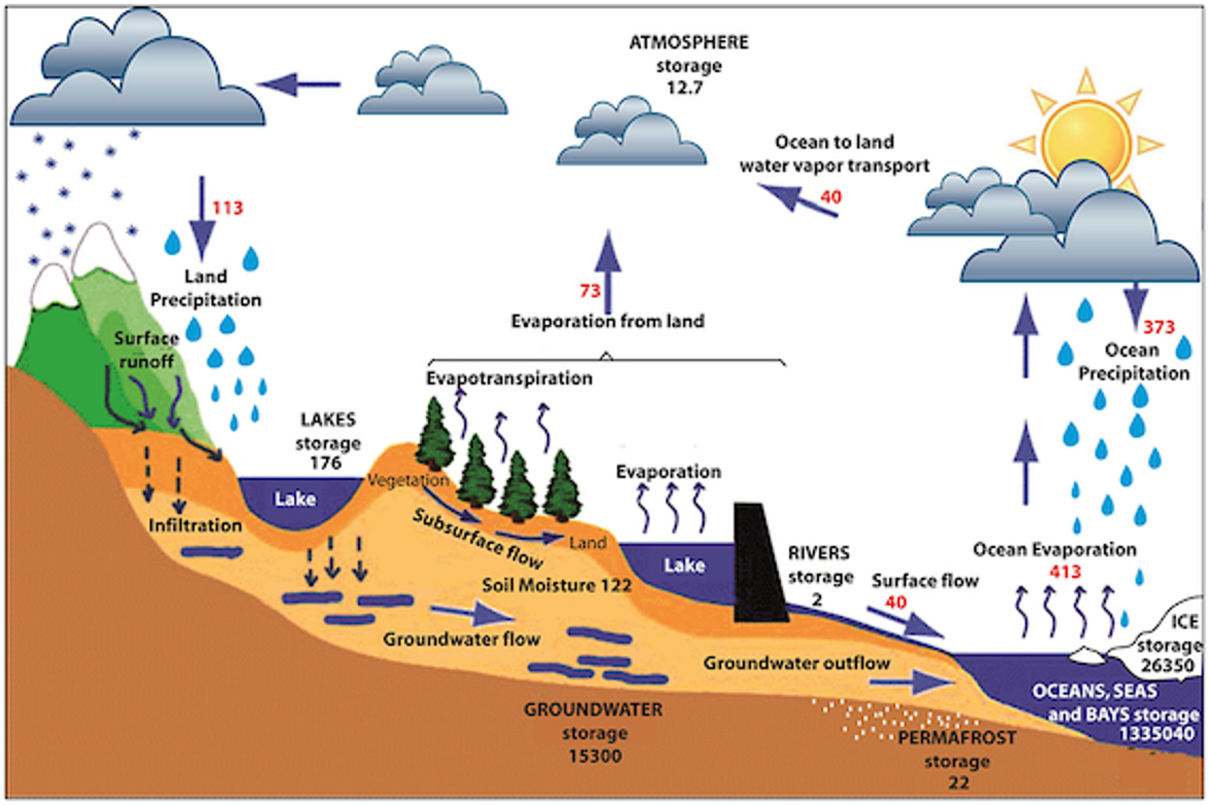

Figure 3.2: The hydrological cycle in terms of storage (black numbers) and water exchanges (red numbers) (adapted with permission of John Wiley and Sons from [88]).

briefly described as the process by which moisture evaporates from one place and eventually precipitates in another, which is maintained by atmospheric, oceanic and hydrologic transport of water. In regions with an oceanic presence, the evaporation ratio typically exceeds the precipitation rate, with the ocean acting as the main source of moisture that is then transported by the atmosphere to the land masses. Land masses represent a natural sink for atmospheric moisture, since precipitation is greater than evapotranspiration. The surplus of surface water then refills rivers, groundwater, and other bodies of water that eventually drain into the ocean, thus completing the cycle. As shown in Figure 3.2, about 90% of the water that evaporates from the oceans returns to them as rainfall, and just 10% is deposited as precipitation over land masses [88]. Roughly two-thirds of this 10% is recycled on land, while the remaining one-third directly flows into the oceans [89].

When water evaporates, the moisture typically remains in the atmosphere for about 10 days before condensing and returning to Earth as precipitation [90, 91]. Precipitation requires the presence of three elements: (1) atmospheric moisture, (2) a cooling process, and (3) cloud condensation nuclei. Cooling can be due to various mechanisms, such as lifting of an air mass through convection, large-scale ascent or flow over a topographic obstacle. It can also occur due to radiation, such as the formation of fog. Condensation in the atmosphere is dependent on the presence of aerosols. The formation, growth, and precipitation of cloud droplets or ice crystals are controlled by microphysics through processes such as collision or coalescence [92].

3.2.2 Water Vapour Flux

The atmospheric transport of water vapor is usually depicted as the total horizontal flux of water vapor integrated vertically. This can be represented as,

$$\Theta = \frac{1}{g}\int_0^{p_s} qV\,dp \tag{3.1}$$

where g is gravity acceleration, p_s is the surface pressure, q is the specific humidity and V is the horizontal wind vector at a specific level. The precipitable water is defined as,

$$W = \frac{1}{g}\int_0^{p_s} q\,dp \tag{3.2}$$

The hydrological balance in the atmosphere can be expressed using the principle of conservation of mass as,

$$\frac{\partial W}{\partial t} + \nabla \cdot \Theta = E - P \tag{3.3}$$

Then, the temporal variation of the precipitable water (3.2) and the divergence of the total horizontal flux of water vapor (3.1) balances the fresh water flux $E - P$ at the surface. The $E - P$ shows the main sinks and sources of water vapor globally. The main net sources $(E > P)$ are found in the subtropical regions with high evaporation, while the main net sinks $(E < P)$ are located in the InterTropical Convergence Zone (ITCZ), the South Pacific Convergence Zone (SPCZ) and mid-latitude storm tracks, where moisture convection results in heavy precipitation.

3.2.3 Determination of Atmospheric Sources and Sinks

There are three main methods to determine the source and sink areas of atmospheric moisture: analytical or box models, numerical water vapor tracers, and physical water vapor tracers (isotopes). Here we present a brief explanation of each one, but a detailed description has been done by Gimeno et al. [88].

Analytical Models

Historically, analytical models have been developed for understanding changes in the surface hydrology of a region. They have been extensively utilized to calculate the recycling ratio [93, 94]. Focusing on the impact of evapotranspiration on local precipitation (also known as precipitation recycling), the analytical models are based on the equation of the vertically integrated balance of water vapor, first reviewed by [95], and written as,

$$\frac{\partial(w)}{\partial t} + \frac{\partial(wu)}{\partial x} + \frac{\partial(wv)}{\partial y} = E - P \tag{3.4}$$

w denotes the water vapor amount in the vertical column per unit of area, u represents the ratio of vertically integrated zonal water vapor flux between w and v depicts the water vapor weighted meridional wind. Many other authors have worked on this concept to implement new analytical models for better estimation of precipitation recycling [96, 97]. Because there is a strong logarithmic relationship between the recycling ratio and area for different regions, Dirmeyer and Brubaker [98] created a global analysis of the recycling ratio on a common area scale. One significant benefit of using these models is their simplicity and low computational

cost. However, their usefulness is limited by several strong assumptions, such as that water vapor from all sources is completely mixed within the atmospheric column. Consequently, the applicability of analytical models is restricted and they can only provide a rough approximation of the recycle ratio.

Physical Water Vapor Tracers

Numerical and analytical models are valuable tools for studying the water cycle, but they must be validated with real physical data. Stable isotopes of hydrogen and oxygen, such as deuterium (D) and ^{18}O, are used for this purpose. They are naturally present in precipitation and water vapor and by analyzing their ratios in different phases, we can characterize phase changes [99, 100, 101, 102]. Since the 1960s, data on isotopic composition in precipitation has been collected and analyzed multiple times. These studies have consistently shown the influence of factors such as temperature, latitude, altitude, and amount on isotopic composition. Moreover, several investigations have utilized isotopic data to verify models and explore atmospheric recycling.

Numerical Water Vapor Tracers

Numerical water vapor tracers, also known as the "water vapor tagging" approach, can be further divided into Eulerian and Lagrangian methods. The Lagrangian method involves tracking fluid parcels as they move through space and time, while the Eulerian method focuses on fixed locations in space and the movement of fluid through them over time as shown in Figure 3.3. Eulerian techniques provide information on the recycled precipitation taking into account the specific origin and destination of the advected moisture [103, 104, 105]. Eulerian methods can be divided into offline and online methods.

2-D moisture tracking models, also referred to as offline Eulerian methods [106], are an alternative to traditional analytical models. These models are particularly useful for computing continental moisture recycling ratios at a global scale. Rather than relying on the traditional analytical model, which assumes a well-mixed atmosphere, the 2-D moisture tracking models use vertically integrated variables for their calculations. However, this well-mixed atmosphere hypothesis can lead to errors in regions where there is a significant vertical shear. In recent years, this assumption has been relaxed by adding an additional vertical level to some offline Eulerian models (i.e., transitioning from a single column to two layers). Thus, the results provided by these models have been considerably improved [107].

Water Vapor Tracers (WVTs), also known as online Eulerian methods, are considered to be the most accurate technique for studying atmospheric moisture sources for precipitation. This methodology involves coupling a moisture tagging technique with a global or regional climate model, which enables WVTs to consider all physical processes affecting atmospheric moisture, such as advection, molecular and turbulent diffusion, convection, and cloud microphysics. However, this technique has some limitations, including the fact that it requires running an atmospheric model and relying on the results of the simulation. Therefore, this method can only provide accurate results if the atmospheric model simulation is realistic. Additionally, the computational cost associated with WVTs is much higher than any of the other methodologies

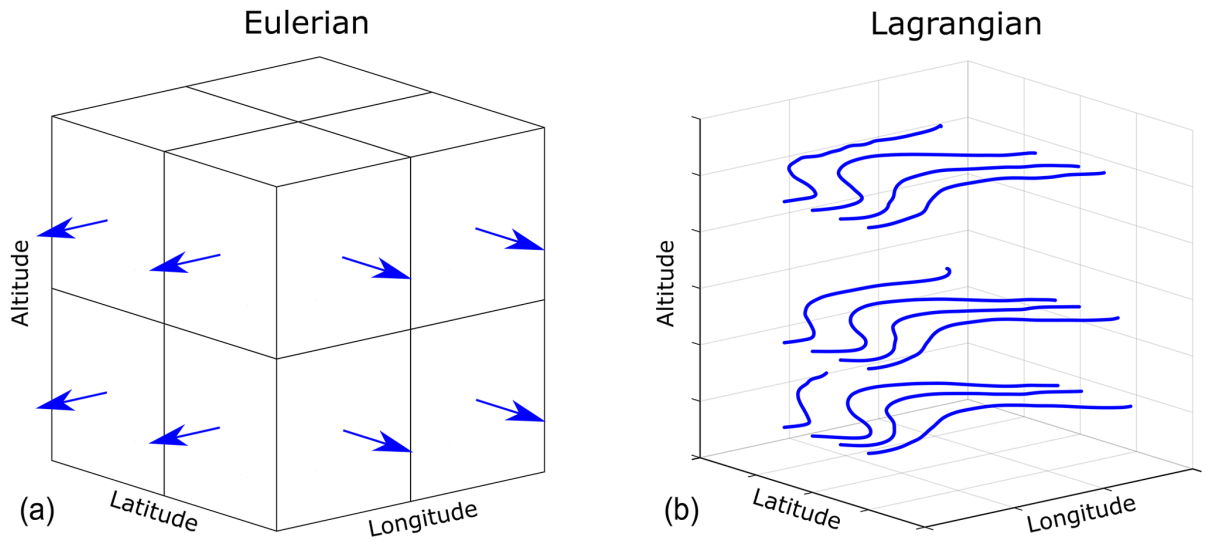

Figure 3.3: Difference between Lagrangian and Eulerian models for tracking moisture. The Eulerian method relies on a grid system, while the Lagrangian method follows the trajectory of individual particles (adapted with permission of Copernicus Publications from [108]).

mentioned above.

Spatio-temporal tracking of individual fluid particles in Lagrangian models is a widely used method for studying moisture sources and sinks. There are two main classes of Lagrangian models: quasi-isentropic back-trajectories and Lagrangian particle dispersion. These models have been used in climate studies of atmospheric water vapor sources and in diagnosing the origin of moisture in extreme precipitation events. The advantage of these models is their computational efficiency and the fact that source regions do not need to be preselected since particles can be tracked in time. However, using reanalysis data for the calculations introduces certain constraints. Some of these models, however, have some simplifications in their formulation that can lead to serious biases. For example, Lagrangian particle dispersion does not clearly distinguish between Evaporation (E) and Precipitation (P) and neglects liquid water and ice, leading to an overestimation of both E and P. On the other hand, quasi-isentropic back-trajectories require evaporation and precipitable water content for calculations but assume the well-mixed atmosphere hypothesis, which assumes that water from surface evaporation contributes uniformly throughout the column. In addition, phase changes along the trajectory of the particles are not taken into account.

Being integrated into climate models, WVT numerical models incorporate more information than analytical methods. Thus, a larger number of processes that can affect moisture are included. Thus, the tracers have a clear limitation. Their accuracy is subject to the accuracy of the results of the climate model. Lagrangian methods have gained popularity in recent years for diagnosing moisture transport. By using backward trajectories of precipitation areas, the origin of the air masses can be determined. The trajectories of the parcels are released backward in time. For each grid parcel k and instant of time t, Dirmeyer and Brubaker [109] identified the evaporative contribution ($R_{i,k}(x,y)$) in each grid point (x,y) as the ratio of the surface evaporation area E between the fraction of precipitable water W,

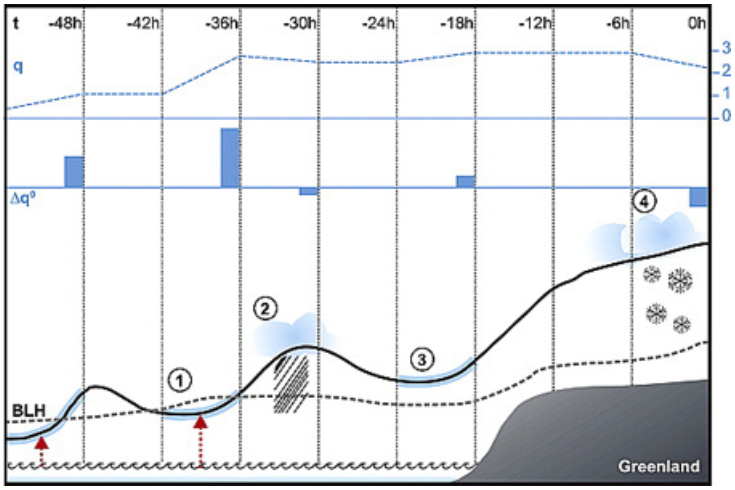

Figure 3.4: Sketch of the approach to detecting updrafts along a reverse path of an air mass traveling from the Atlantic Ocean towards Greenland (adapted with permission of John Wiley and Sons from [111]).

$$R_{i,k}(x,y,t) = \frac{E(x,y,t)}{W_i} \tag{3.5}$$

where i index represents the grid box of the target area where precipitation occurs. In terms of area A composed by n grid points, the total mass of evaporation using K initial released particles is defined as,

$$E_A(x,y) = \sum_{i=1}^{n} \sum_{k=1}^{K} \sum_{t=1}^{t_f} R_{i,k}(x,y,t) \tag{3.6}$$

being t_f the time for the longest backtracked particle. Stohl et al. [110] developed a similar methodology to study the gains and losses along the trajectories of the k particles, considering the quantity q defined as the specific humidity that is calculated for each point of the trajectory.

$$(e-p)_k = m\frac{dq}{dt} \tag{3.7}$$

$(e-p)$ refers to the increase or decrease of specific moisture along the path of each trajectory, and m refers to the mass of the parcel. The surface freshwater flux in an area A can be determined by introducing a significant number of computational air particles K into the computational atmosphere domain. This surface freshwater flux is described as,

$$E-P = \frac{\sum_{k=1}^{K}(e-p)_k}{A} \tag{3.8}$$

This methodology allows the identification of net moisture loss or gains both along individual particle trajectories and on a regular grid. The origin and destination areas of evaporation in a specific region can be traced and established based on the data collected from the movement of air particles. The main limitation of this methodology is the inability to clearly separate evaporation and precipitation [112, 113]. In addition, $(E-P)$ is calculated by taking the time derivative of moisture along the particle trajectories. If the reanalysis data used to

feed the model do not accurately calculate the water balance (with the increment of analysis often being the most important factor), then the method can result in substantial inaccuracies. Moreover, the gains attributed to a location at a given instant may not effectively contribute to the precipitation phenomenon. These gains may have precipitated in an intermediate step between their evaporation and the final precipitation event. Sodemann et al. [111] presents a new method to properly estimate the contribution (and consequently the weight) of each evaporation grid point for each simulated trajectory. This is an iterative process that recalculates increments in moisture (evaporation) related to previous intermediate losses (precipitation) prior to the target precipitation event in order to obtain realistic evaporation values. Considering a trajectory as shown in Figure 3.4, at $t = -48h$, the gain fraction with respect to the humidity value (q_n) at that n-instant is calculated as,

$$f_n = \frac{\Delta q_n}{q_n} \tag{3.9}$$

with Δq_n the gain of humidity of a certain particle. Since another positive absorption is given in a next m-time step $t = -36h$, this new uptake reduces the significance of the previous one. So all the previous fractional contributions have to be recalculated as,

$$f_m = \frac{\Delta q_n}{q_m} \tag{3.10}$$

Similarly, when intermediate precipitation occurs, the previous positive contributions Δq_n have to be recalculated considering this loss. Then,

$$\Delta q'_m = \Delta q_m + \Delta^0_{q_n} \cdot f_m \tag{3.11}$$

In this way, we obtain corrected evaporation values that are more realistic.

3.3 Atmospheric Models

For decades, researchers have been studying the sources of moisture that lead to rainfall. Recent years have seen significant advances in the tools and techniques used for this purpose. Determining the origin of precipitation is challenging through observations alone, so most researchers use numerical moisture tracking models. The present thesis examines the sources of moisture in two catastrophic flood events in the WMR, comparing an offline Lagrangian and an online Eulerian approach. The moisture source tracking was carried out previously using the WRF-WVTs online Eulerian model described by Insua-Costa and Miguez-Macho [114]. The obtained results have been presented in a previous publication [83]. The aim of our study is to replicate this methodology, using two offline Lagrangian models, namely the FLEXPART-WRF model [115] and the U-Track model [108], with the purpose of intercomparing the results obtained through all methods. Therefore, in the following subsection, we will give a brief explanation of these models.

3.3.1 WRF-WVTs

This Eulerian-online method consists of a moisture tagging tool coupled to a regional or a global atmospheric model. The WRF Water Vapour Tracers (WRF-WVT) [114] is implemented

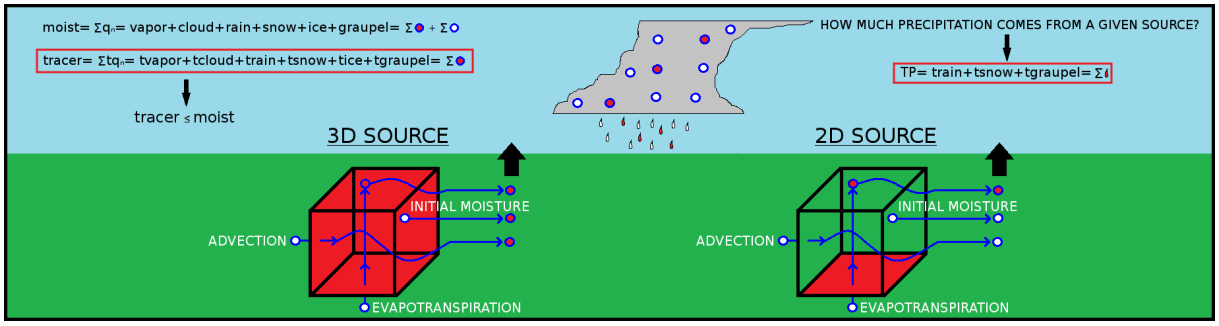

Figure 3.5: 3D and 2D moisture sources tagging by WRF-WVT moisture tracer method (adapted with permission of Copernicus Publications from [114]).

in the WRF model version 3.8.1 [116]. This tracer method is based on implementing the total moisture forecast equation with moisture tracers as,

$$\frac{\partial q_n}{\partial t} = -\vec{v}\nabla q_n + v_q \cdot \nabla^2 q_n + \left(\frac{\partial q_n}{\partial t}\right)_{PBL} + \left(\frac{\partial q_n}{\partial t}\right)_{microphysics} + \left(\frac{\partial q_n}{\partial t}\right)_{convection} \tag{3.12}$$

q_n denotes the six different moisture species considered: water vapor, cloud water, rain water, snow, ice, and graupel. The first two terms on the right-hand side of the equation correspond to the effects of advection and molecular diffusion, while the last three terms correspond to trends resulting from parameterized turbulent transport (Planetary Boundary Layer, PBL scheme), microphysics and convection. The last terms consider subgrid effects that affect atmospheric humidity, such as phase changes and precipitation, or redistribution by convection and turbulent diffusion.

The moisture tagging technique involves the creation of new variables that track the different moisture species, allowing for a more accurate representation of the behavior of water vapor, cloud water, rain water, snow, ice, and graupel. Although the prognostic equations for total moisture and WVTs have the same form, the tagged moisture does not evolve independently of total moisture. The WVTs method is therefore classified as an "online" Eulerian approach, as the prognostic equations for tracer moisture must be solved together with the governing equations of the model, including the turbulence (PBL) scheme, microphysics, and convection. In contrast, advection and diffusion routines can be called for tracers independently of total moisture. It is important to use a positive definite, mass-conserving advection numerical scheme to minimize numerical errors in WVTs calculations. This method can track 2D and 3D moisture sources, as shown in Figure 3.5. Two-dimensional sources are related to surface evapotranspiration fluxes, while three-dimensional sources are related to the whole atmosphere located over the interest region or just a portion of it.

In this method, simulations run forward in time, and consists of calculating the proportional impact of the different sources of humidity by being able to evaluate different precipitation parameters, such as total precipitable water, global precipitation, rain, snow or graupel. Let it be $\overline{P}$ the average total precipitation, the relative contribution of each source S can be expressed as:

$$RC_{TP_S} = 100 \cdot \frac{\overline{TP}_S}{\overline{P}} \tag{3.13}$$

where $\overline{TP}_S$ indicates the mean total precipitation from source S.

3.3.2 FLEXPART-WRF

FLEXPART-WRF v3.1 Lagrangian model, developed from the FLEXPART v9.2, is able to handle different map projections used by WRF, such as Lambert conformal, stereographic, and Mercator. This model is based on various WRF variables, but the key meteorological fields used to compute the advection of air through resolved winds consist of 3D horizontal and vertical wind fields, 2D latitude and longitude fields, and a map factor field to correct the displacement of the trajectories. This model allows to select different parameterizations [115]. The convective parameterization scheme used in FLEXPART is based on the work of Emanuel and Zivkovié-Rothman (1999) [117]. This approach relies on the grid-scale temperature and humidity fields to parameterize convection and calculates a displacement matrix to provide the necessary mass flux information for particle redistribution. Turbulence can be treated using different options. The option recommended by the authors is the one also implemented in FLEXPART, which allows for the use of the Hanna scheme [118] as the PBL turbulence parameterization. Another option is to employ the turbulent kinetic energy (TKE) from the fields provided by WRF. But also, turbulence can be entirely deactivated, causing FLEXPART to function as a non-dispersive Lagrangian trajectory model. In correlation with turbulence, there is a vertical mixing parameter that can assume Gaussian vertical mixing as long as turbulence is considered. Selection of various treatments for specific PBL and surface parameters, such as PBL height, surface sensible heat flux and friction velocity, can also be performed. These values can be taken directly from the WRF, or diagnosed by FLEXPART.

In terms of trajectory processing, the particles can be released at specific locations or, given a model domain, to fill the whole domain with a user-selected number of particles. These particles are then distributed throughout the model domain based on air density, assigning each particle the same mass, resulting in an accurately total atmospheric mass. Once initialized, the particles move freely within the atmosphere. At each time interval, an ASCII output file is produced containing 13 variables of interest. The initial variable represents the unique identification number for the particle, and the following four variables denote the location of the particle (longitude, latitude, and altitude) and the simulation's time at which the particle was released. The remaining variables include the topography, potential vorticity, specific humidity mass, air density, planetary boundary layer height, tropopause height, temperature at that location, and mass of the particle.

Initially, once the simulation finishes, it is necessary to choose the trajectories of the particles that have actually participated in the occurrence of the event. This process entails the selection of a specific threshold value of dq, which is able to identify a rainfall situation at the precise position and time where the event occurred. Thus, the subset of particles exceeding this threshold will be used for further analysis. Knowing the position of a particle and the value of the associated humidity, we can calculate the $E-P$ field as described in Eq. 3.8 for the region of interest. In this methodology, the relative contribution of each source is defined based on the

evaporation ratios as,

$$RC = 100 \cdot \frac{E_S}{E_T} \tag{3.14}$$

where E_S is the total water vapor gained over the source S, and E_T is the total evaporation estimated for the total domain area. Sodemann et al. [111] also proposes to retain only moisture uptakes from particles below 1.5 times the PBL height (BLH), since water vapor uptakes in the free atmosphere cannot be due to a surface flux, but to deficiencies in the methodology. This effort to minimize the errors of the method results in the reformulation of Eq. 3.14 as,

$$RC_{BLH} = 100 \cdot \frac{E_S|_{BLH}}{E_T|_{BLH}} \tag{3.15}$$

where $E_S|_{BLH}$ and $E_T|_{BLH}$ are calculated in the same way as E_S and E_T, but just for air parcels within the boundary layer.

3.3.3 U-Track-atmospheric-moisture model

U-Track is a model that tracks moisture based on Lagrangian trajectories, developed by [108]. The model utilizes large quantities of moisture simulated particles that are released randomly at various heights and locations within cells over the interest region. The introduction of these particles is accomplished through the process of evaporation, which subsequently becomes integrated into the atmosphere. The movement of these particles is then tracked using wind speed and direction reanalysis data. U-Track was developed through a comprehensive sensitivity analysis that assessed the impact of various assumptions and uncertainties on the accuracy of moisture tracking simulations, as well as hydrologically relevant statistics [108]. In each time step, the moisture budget is assessed for the parcel. If there is no precipitation at the parcel's location, all the evaporated moisture remains within the parcel. However, if precipitation occurs at the parcel's location, a portion of the moisture that is still present in the parcel (which is represented by the precipitation over all the precipitable water of the entire atmospheric column P/PW) is allocated to rain out at that location. This assumption assumes that all the moisture in the atmospheric column has an equal chance of raining out. As a result, the amount of original evaporation remaining in the parcel decreases as moisture is transported downwind.

Although the implementation of this model has not been openly exposed and discussed, the authors have conducted an extensive sensitivity study of the model, which introduced the parameters that the user can vary. 2D and 3D forcing data can be considered to investigate the impact of vertical variability of atmospheric moisture transport on the results of moisture tracking. In the 3D model, the released moisture is distributed through the atmospheric column as a function of its precipitable water content. When 2D data is used for forcing, there is no vertical variability in horizontal transport. Another control parameter is the vertical mixing period. Considerable vertical mixing may occur in the atmosphere due to turbulence, but the rate of this mixing is unknown, so there is no other model with which to compare the results. The authors evaluated the impact of eight different rates of vertical mixing on the sensitivity of downwind evaporation footprint. These eight rates included those that accounted for large-scale vertical flow in the ERA5 reanalysis data (ω), as well as four different randomized

mixing probabilities. These probabilities corresponded to full vertical mixing taking place on average every hour, every 6 hours, every 24 hours, and every 120 hours. Optimal vertical mixing occurred every 24 hours during the simulations. Several other parameters of the simulation can be adjusted, including the amount of tracked particles, the height at which they are released, the degraded vertical atmospheric profile, and the integration time step.

The moisture tracking process can be summarized in three sequential steps: (1) the initial release of moisture from the land surface into atmospheric moisture parcels, (2) the calculation of the parcels' trajectories as they move through the atmosphere, and (3) the allocation of the moisture within the parcels to precipitation events that occur at the location of each respective parcel. The allocated moisture is considered until 99% of the moisture is allocated, or until the moisture has been in the atmosphere for 30 days, whichever comes first. Finally, the procedure determines the downwind precipitation locations of the moisture that evaporated at the starting point, which is known as the downwind precipitation footprint. The relative contribution (RC) for a certain S-source can be defined as,

$$RC = 100 \cdot \frac{P_S}{TP} \tag{3.16}$$

where P_S corresponds to the moisture allocated to the S-source and TP the total precipitable water.

Chapter 4

Evaluation of a Lagrangian Model in the Ría de Arousa

*The results from this chapter have already been published as S. Cloux[1], S. Allen-Perkins[2], H. de Pablo[3], D. Garaboa-Paz[1], P. Montero[2], & V. P. Muñuzuri[1]. "Validation of a Lagrangian model for large-scale macroplastic tracer transport using mussel-peg in NW Spain (Ría de Arousa)". Science of the Total Environment, 822, 153338. 2022.
DOI: https://doi.org/10.1016/j.scitotenv.2022.153338

[1] CRETUS Research Center, Nonlinear Physics Group, Faculty of Physics, University of Santiago de Compostela, Spain.
[2] INTECMAR, Inst.Tecnoloxico para o Control do Medio Marino de Galicia, Vilagarcia de Arousa, Spain.
[3] MARETEC, Instituto Superior Tecnico, Universidade de Lisboa, Portugal.

4.1 Introduction

Marine debris has become a major concern in recent years [19, 20, 21]. Plastic debris are found in rivers, oceans and beaches around the world, resulting from poor management of this type of waste on land. These items present a major problem for the marine environment, as well as for the health of marine wildlife and humans. Plastic items remain in the ocean for years, breaking down into small fragments due to various agents such as wind, salinity and mechanical stress caused by ocean currents and waves [22, 23] (see Figure 4.1). These fragments can be classified into macroplastics, which are larger than 0.5 *cm* in diameter, and microplastics, which are smaller than 0.5 *cm* in diameter. The ingestion of these small bodies into the food chain is an unavoidable fact that has already affected numerous species, not only physically, but also as toxic agents due to the chemicals they may contain [119, 120, 121]. The greatest concern with these particles is their incorporation by a variety of living organisms, from filter-feeding plankton, mollusks, fish, birds, turtles, whales and many others, to humans [24, 25, 26, 27, 122, 121]. Additionally, the accumulation of plastic debris in certain areas, known as ocean *garbage patches* or *hot spots*, can have major economic impacts by damaging fishing and tourism industries. Therefore, understanding how plastics move along the ocean is crucial for understanding the environmental impact of plastic pollution and for developing effective management strategies.

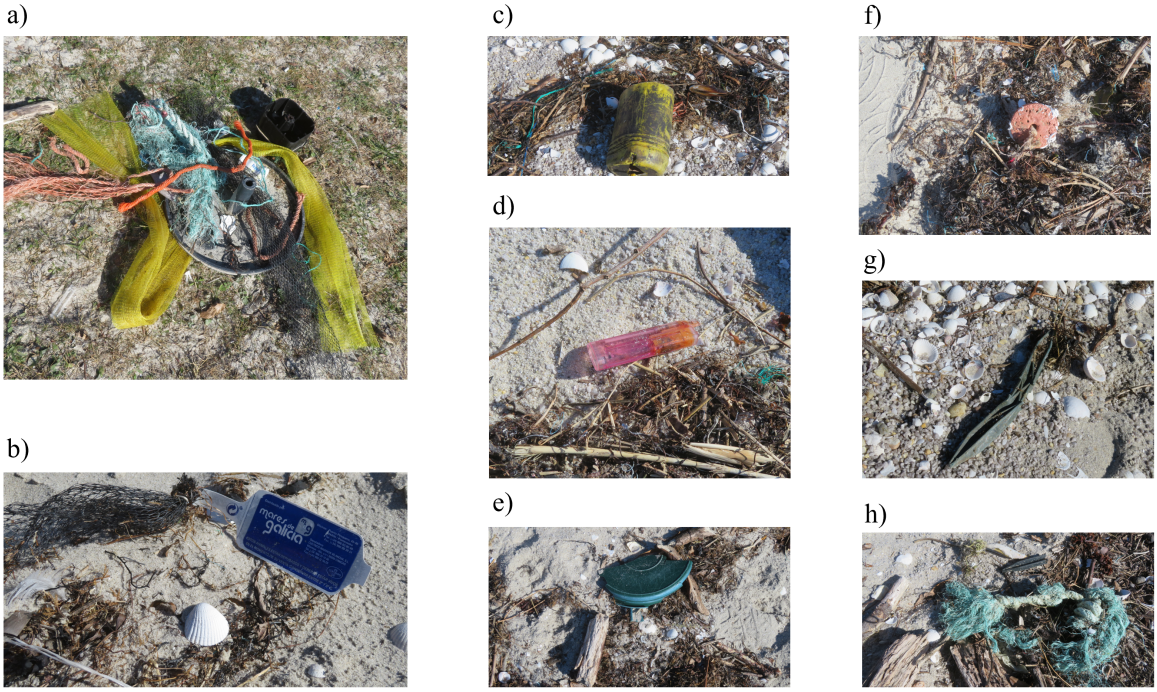

Figure 4.1: Different types of macroplastics on the Barraña beach.

As it was exposed in Chapter 2, the movement of marine plastics through the ocean is not well understood, despite being a major pollution issue. There are a variety of techniques that are used to determine the presence and distribution of plastic in the oceans. Measuring the presence and quantity of microplastics in the open ocean is a challenging task. Due to their small size, microplastics can range from values below 0.5 *cm* to the nanoscale, making them difficult to classify and quantify [123, 19, 124]. The most prevalent method for collecting microplastics is by using manta trawl nets to capture these tiny particles from the surface waters. Afterwards, in laboratory setting, the quantity, size, type and polymer can be analyzed by various optical (microscopy) and chemical (e.g. spectroscopy) techniques [125]. Other approaches include monitoring plastic in the stomachs of marine animals, for example, for pelagic species such as sea birds and marine mammals. This can be useful to detect the ingestion of microplastics [126].

Remote sensing technologies, such as satellite imagery and aerial photography, are also commonly used to detect plastic pollution in the oceans. For example, synthetic aperture radar (SAR) based on satellites can detect floating plastic debris on the ocean surface, while thermal infrared (TIR) sensors can detect plastic particles below the surface [127, 128]. In addition, passive or active drifters have been used in some studies to track the movement of plastics in ocean currents, providing a realistic trajectory that the plastic would follow and a proper understanding of circulation patterns and areas of accumulation [45]. However, the best approach for studying the impact of plastics is the use of Lagrangian transport tools, which are commonly used in marine litter transport studies. These models can track the movement and origin of plastic in the ocean, as well as its fate, by utilizing velocity fields to provide the

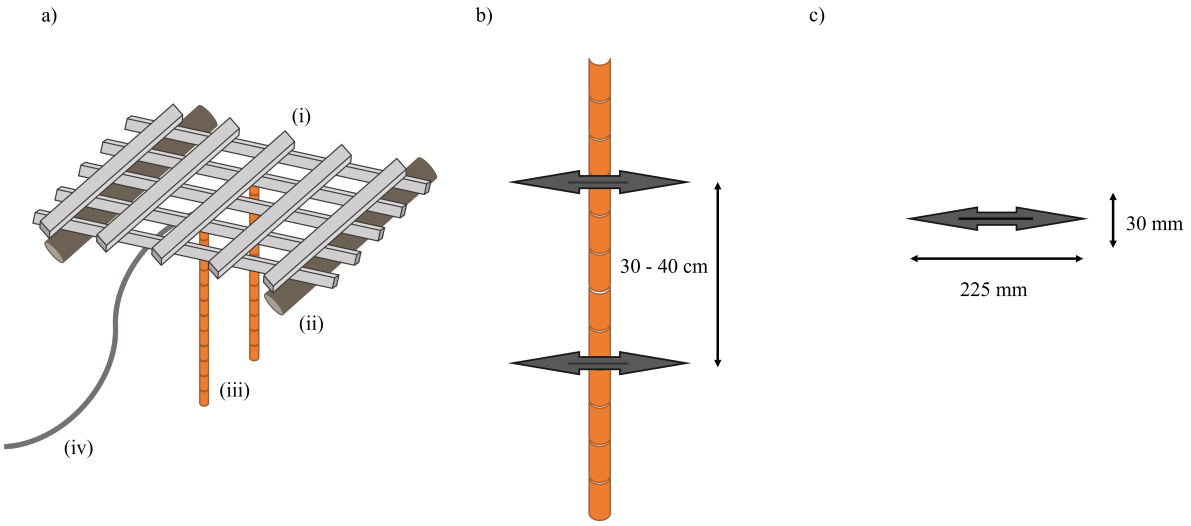

Figure 4.2: Schematic of a mussel cultivation raft. (a) Shows the main components of the pan: (i) wooden structure, (ii) floats, (iii) cultivation ropes and (iv) anchoring. (b) Shows the arrangement of the mussel-peg on the rope and (c) the dimensions of the mussel-peg.

position of plastics at each time step [129, 66, 130, 68].

In this study, we validate the MOHID-Lagrangian model using data collected from beaches. To do so, we focus on mussel-pegs, which are plastic items used in the cultivation of mussels in the Galician estuaries (see Figure 4.3). Mussel cultivation is carried out using mussel rafts, which are floating nurseries consisting of a wooden structure to which mussel ropes are attached. These structures are anchored to the seabed with a chain (see Figure 4.2). To attach the mussel larvae to the ropes, a fine, biodegradable rayon net is used, allowing the mussels to grow and become heavier over time. As the mussels grow, the load is distributed among more ropes. Wooden or plastic sticks known as mussel-pegs are placed every 30-40 *cm* on mussel ropes to prevent mussel clusters from breaking off and provide a better grip for the mussels, as shown in Figure 4.3a). These plastic sticks are 225 *mm* long and 30 *mm* wide, as shown in Figure 4.3b). During the process of threading, unfolding, and extracting the mussels, the plastic sticks can fall into the sea and become marine debris, and they can also break during the extraction process. These sticks are frequently found on the Galician coasts and can serve as marine indicators. This study is conducted in the Ría de Arousa, a part of the Rías Baixas that is particularly active in mussel production. Given the proximity between the release point and the shore, it is assumed that the properties of the mussel-pegs, including their density, do not change during their journey. Furthermore, since they are transported at the upper sea level, they can be considered ideal Lagrangian tracers.

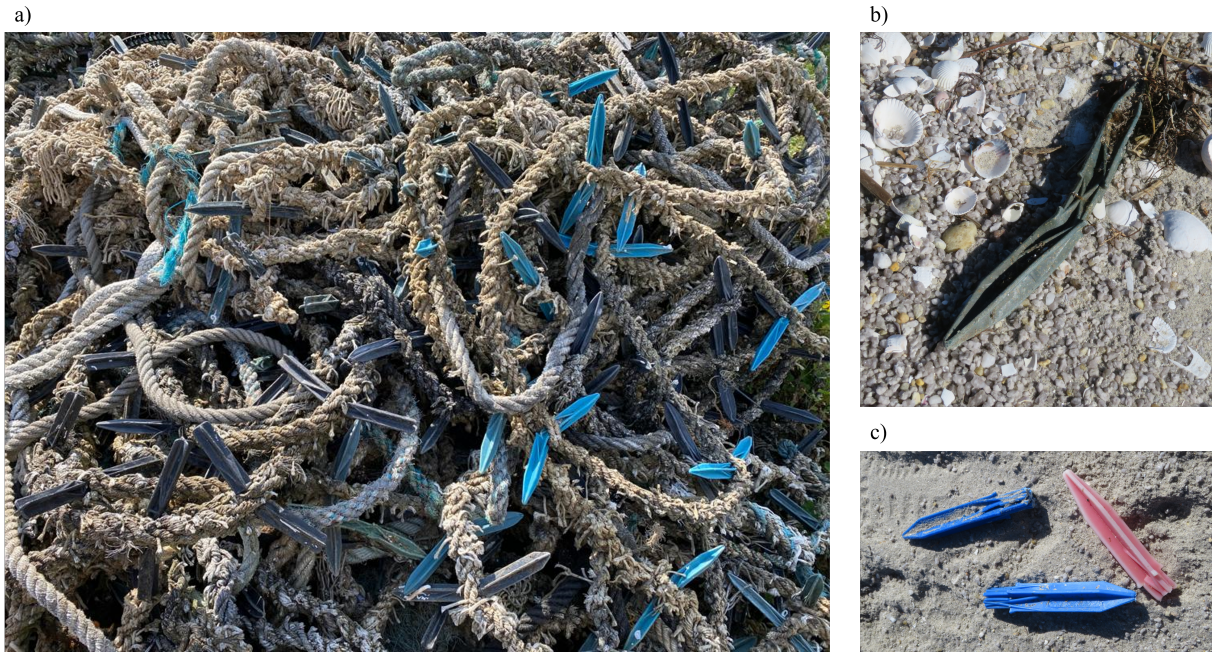

Figure 4.3: Different mussel-pegs situations. (a) Capture of mussel-pegs on the cultivation rafts, (b) single mussel-peg and, (c) broken mussel-pegs on the Barraña land coast.

4.2 Study Area

The coastline of Galicia spanning 1195 *km* along the northwest coast of the Iberian Peninsula according to the Instituto Nacional de Estadistica [131], is known for its rugged cliffs, long sandy beaches, and charming fishing villages. The diverse topography, soil, climate, and biogeography were instrumental in shaping the landscapes of Galicia. Additionally, the role of the sea and its erosive and accumulative action on the coastline must be considered. Marine action can lead to erosion in some areas and accumulation in others, resulting in an erosion/accumulation balance. This balance is evident in the high degree of mobility of rocky coastlines, as well as the abundance of beach and dune systems. The Galician coast features various rock types, including granite, slate, gneiss, and basic rocks, each with unique characteristics that affect their behavior in the face of marine processes. These rocks have varying degrees of resistance to erosive agents and waves, specifically along the coast.

The Galician coast is characterized by moderate to high energy waves, with 80% of waves being between 1 and 2.5 meters high. The highest waves, between 3 and 5 meters, occur during the fall and winter months, primarily coming from the west and northwest during storms. Although the percentage of waves with heights greater than 4 and 5 meters is small, these intense waves can have significant effects on coastal dynamics. Over time, various mechanical erosional processes have shaped the Galician coast. Beaches, which are depositional landforms composed of coastal sediments, vary greatly in their diversity. In Galicia, 11 different types of beaches have been classified based on their exposure to the tide, surface area in relation to it, amount of sand and rock, presence and influence of river mouths, and human activity. Figure 4.5 a) shows an aerial view of Barraña beach, which is a long sandy extension, while

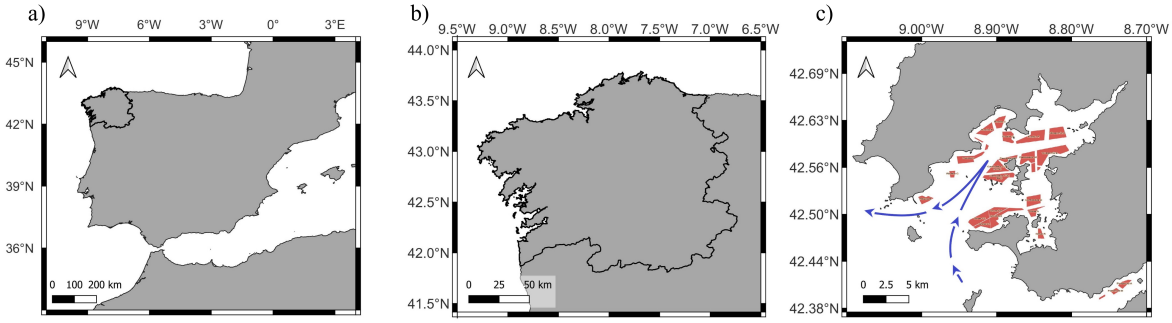

Figure 4.4: (a) Galician coast as represented by a solid black line on the left map, (b) Galician Rías division and (c) the spatial distribution of mussel rafts, represented by red polygons along the Ría de Arousa and the surface circulation (blue line).

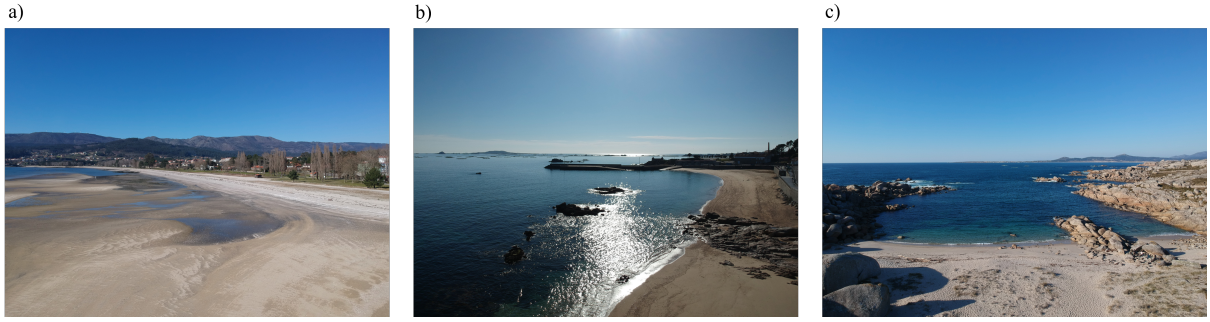

Figure 4.5: Three examples of different type of beaches along the Ría de Arousa. (a) Barraña beach (b) Castiñeiras beach and (c) Cabo Couso beach.

Figure 4.5c) shows a rocky beach at Cabo Couso. Coastal areas may also have anthropogenic structures, as shown in Figure 4.5b). Ideal beaches for simulation data comparison would have a favorable orientation for the tide, dimensions that are on the scale of the simulation resolution, and no natural or anthropogenic obstacles that interfere with the movement or retention of floating particles. It is worth mentioning that Galicia is known for frequent storms and gales, which play a fundamental role in many aspects, including the transport of marine debris along its coasts. These meteorological events are characterized by strong winds and heavy rainfall.

The Rías, which are indentations in the coast caused by flooding river valleys, are a unique feature of the Galician coast, offering not only beautiful scenery but also a rich ecosystem and diverse range of activities such as fishing, seafood, and aquaculture. Geographically, the Rías are traditionally divided into Rías Altas and Rías Baixas based on their position in relation to Finisterre, the westernmost cape of Galicia. The Ría de Arousa (shown in Figure 4.4) is a large estuary located on the northwest coast of the Iberian Peninsula, part of the Rías Baixas region. It covers an area of approximately 230 km^2 and can be divided into two zones: an inner zone, which is more exposed to fluvial processes and features shallower, isolated habitats, and an outer zone, which has greater interaction with oceanic processes and features deeper, exposed habitats. The average sea level oscillation is around 2.5 m, making it a meso-tidal estuary. The surface circulation in the Ría is shown in Figure 4.4 c) by the blue line. As can be seen, a

current enters from the south and flows into the innermost part of the ria. This circulation then leaves again to the outside through the northwestern part of the estuary. The beaches of the Ría de Arousa are numerous and varied in type, mainly due to the intense fracturing of the rock and tertiary erosion of granites. However, most of the beaches selected for data collection are of the platform type, which have a significant percentage of intertidal rocky area exposed during low tide and that affects particle retention on these beaches.

4.3 Methodology

4.3.1 Beaching Collection Data

To gather a comprehensive range of ocean-meteorological situations along the coast, several locations were selected for the beaching collections. The sampling plan was designed to identify the main areas of litter accumulation along the coastline of Ría and Illa de Arousa. The selected beaches met the following criteria: (1) they were made up of sand or gravel and exposed to the open sea, (2) were accessible to samplers throughout the year, and conducive to the removal of marine litter, and (3) were not subject to other litter removal activities. A weekly frequency was established, and data collection was always conducted one hour after high tide to avoid sampling being affected by the rising tide. Furthermore, the collected data was backed up with a photograph. During each collection, the number of mussel pegs found, both whole and broken, was counted and removed from the beaches.

The sampling of all selected beaches was conducted in two campaigns: A) Illa de Arousa, which was carried out between October 2018 and April 2019, and B) Ría de Arousa, which was conducted between October 2020 and March 2021. The first sampling on Illa de Arousa was performed through citizen action, specifically by students from the Illa de Arousa Secondary Education Institute. To ensure the quality and accuracy of the samplings, filters were established to consider the collected data reliable. First, it was verified that each sampling had both a record and a photo. Then, the date and time of the record had to match the date and time of the photo. Additionally, it was confirmed that the number of sticks recorded matched the number of sticks delivered by the student. Out of the expected 986 samples, 767 (77.78%) met the established filters. A total of 9,205 toothpicks were collected from them, resulting in the removal of 141,245 kg of plastic from the sea (estimated based on an approximate weight of 26 g per whole toothpick). The number of samples taken on each beach is not evenly distributed, with some beaches having less than 25% of samples taken and others having more than 90% of samples taken. To enable solid comparisons between different beaches, it was decided to analyze only those beaches with a sampling rate above 66.66% for the 27-week duration of the campaign. Experienced technicians in coastal sampling regularly performed sampling work on the points located on the coast of this estuary, ensuring the integrity and accuracy of the data in this collection did not require verification.

4.3.2 Lagrangian Simulation

This study investigates the accumulation of marine litter along the Ría de Arousa coast, considering three different scenarios presented in Table 4.1. All three scenarios cover the same spatial domain, the Ría de Arousa (see Figure 4.6), but differ in the simulated time period. The

Simulation	Initial Date	End Date	Resolution	Beaching Factor	Measures
(1)	October 2018	April 2020	3h	80%	Percentiles
(2)	October 2018	April 2019	1h	20% 50% 80%	RA
(3)	October 2020	March 2021	1h	20% 50% 80%	RA

Table 4.1: Setup and measurements obtained from the simulations for the three scenarios considered in this study. (1) Considers a period of 1.5 years with a beaching factor of 80% to calculate the percentiles throughout the Ría de Arousa. (2) Considers a 6 month period to calculate the relative accumulation in the Illa de Arousa using the 20%, 50%, and 80% beaching factors. (3) Considers a 5 month period to estimate the relative accumulation in the Ria de Arousa using the 20%, 50%, and 80% beaching factors.

first scenario focuses on the overall accumulation over a 1.5-year period (October 1, 2018 to April 1, 2020). The second scenario is related to the Illa de Arousa collection from October 1, 2018 to May 1, 2019, while the third scenario covers the period from October 1, 2020 to April 1, 2021 and is related to the second beach collection along the north of the Ría de Arousa shore. These time periods were selected based on beach monitoring data. To estimate the accumulation ratios along the coastal line, the Ría de Arousa coastal line is divided into 427 segments, each measuring approximately 1000 m in length by 100 m in width. These dimensions are chosen to ensure the best reproduction of the coastline and accurate definition along the coast.

In the first simulation, percentiles (P25, P50, P75, P95) are calculated for each segment not only to distinguish between high and low accumulation zones but also to show the spatial distribution of marine litter within the Ría de Arousa. Certain days in this simulation are also selected to show the influence of different wind orientations. In the case of the Illa de Arousa, it is observed that certain beaches are situated between two distinct sections of coastline. Furthermore, several of the sampled beaches are found to be located within the same coastal segment. Consequently, both the beaches and their respective samplings are redefined and assigned to new segments (S1, S2, S3, S5, S6, S7, S8, and S9) as shown in Figure 4.6. In the third scenario, nine beaches are selected. A total of 18 study areas are used for the comparison of simulated and experimentally collected data. Note that, since the extent of the buffer may be larger than the extent of the shore where collections take place, the estimated accumulation may be greater than the actual accumulation. To correct this, an area factor is used. This factor is calculated as the ratio of the monitored beach area to the computational buffer area.

The simulation covers an area ranging from 9.15°W to 8.15°W and from 42.2°N to 42.6°N with a spatial resolution of 200 m and a temporal resolution of 1 h. Only for the first simulation, a 3-hour resolution is assumed. Lagrangian particles are released from all emission points every hour throughout the simulation period. Emission points are determined based on the mussel raft distribution and are located in the same place as shown in Figure 4.4. To account for mussel-pegs coming from other estuaries with shellfish activity, two additional emission points are included at the northern and southern edges of the simulation domain using a polygon

type emission. For each polygon, emission points are placed every 140 m along the polygon geometry. In the case of external sources, a regular emission is defined with an area of $9km^2$. Considering the uncertainty surrounding the exact timing of mussel-pegs release into the sea, a continuous emission approach is set. Any alternative emission strategy, such as those restricted to 4 or 6 hours per day, could introduce inaccuracies in the results. In case we would consider a 4-hour emission coincided with the tidal ebb, the particles in the estuary would be completely depleted, further highlighting the need for a continuous emission approach to ensure statistically significant results. To simulate three possible retention scenarios (high, medium, and low), simulations are run with different probabilities of stranding. Trends are calculated using relative accumulation ($\%\ RA$) for each beach, and for each study area, the mean accumulation is obtained every 4 h to smooth out any atypical effects due to specific weather conditions. For each time period considered, the total accumulation (A_{TOT}) and the maximum accumulation among all study areas (A_{MAX}) are obtained. The relative percentage for each region is determined by dividing the accumulation of that area by the maximum accumulation.

$$\%RA = \frac{A_{TOT}}{A_{MAX}} \tag{4.1}$$

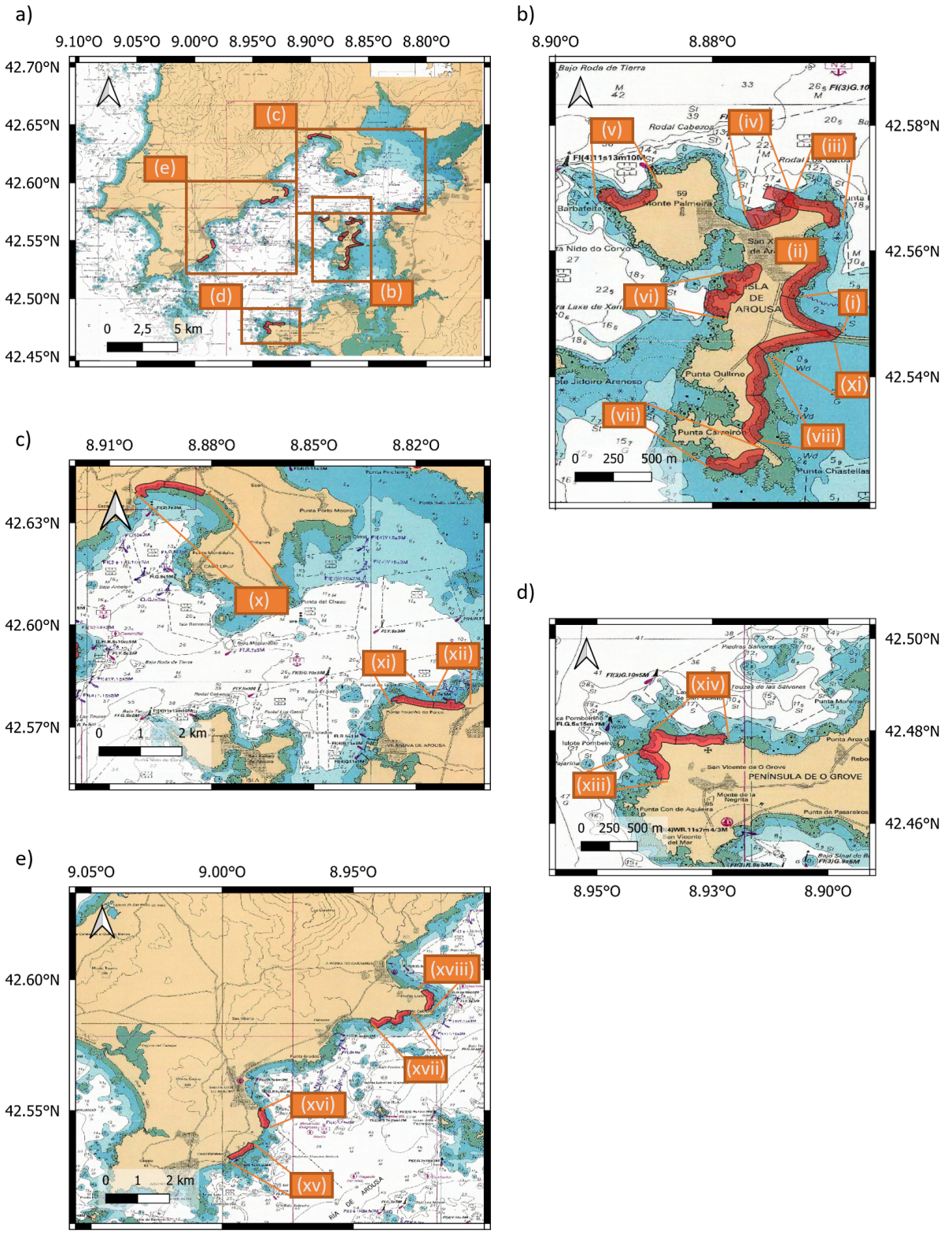

Figure 4.6: Navigation cards for the Ria de Arousa (a). The shaded areas corresponds to: (b.i) S1, (b.ii) S2, (b.iii) S3, (b.iv) S4, (b.v) S5, (b.vi)S6, (b.vii) S7, (b.viii) S8, (b.vix) S9, (b.x) Barraña, (b.xi) Porco, (b.xii) Aduana, (b.xiii) Castiñeiras, (b.xiv) Carreiro, (b.xv) Mosqueiros, (b.xvi) Fontán, (b.xvii) Illa, (b.xviii) Niñeiriños.

4.4 Results

4.4.1 Spatial Distribution of Accumulation along the Coastal Line

In the longest simulation, which covers one and a half years, the distribution of floating particles along the 429 segments of the coastline is estimated and presented in Figure 4.7a). The total accumulation is calculated by analyzing the temporal distribution of debris accumulation for each coastal segment. To establish thresholds for very low, low, medium, high, and very high accumulations, percentiles (P25, P50, P75, and P95) were used. The outermost regions have the lowest accumulation rates due to being most exposed to oceanic action. Conversely, higher accumulation rates were found towards the inner part of the estuary. As the currents enter from the south and drain towards the north, the main accumulation zones are observed in segments oriented towards the south and southeast. This is depicted in Figure 4.7, which shows two distinct accumulation zones in the northeast of the estuary and northwest of the central island (A Illa). The entire intermediate inner region displayed high accumulation values above P50. In this simulation, the influence of wind on the accumulation of debris is examined. Figure 4.7b) represents an easterly wind on the 30th January 2019, Figure 4.7c) illustrates the impact of a southeasterly wind on the 7th May 2019, and Figure 4.7d) depicts the effect of a northwesterly wind on the 10th January 2019. These three scenarios demonstrate the significant influence of wind on the accumulation of debris. An easterly wind results in higher accumulation on coastlines with the same orientation. A northwesterly wind, on the other hand, favors the drainage of the estuary and leads to lower accumulation in the innermost zone and higher accumulation in the outermost regions. Lastly, a southwesterly wind favors high accumulation on beaches with the same orientation and located in the interior region.

4.4.2 Comparison between Monitoring Data and Simulated Data

When comparing monitoring data to simulated data, the results are grouped by segments. The simulation results take into account the average accumulation every 4 hours for the considered buffers, and then estimate the temporal accumulation per buffer. The results are presented from two perspectives: (1) for the entire simulation period and (2) separated by months.

Illa de Arousa

Figure 4.8 shows the results for nine different coastal line segments for the first time period of collection data in beaches, from October 1, 2018 to May 1, 2019. It is important to note that the comparison is based on trends, not raw data. Both data series are normalized to the maximum value found in each study region. The stranding factor is being varied to determine which one results in the best accumulation. In most cases, the 20% stranding factor provides the best fit. The Illa de Arousa area is mostly rocky, so it is unlikely that mussel-pegs reach sandy areas. However, the computational model reproduces the general trend of accumulation in the studied areas, with the exception of segments S4 and S9. The case of S4, in particular, illustrates the negative effects of inadequate reproduction of the coastline. This segment corresponds to the harbor of Illa de Arousa.

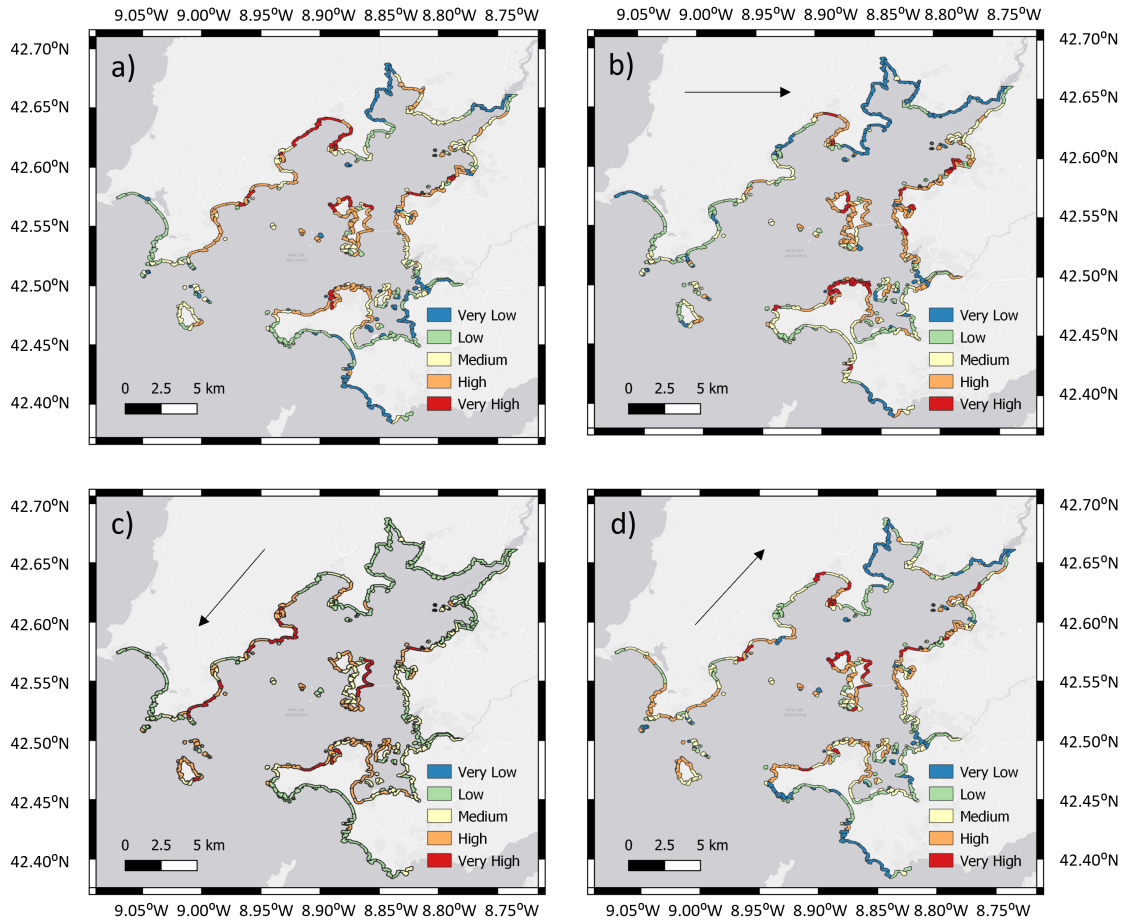

Figure 4.7: Accumulation ratios in the Ría de Arousa along the 427 segments for a period of one and a half years (from 2018 October 1 to 2020 April 1) obtained from the computational model. The classification 'very low' corresponds to accumulation values below P25; 'low', between P25 and P50; 'medium', between P50 and P75; 'high', between P75 and P95; and 'very high', above P95. The black arrow shows the wind direction. a) Considers the whole time period, b) corresponds to an easterly wind, c) corresponds to a southeasterly wind action, and d) corresponds to a northwesterly wind action.

This zone is strongly surrounded by rafts, so it is very likely to record high values of accumulations in the monitoring. Here the presence of dikes and pontoons affects retention in the area, resulting in high retention of mussel-pegs, as evidenced by monitoring data. But the reproduction of the shoreline is too rough in this region. Its shape is not conducive to particle arrival and retention. Thus, few simulated particles can be stranded on this beach. S9 is an example of how the presence of anthropogenic constructions acts as artificial drivers or barriers. Despite being an area well exposed to tidal action and highly influenced by wind, the bridge connecting the island reduces the effect of this phenomena, causing fewer particles to reach this study area (as shown in monitoring data). However, this blocking does not appear computationally, thereby leading to greater accumulation results. Finally, the relative contribution of the two external emission sources is calculated. Only 3% of the particles that reach the coast come from external sources. This is expected as these sources primarily affect the outermost regions, which are most affected by oceanic action, and thus only a small

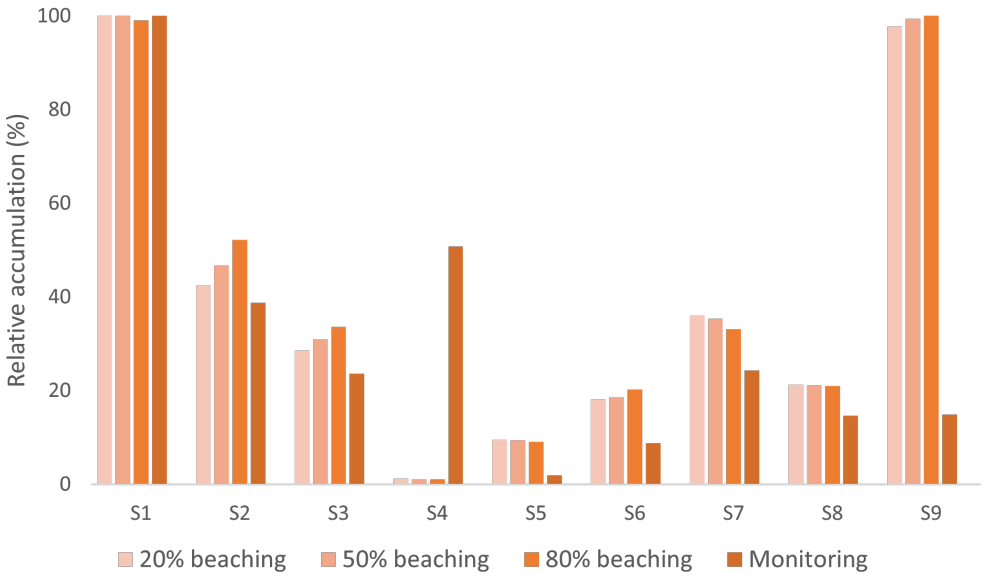

Figure 4.8: Comparison of trends in the accumulation of mussel-pegs for different shore segments in the Illa de Arousa from October 2018 to April 2019. Simulations have been performed for different beaching values: 20% (light orange), 50% (medium orange) and 80% (dark orange). The monitoring data are shown in brown.

fraction of particles emitted by these sources are stranded on the coast. These outcomes are reasonable for two primary reasons: Firstly, the emission boxes have been located near the simulation limits outside the estuary, which means that a part of the emissions will exit the simulation domain. Secondly, the external circulation does not enable the particles to penetrate and reach the innermost locations of the estuary. Nonetheless, the pattern of accumulation differs significantly for both sources, as shown 4.9. The simulated emissions in the upper area primarily impact the northern outer region of the Ría. In contrast, the simulated emissions in the lower section of the estuary are positioned at more inland locations, which is coherent with the circulation of the estuary.

Figure 4.10 illustrates the monthly comparison between simulated and monitoring data. The utilization of higher temporal resolution reveals a greater number of discrepancies when compared to previous representations. It is essential to identify the factors that may contribute to the disparity between simulated and monitoring results. The primary and most significant factor is the relationship between the study area's orientation and intertidal motion. As the beach becomes more oriented toward the tidal movement, the number of computationally accumulated particles increases. However, the bathymetry of the region can result in accumulation values that are not similar to the computational estimation. The presence of rocky regions near the coast may act as a low retention factor, resulting in monitoring data on the beach that is lower than expected. In the case of Illa, this phenomenon occurs in regions S2, S3, S5, and S6, which are heavily affected by intertidal motion. This implies that as the number of particles passing through an intermediate zone increases, the accumulation recorded in that zone also increases, assuming a stranding rate of 80%. This effect is particularly pronounced in regions S7 and S9 due to their southern orientation, which results in a higher number of particles being received during rising tides. Figure 4.6 illustrates that all areas of the

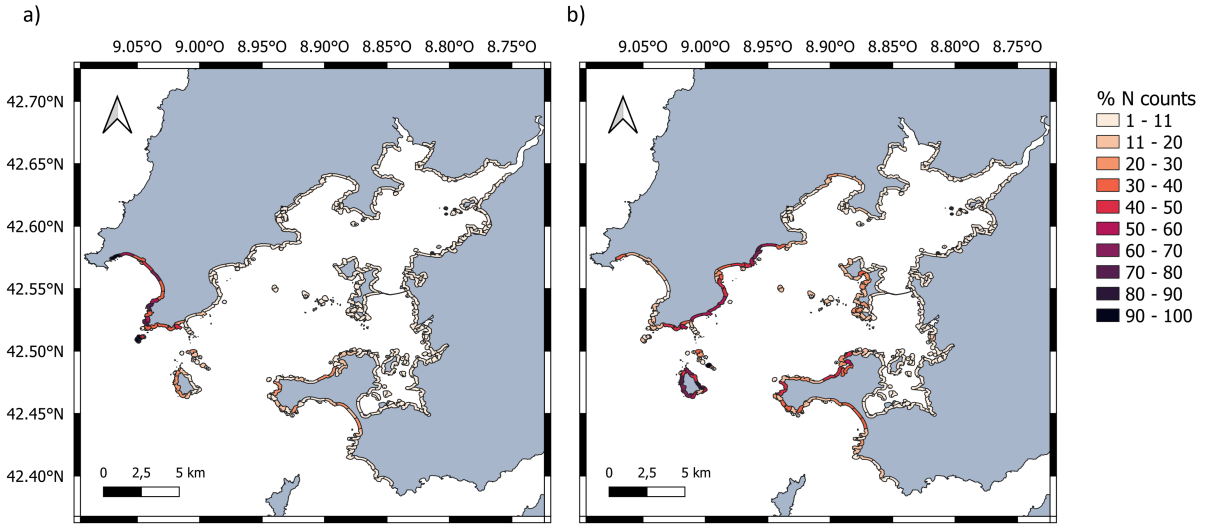

Figure 4.9: External source's contribution in the Ría de Arousa. (a) Present the relative contribution for the upper emitter and (b) for the lower emitter.

island possess rocky intertidal zones that have an impact on monitoring data at the beaches, as this value is usually lower than that estimated by the model. In cases where the collection value is higher, it may be due to a specific synoptic situation on the day of collection. As the westernmost area of the Iberian Peninsula, Galicia, and particularly the west coast, often experiences various atmospheric phenomena originating from the North Atlantic. Specifically, in October 2018, two hurricanes reached the coast of Galicia, leading to an anomalous synoptic situation. The month of November 2018 was characterized by the occurrence of a severe storm, resulting in atypical wind conditions. Finally, the month of December 2018 was characterized by high-altitude squalls during the first 20 days of the month. All of these synoptic situations can affect the monitoring data. The case of S4, as previously mentioned, presents a representation problem, as the orientation of the buffer representation means that few particles reach this area. Finally, regions S1 and S8 are the best estimated regions throughout the entire period. With regards to the beaching parameterization, no differences are observed in this particular study.

Ria de Arousa

In the Ría de Arousa, we calculate the same trends as in the previous subsection. We find similar results in the trend of the simulated data compared to the monitoring data (see Figure 4.11) for the accumulation over the entire simulation period. The Barraña beach has the maximum accumulation value in both the simulation and beach collections, while the minimum value is estimated for Nineiriños using both methodologies. Monitored data for this beach show a concentration of 0.31% with respect to the total litter collected on all beaches sampled. There is a clear discrepancy between simulation and observation for Carreiro beach. This beach is located in a highly exposed area of the estuary to oceanic action, and its position makes it possible that the accumulations observed on the beach come from points outside the

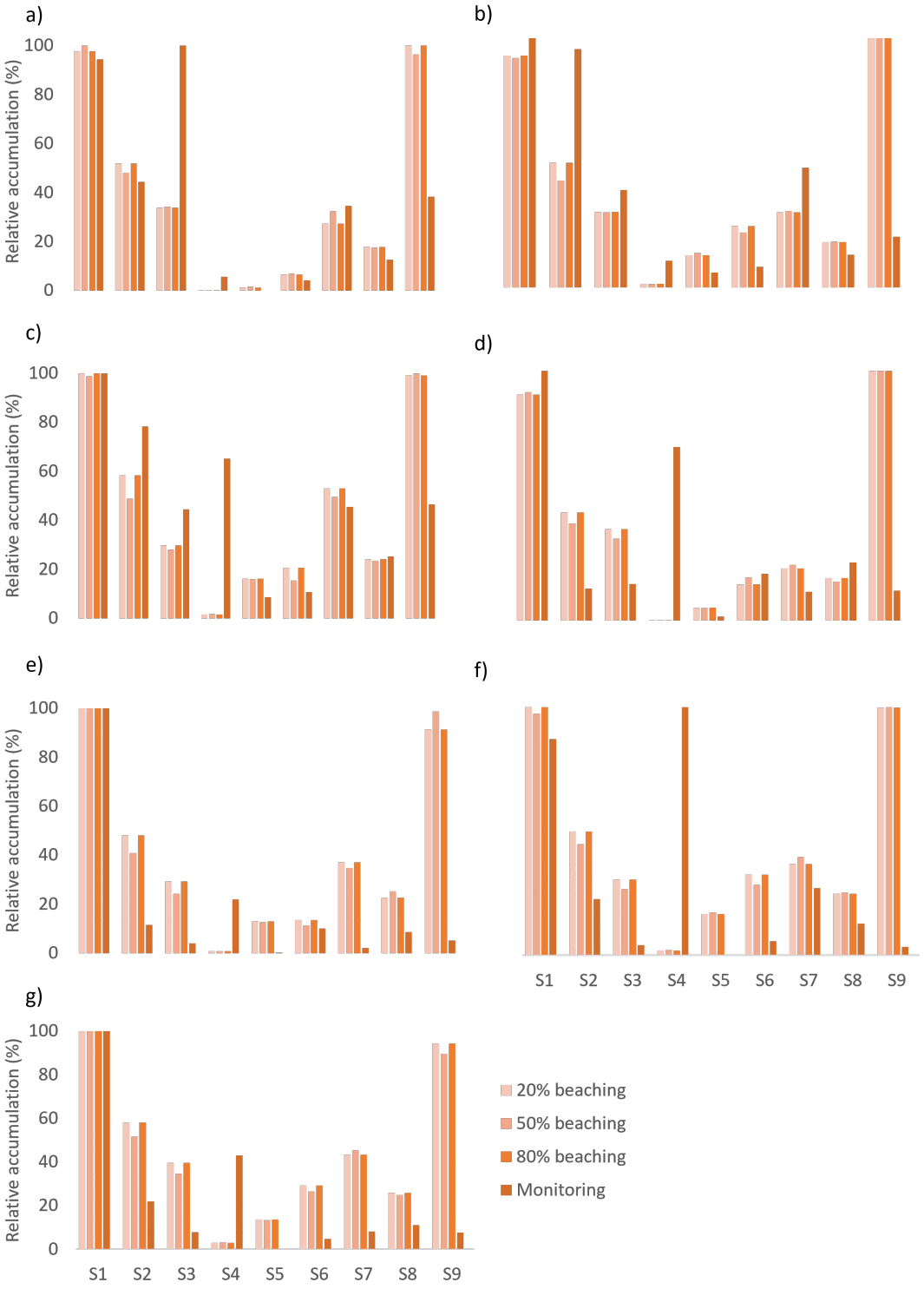

Figure 4.10: Comparison of trends per month in the accumulation of mussel-pegs for different shore segments in the Illa de Arousa from October 2018 to April 2019. Simulations have been performed for different beaching values: 20% (light orange), 50% (medium orange) and 80% (dark orange). The monitoring data are shown in brown.

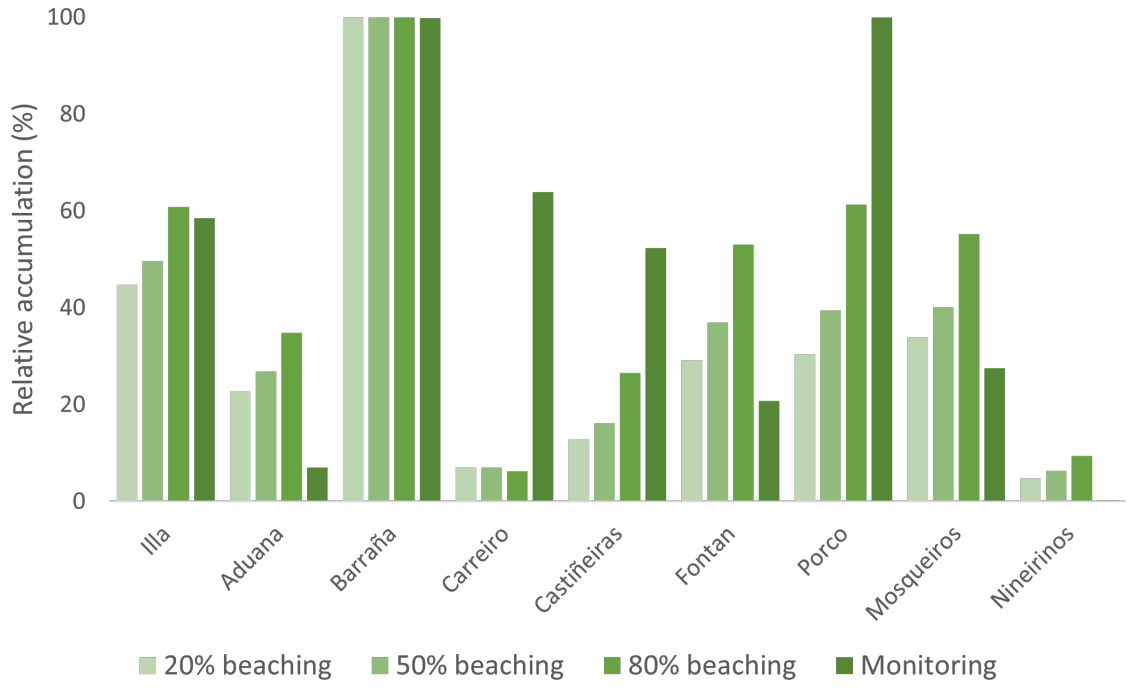

Figure 4.11: Comparison of trends in the accumulation of mussel-pegs for different beaches along the Ria de Arousa from October 2020 to March 2021. Simulations have been performed for different beaching values: 20% (light green), 50% (medium green) and 80% (dark green). The monitoring data are shown in darkest green.

estuary, particularly from the mussel cultivation areas of Ría de Pontevedra. Despite efforts to overcome this fact with two external emission sources, the percentage of particles reaching the coast from external sources, as in the previous scenario, is around 3%. The behavior of beaching for the last studied regions is similar to the previous case. The highest values of relative accumulation occur for a beaching value of 80%, while the lowest values are recorded for a beaching of 20%.

Figure 4.12 shows the accumulation values by month. The relationship between beach orientation and intertidal movement is evident in cases such as Illa and Fontán beaches. The model estimates higher values than those found on the beaches due to intertidal movement hindering mussel-peg accumulation. The ocean's influence must also be considered, with the model showing lower accumulation values in areas with more oceanic circulation, as seen in the Carreiro and Castiñeiras regions. However, at Carreiro beach, high accumulation values are recorded in the beach collections. This is because, although it is located in one of the furthest areas of the Ria, its orientation does not allow for the estuary's dynamics to effectively clean the area. Additionally, being a rocky area, the dynamics in this region are slower in reality than what the model predicts. In the case of Castiñeiras, its orientation causes the oceanic action to have a greater effect, so lower values are found in both methodologies. Moreover, it may happen that artificial constructions such as seawalls are not included in the coastal management plans, so they are not taken into account in the simulations. However, these types of structures have an impact that reflects in the monitoring data, as in the case of Aduana beach, where a dike prevents the accumulation of more sticks than those recorded in the monitoring. Therefore, the

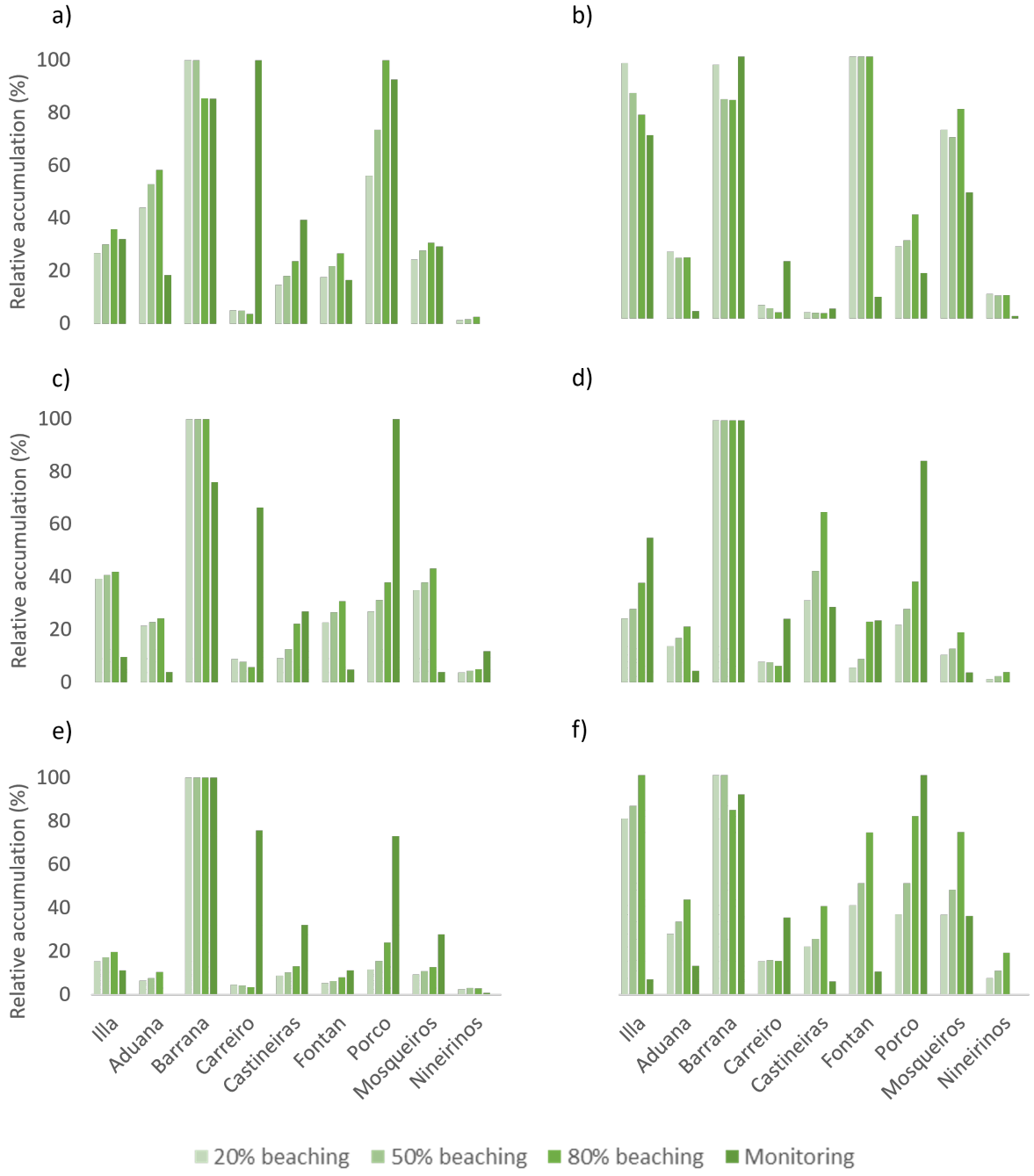

Figure 4.12: Comparison of monthly trends in the accumulation of mussel-pegs for different beaches along the Ria de Arousa from October 2020 to March 2021. Simulations have been performed for different beaching values: 20% (light green), 50% (medium green) and 80% (dark green). The monitoring data are shown in darkest green.

Lagrangian model on this beach always reports higher values than those actually found in the collected ones. Finally, for locations that do not present any of these factors, as is the case of Barraña and Porco, the beach monitoring data is well reproduced computationally. During this study period, the months of January and February are characterized by the occurrence of storms that affect the region. In these months, Galicia suffered four different strong storms. In

our comparison, both months stand out for presenting disparities between the simulated data and the monitoring data. In terms of beaching factors, it can be concluded that there are no significant differences observed in most cases. However, it should be noted that in cases where the circulation favors the appearance of a greater number of particles in a particular study region, the established percentage should be taken into account. This is because a higher percentage can lead to greater disparity between results with different stranding, such as what was observed in the case of Porco beach during the months of October and March.

4.5 Discussion

In this study, we introduce a recently developed Lagrangian technique, the MOHID-Lagrangian model, which has been validated using monitoring data. It should be noted that while the validation of these models must be carried out on a regional scale, they can be applied on a global scale. The validation work is carried out using data collected from seafood activity in Galicia, particularly the Rias Baixas. During mussel collection on the rafts, plastic mussel-pegs are released into the sea. These pegs have the unique feature of remaining on the surface until they reach the coast due to their morphology. Furthermore, since the rafts are located close to the coast, it can be assumed that the path that the mussel pegs follow until they reach the coast is short enough so that phenomena such as biofouling do not affect their movement. The strength of this study lies in the fact that the sources of marine litter are well-known, which allows the use of monitoring data to validate the MOHID-Lagrangian model. However, the precise reproduction of this situation is complex as the actual emission of mussel-pegs is not known, and the residence time and precise origin of the mussel-pegs are undetermined.

The validation process can also be affected by challenges inherent in the sampling process. Ensuring the safety of sampling personnel is always the main priority, resulting in samplings being conducted exclusively during daylight hours and being suspended in situations where safety could be compromised, including adverse weather conditions and COVID-related protocols. As a result, there may be multiple situations that prevent a collection from taking place, interrupting the monitoring time series. Furthermore, collections in the Illa de Arousa region rely on citizen action, involving untrained personnel. Weekly sampling is conducted on different days of the week, depending on the criteria of the sampler, and the recommendation to sample two hours after the tidal peak is not systematically followed. Thus, this wide disparity in collection times complicates the characterization of the meteorological situations represented in the data, potentially affecting the comparability of results. However, beach collection data is highly valuable for determining whether computational models, in this case, the MOHID-Lagrangian, are capable of reproducing observational results.

To assess the accuracy of the model, simulations have been performed in a domain spanning from 9.15°W to 8.15°W and 42.2°N to 42.6°N, with a spatial resolution of 200 m and temporal resolutions of 3 hours and 1 hour. The emission points have been located where mussel ponds were present, and Lagrangian particles have been released hourly throughout the simulation period. To account for external sources, two additional emission points have been placed at the edges of the domain. To estimate contributions along the coastline, it has been divided into 429 segments of 1 km long by 100 m wide. The stranding probability has

been varied to simulate three different retention scenarios, with stranding factors of 80%, 50%, and 20% representing high, medium, and low retention zones, respectively. The relative accumulation trends have been calculated using the %RA for each beach.

During the simulation period of one year and a half, we used a three-hour resolution to analyze the spatial distribution of particles released along the coastline and evaluate the model's responsiveness to known parameters, such as the wind effect. Additionally, we located two emission areas in the lower and upper outer parts of the river to consider contributions from external sources. Based on the results of this examination, we can draw certain conclusions.

- Using the P25, P50, P75, and P95 percentiles, it is possible to identify qualitative differences in the areas of debris accumulation along the coast. Regions that are particularly vulnerable to oceanic activity show the lowest accumulation ratios. The highest densities of marine debris are found along the outer edges of currents within the estuary, and this phenomenon is attributed to the circulation patterns exhibited by these currents.
- It is determined that wind plays a crucial role in the distribution of marine debris. The accumulation of debris in specific areas varies based on the direction of the wind. Hydrodynamic models take into account the influence of wind to estimate the value of surface currents, thus making it reasonable that this phenomenon affects the results.
- Only 3% of the particles that reach the coast come from external sources. This is expected because these sources primarily affect the outermost regions, which are most influenced by oceanic activity. In these regions, the particles are subject to different dynamics than those of the estuary and may be coupled to the Atlantic Meridional Overturning Circulation (AMOC).

Upon comparing the model to the monitoring data collected on the coasts, it has been determined that the results are highly favorable for both study periods. In both scenarios, it was demonstrated that the general trend of each area for the entire time period could be accurately reproduced, with the exception of two regions within Illa, and one in the Ria.

- In the case of Illa, most of the regions exhibit a similar tendency between the simulation and monitoring results. However, segments S4 and S9 highlight the importance of considering anthropogenic structures during the interpretation of results. These structures can act as artificial drivers or barriers. In the case of S4, a poor reproduction of the coastline causes the simulation to register lower values than those monitored. The monitoring values are also increased due to the high retention caused by the harbor and pontoons. In the case of S9, the presence of the bridge connecting the island reduces the effect of the wind, causing fewer particles to reach this study area (as shown in monitoring data). However, this blocking effect does not appear in the simulation, resulting in greater accumulation results. Thus, knowledge of the study area is essential in determining if it can be accurately represented computationally. Spatial resolution issues can lead to unexpected and erroneous results.
- All study areas exhibit comparable monthly patterns, except for November and December, which display atypical behavior. This unusual behavior during these months may be attributed to the impact of North Atlantic hurricanes.

- Regarding the Ría comparison, the Lagrangian model adequately replicates the general trend, except for Carreiro and Aduana beaches. From a computational standpoint, Carreiro beach is one of the least contaminated areas of the study. This is due to the fact that it is in an outer area of the estuary, quite exposed to high variability. In Aduana, the presence of a dike blocks the entrance of mussel-peg, but this structure is not represented in the computational coastal line. Thus, disparities appear between simulated and monitoring data.

- The impact of tides is evident, as the computed accumulation values in beaches that are well-exposed to tidal action exceed those recorded in beach samples.

- Regarding the sensitivity study of the beaching factor, it has been observed that, in most cases, the differences between the established beaching values of 20%, 50%, and 80% are relatively similar. However, significant variations are sometimes observed, which can be attributed to the fact that the simulation may not accurately represent the precise beach exposure. The beach topography, such as rocks and algae, can influence the retention of floating particles and may not be accurately simulated in the coastline model. Nevertheless, it is not possible to establish a linear correlation between the beaching factors that would fit well with each beach.

Considering all of the above, we can conclude that the results are satisfactory and that the MOHID-Lagrangian model is a useful tool in the study of Lagrangian transport in oceans. However, a good understanding of the emission sources and the target study areas is necessary to ensure accurate reproduction of the processes involved.

Chapter 5

Estimation of marine debris in the North Atlantic area

*The results from this chapter have already been submitted as S. Cloux[1], P. Pérez[2], H. de Pablo[3] and V. Pérez Muñuzuri[1], "A regional Lagrangian model to evaluate the dispersion of floating macroplastics in the North Atlantic Ocean from different types of sources in the Iberian Peninsula.". Submitted to Science of the Total Environment, 2023.

[1] CRETUS Research Center, Nonlinear Physics Group, Faculty of Physics, University of Santiago de Compostela, Spain.
[2] Centro Oceanografico de Vigo, Instituto Espanol de Oceanografia, CSIC, Vigo, Spain.
[3] MARETEC, Instituto Superior Tecnico, Universidade de Lisboa, Portugal.

5.1 Introduction

The amount, patterns, and origins of plastic debris found on coasts and in the open ocean remain largely unknown [132]. However, there is a general agreement that this type of pollutant exerts negative effects on marine and coastal ecosystems, fisheries, and tourism [133, 134]. Accurately determining the quantity and extent of microplastics in the open ocean is a highly complex task. Since microplastics range in size from less than 0.5 *cm* to nanometer dimensions, classifying and categorizing them is a formidable challenge [123, 19, 124].

Determining the sources and accurately estimating the quantity of plastic waste entering the ocean poses a challenging task. Plastics can enter the ocean through a variety of pathways, including rivers, land-based sources such as litter and wastewater, as well as maritime activities such as fishing and shipping. Visual analysis of plastic waste areas, remote sensing, and statistical methods are useful for estimating the quantity of plastic debris going into the ocean [135, 136, 137]. In the case of rivers, the amount of plastic waste released can be linked to the size of the river basin and the population living in the area [138]. However, determining the exact amount of plastic debris entering the ocean or rivers can be challenging, as it depends on various factors such as river flooding, estuary residence time, and retention areas [139]. Bauer-Civiello et al. [140] also examined the role of stormwater systems as a rarely recognized source of plastics in rivers. Other sources of plastic debris, including coastal population centers, ports, and bathing areas, can also be identified on land [141, 142]. Additionally, it

can be difficult to link this information with the amount of plastic in the ocean, as plastics can degrade or disintegrate over time, making it challenging to trace the origins of plastic particles found in the ocean. Nonetheless, efforts are being made to improve our understanding of the sources of plastic pollution, including the use of models and monitoring systems to track the flow of plastic debris in and around coastal regions.

There are several methodologies used to account for plastics in the ocean, each with its strengths and limitations. One common method is visual surveys, in which researchers visually count and classify plastic debris in a given area. This method is relatively inexpensive and can provide valuable insights into the distribution of plastic in different regions of the ocean. However, it is limited by the fact that it can only capture surface-level debris and miss small or submerged particles. Another approach is the use of trawling nets, which collect plastic particles as they are dragged through the water. This method provides a more comprehensive view of the types and sizes of plastic in the ocean, including microplastics. However, trawling nets can also collect natural debris, making it challenging to distinguish between plastic and non-plastic particles. In recent years, advanced technologies such as drones and remote sensing have been employed to map and quantify plastics in the ocean. These methods can cover large areas of the ocean quickly and efficiently, providing more comprehensive data on plastic distribution. However, they are still limited by the fact that they can only detect plastics on the surface, and they may struggle to differentiate between plastic and other materials. Overall, a combination of methods is often used to gain a more comprehensive understanding of plastic pollution in the ocean, taking into account the strengths and limitations of each approach. This information is crucial for developing effective strategies to mitigate plastic pollution and protect marine ecosystems. This study aims to examine the spread of floating macroplastics that originate from various sources along the Atlantic coast of Spain and beyond. The analysis will encompass not only a regional area but also a broader scale, determining potential accumulation areas and evaluating the impact of emissions from different sources.

5.2 Study area

This research focuses on the North Atlantic region, as illustrated in Figure 5.1a). The distribution of plastic materials in the ocean is closely linked to the behavior of surface currents. Therefore, it is important to understand the hydrodynamics of the region we are examining. The dynamics of the North Atlantic region are typically initiated by the Gulf Stream [143, 144], which flows parallel to the east coast of North America until it reaches Cape Flanders, as depicted in Figure 5.1a). The Gulf Stream bifurcates near the Newfoundland Banks, resulting in two branches [145, 146, 147]. One of these branches continues its eastward flow at a latitude of 52°N, and forms the North Atlantic Current. Mann [147] identified the area around 42°N and 42°W as the central point of a persistent anticyclonic gyre. As the current reaches the western coast of Europe, it separates into two distinct branches: one flows northward and becomes the Arctic Current, while the other flows southward and evolves into the Canary Current, the Atlantic Subtropical Current, and ultimately the North Equatorial Current. This current flows westward towards the Caribbean Sea and the Gulf of Mexico, thus forming the basis of a large-scale circulation pattern known as the Atlantic Meridional Overturning Circulation (AMOC). This circulation also encompasses

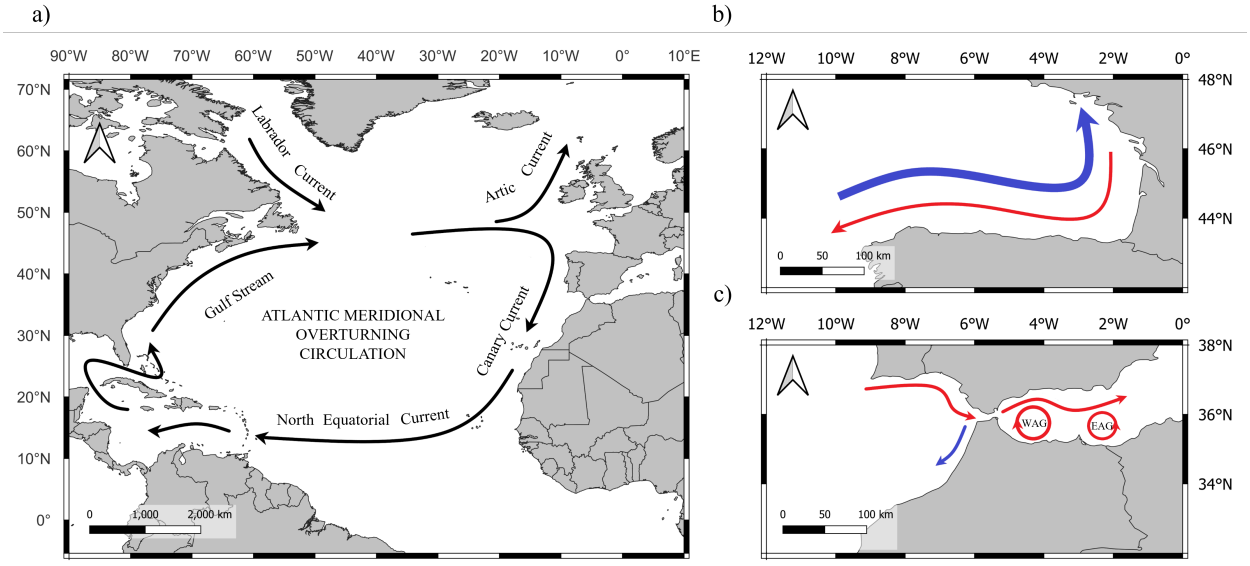

Figure 5.1: Surface currents in the study area. a) General circulation in the Atlantic Ocean, b) the seasonal behavior of the currents in the Bay of Biscay and c) in the South of Spain. The red arrows denote the dynamics for the warmer seasons, while the blue arrows represent the dynamics for the colder months.

and involves other movements that originate in various sub-regions of the North Atlantic Ocean.

In the Iberian Peninsula, there are four specific areas that merit special attention: the Bay of Biscay, the Gulf of Cadiz, the Alboran Sea, and the Canary Islands. The dynamics of the Bay of Biscay have been extensively studied [148]. The behavior of surface currents in this area is characterized by seasonal variations that are strongly influenced by prevailing winds [149]. During the winter season, the current flows eastward along the Spanish coast and northward along the French coast, while in the summer season, a weaker counter-current is observed with an intensity that is three times lower, as shown in Figure 5.1b). The water masses present in this region, as well as along the western coast of the Iberian Peninsula, originate from either the North Atlantic Ocean or from interactions between water masses from the North Atlantic Ocean and the Mediterranean Sea [150]. An analysis of drifting buoy data has shown that the strongest movements in the Bay of Biscay are associated with high-frequency tides and inertial waves [151]. The estimated mean size of eddies in the Bay of Biscay is about 45 *km*, and their occurrence exhibits a seasonal variability, with a relatively high number of eddies observed during the first half of the year and a relatively low number during the second half of the year. A Lagrangian numerical analysis has revealed that although the slope current system plays a significant role in the inflow and outflow of the Bay of Biscay, it is not capable of transporting water masses in a continuous and uninterrupted manner [148].

In the Mediterranean Sea, plastic accumulation is a well-known problem due to its closed nature and complex circulation patterns characterized by multiple gyres and eddies [152, 153]. The circulation is further influenced by the North Atlantic currents and the region's bathymetry, which governs the circulation at various depths, leading to significant impacts from upwelling and downwelling processes on surface circulation [154]. The Western Mediterranean Basin, also known as the Alboran Sea, is driven by mass intrusion through the Gibraltar Strait

that compensates for evaporation losses, as well as wind forcing. The surface circulation is characterized by a frontal Atlantic jet around two large-scale anticyclonic gyres: the Western Alboran Gyre (WAG) and the Eastern Alboran Gyre (EAG) (see Figure 5.1c)). Sudden changes in the WAG, such as its collapse or the eastward migration of the Atlantic jet, have been observed [155, 156]. Such changes lead to the transformation of the Atlantic jet into a coastal jet that follows the African coast during autumn and winter [157], resulting in seasonality in the surface circulation of the Alboran Sea [158]. In the northern part of the Western Mediterranean Sea, the Atlantic waters flow eastward up to the Corsica and Sardinia Islands, where they are driven northward along the western Corsican coasts to form the Western Corsica Current. Later, this merges with the Eastern Corsica Current in the Ligurian Sea to form the Northern Current. This current is mainly formed by the Atlantic Waters in surface and Levantine Intermediate Water in subsurface [159]. Several oceanographic campaigns have described the seasonal variability, mainly represented by a well-defined episode of narrowing, deepening, and offshore drift from late January to mid-March [160].

The dynamics of the Gulf of Cadiz in the Atlantic Ocean are intricate, and closely connected to those of the Mediterranean Sea [154]. In the summer months, an anticyclonic pattern on the open sea surface promotes circulation towards the Strait of Gibraltar. However, during late autumn and early winter, the circulation shifts in a southwesterly direction, as illustrated in Figure 5.1c). Large-scale atmospheric models have identified the influence of wind in the region, particularly in winter. Easterly winds, corresponding to a negative North Atlantic Oscillation (NAO) value, cause local forcing [161].

The oceanic dynamics of the Canary Islands are characterized by subtropical gyres [162]. They have demonstrated that the region experiences an intense seasonal cycle in the southern part of the islands, with significant differences in transport between spring and fall. The main water mass transport also shows slight variations in location and intensity for Surface Waters and North Atlantic Central Waters.

5.3 Methodology

5.3.1 Numerical Simulations

Two 7-year simulations were conducted from January 2015 to December 2021 for this study. The first simulation involves only Lagrangian particles that move through the study domain without being trapped on the coast. In the second simulation, a 50% beaching coefficient is introduced to investigate its impact on dispersion. This choice is arbitrary, aimed to avoid excessively high or low retention rates. The study focuses on three types of potential sources: rivers, on-land sources, and marine traffic sources, each of which is described in detail in the following subsection. Considering the results without beaching, the relative accumulation of each type of source in the North Atlantic domain is determined. For this purpose, a grid covering the North Atlantic Ocean domain is used with a resolution of 0.5 degrees, while for more specific domains such as the Bay of Biscay, the Alboran Sea, and the Mediterranean Sea, a higher resolution of 0.25 degrees is used. The concentration is expressed in terms of the number of particles per unit area, but this net value is not realistic since the

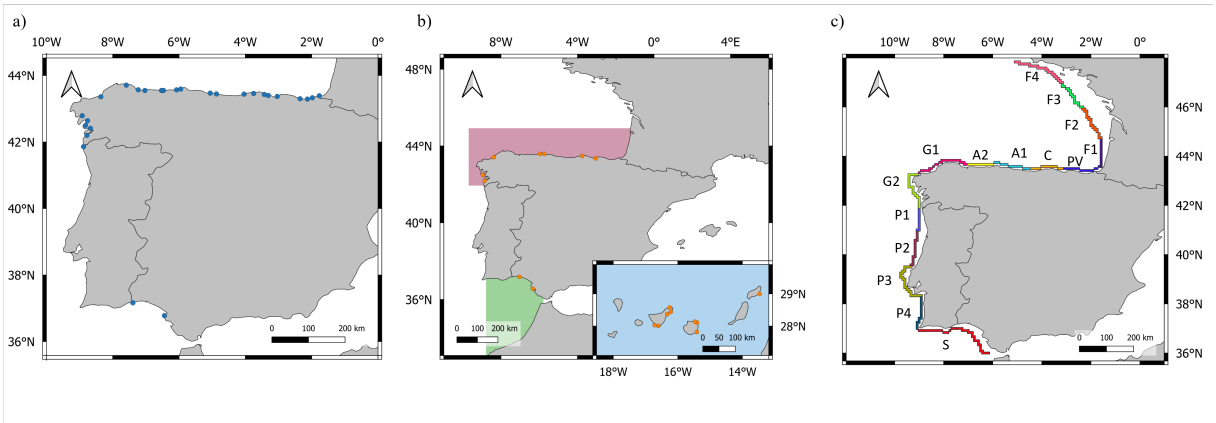

Figure 5.2: Emission sources considered in this study: a) emission points (blue points) of the 27 rivers considered; b) emission points (orange points) of the 18 land-based points considered; c) maritime traffic emission segments (considering also France and Portugal). The 3 regions considered in the study are shown in figure b): R1, northern region (red shadow), R2, southern region (green shadow) and R3, canary region (blue shadow).

model emission value is not accurate. Therefore, the concentration values estimated for the entire period are normalized with respect to the maximum estimated concentration value. The relative accumulation ($\%\ RA$) is calculated as the ratio of the accumulation in each cell (A_i) and the maximum recorded accumulation (A_{MAX}) in the grid for the whole 7-year period, as follows:

$$\%RA = 100\frac{A_i}{A_{MAX}} \tag{5.1}$$

We estimate dispersion by calculating the relative dispersion for all point sources at the end of the simulation relative to their origin. We group the results by emission region and plot a statistical distribution for each region, both for latitude and longitude. We also investigate the impact of the beaching factor on dispersion, analyzing only point sources located on the coast (rivers and on-land positions), as we have well-known coordinates for these sources. For maritime traffic emissions, emissions are made from a polygon parallel to the coast, with the model assigning emission points within the polygon, separated by a user-defined resolution. However, the exact emission points are not well-known, and we cannot use the results of maritime traffic in the dispersion calculation.

We also calculate the number of particles from each marine source within the semi-enclosed regions and group these accumulations by month to observe variations in the presence of particles from a given source over a region throughout the simulated period. For a particular month, we determine the relative percentage of each marine source by dividing its contribution by the total contribution of all sources for that month. Additionally, we examine the seasonality of simulated particles in three semi-enclosed regions of the domain (Bay of Biscay, Gulf of Cadiz, and Alboran Sea) to understand the temporal evolution of accumulations in these regions. Open regions do not experience accumulation phenomena. It was also estimated the potential transboundary pollution coming from France and Portugal.

Source	Type	Variable Rate	Weighted	Measure
Rivers	Point	Yes	Yes	Concentration and Dispersion
On-Land	Point	No	Yes	Concentration and Dispersion
Marine Traffic	Polygon	No	No	Concentration and Seasonality

Table 5.1: Characteristics of the considered sources.

5.3.2 Emission Sources

Despite the widespread belief that most plastic waste originates from land-based sources, particularly heavily populated inland areas, the origin and fate of this waste remain incompletely understood. While some studies suggest that marine sources may also contribute significantly, there is a significant discrepancy between the estimated amount of plastic waste generated on land that enters coastal waters and the amount actually observed at sea. This highlights the need for a better understanding of the movement and fate of plastics, as well as the timing and manner of their release, which continues to puzzle the scientific community. As a result, caution must be exercised when interpreting results related to plastic waste emissions.

In the MOHID-Lagrangian model, emissions are characterized by their location, release time, and emission rate, with the release time typically coinciding with the start of the simulation, and the rate controlling the way particles are emitted. The model considers three types of particle sources: (1) river discharge, which is thought to be the primary route for waste to enter the oceans from land; (2) on-land emissions, which include areas with a higher likelihood of serving as sources of marine litter, such as population centers, ports, bathing areas, and solid waste dumps; and (3) offshore emissions, which account for the impact of maritime traffic. Table 5.1 provides a summary of the configuration of each source.

Rivers

This study focuses on 27 rivers that flow into the Atlantic Ocean along the Atlantic Iberian Peninsula coastline. These rivers are categorized into 6 River Basin Districts (RBD): Eastern Cantabrian, Western Cantabrian, Galicia-Costa, Miño-Sil, Guadiana, and Guadalquivir. The study estimates the emission rates of plastic waste into the ocean using historical gauging records from monitoring networks (`https://sig.mapama.gob.es/redes-seguimiento/`). The river discharge flow corresponds to the assigned emission rates, and the model uses daily flow data. However, for some rivers, daily flow data were unavailable, so the mean flow for the month was used as the daily flow. In the absence of data for the corresponding month, the monthly mean flow of the time series was used. The study determined the emission points based on the locations of the river mouths, as shown in Figure 5.2a). The flow values were weighted according to the study conducted by González-Fernández et al. [138], which established a correlation between visual monitoring of floating macrolitter at the mouth of 42 rivers and streams across Europe, the size of their basin, the associated population, and the

mismanaged waste. This correlation allowed for the estimation of the relative contribution of the main European rivers to the annual floating macrolitter load of the Atlantic Ocean.

On-land points

The study of on-land emissions involved 18 point sources, which were identified based on the Analysis of Pressures and Impacts of the Marine Strategy (MAPAMA and CEDEX, 2012) report. This report evaluated and mapped the potential entry points of plastic debris into the sea from land for Spanish marine demarcations, including coastal population centers, ports, bathing areas, solid urban waste dumps, and rivers. A score ranging from 1 to 10 was assigned to each 10 *km* coastal cell, with higher scores indicating greater magnitude. To select the emission points, the study focused on areas with the highest pressure values, specifically cells with scores among the top three in the demarcation. A single representative emission point was established for each of these zones (refer to Figure 5.2b)). As the emission rate of this type of source is highly uncertain, a weighted and standardized continuous emission was established based on the scores assigned by [163, 164, 165].

Marine traffic

Due to the challenge of precisely locating all possible maritime emission sources, including aquaculture facilities, fishing vessels, merchant ships, and recreational boats, it was decided to consider an emitting area that encompasses all potential maritime emission points. Therefore, an emission perimeter was established around the Iberian Peninsula and the French coast, 10-12 *km* from the coast and at a depth of 92-130 *m*, Figure 5.3. This perimeter coincided with the highest density of marine traffic based on available data from EMODnet. As most of the maritime activities are concentrated in a band parallel to the coast, a polygon emission approach was used. For the first part of the study, only Spanish maritime sources were considered, while contributions from France and Portugal were taken into account for the final part of the analysis to estimate transboundary pollution. Maritime traffic on the Canary Islands was not included because the available data from EMODnet only indicated two types of maritime activities: ferry routes and recreational fishing, which are not significant sources of plastic pollution. To address the uncertainty surrounding emission rates of this type of source, we applied a continuous emission.

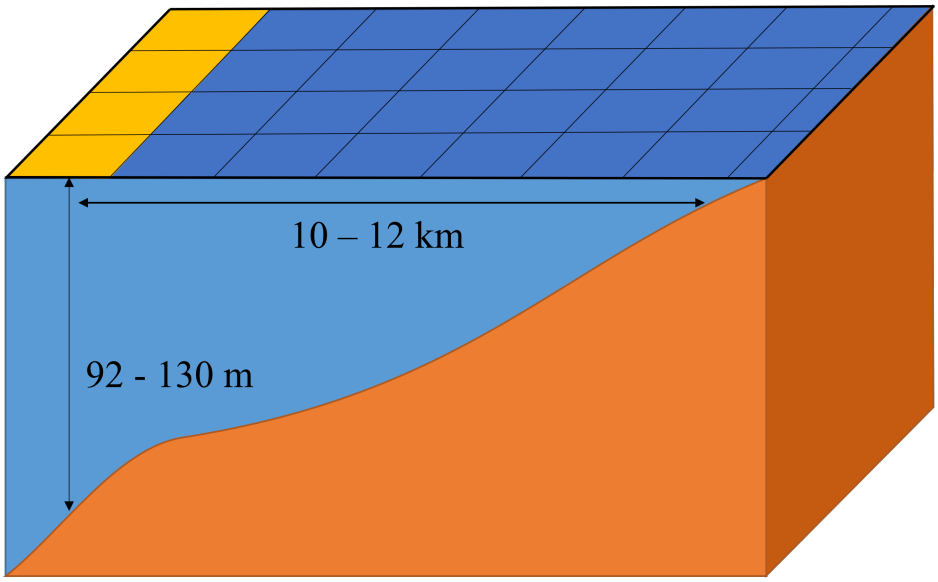

Figure 5.3: Sketch of the coastal perimeter established to simulate the incidence of maritime traffic.

5.4 Results

5.4.1 Concentrations

Figure 5.4 displays the relative concentrations in the North Atlantic Ocean over a 7-year period for the three types of sources considered: a) rivers, b) on-land, and c) maritime traffic. Beaching processes are not taken into account in this analysis. As the number of particles emitted is unrealistic, the resulting concentration values may also be unrealistic. Therefore, the accumulation of each cell is presented as a percentage of the maximum accumulation value obtained for each type of source (*% RA*). The representations of these accumulations are generated using Jenks' Natural Breaks, a technique that groups similar values together and maximizes differences between classes. As a consequence, the divisions for the results of each source may not be identical. Furthermore, it is not possible to compare results for the three emission cases because relationships between the types of emissions cannot be established. However, it can be generally noted that emission rates and the type of sources significantly influence the results. A time-varying emission (rivers) leads to lower concentrations than a continuous emission (on-land). On the other hand, an extensive emission (maritime traffic) results in higher accumulations than a point emission.

The highest concentration for river emissions is recorded in the south of the peninsula, in the Gulf of Cadiz. This finding is consistent with the significant contribution made by the Guadiana and Guadalquivir rivers, as reported by [138]. Note that the accumulation zones are also displaced towards the Alboran Sea, with the highest values assigned to the northern coast of Morocco, which is in line with the circulation patterns in this area. The presence of eddies and their weakening and collapse encourage the retention of particles along the Mediterranean coast of Morocco. In the north of Spain, the highest accumulation values are observed on the Spanish side of the Bay of Biscay. The semi-enclosed nature of this region facilitates the retention of particles. There are also accumulations in the rest of the Atlantic area, but below

0.1%. The Canary Islands appear to be unaffected by pollution originating from peninsular rivers. The results suggest that pollution associated to rivers flow may be widespread, but its impact is more significant at the local scale.

The accumulations resulting from on-land emissions are comparatively more intense than those from river emissions, which can be attributed to the consideration of continuous emissions. In addition to the Gulf of Cadiz, notable accumulations are observed in the Bay of Biscay, with higher concentrations appearing parallel to the French coast. Despite having fewer emission points, the Cantabrian and Galician coasts register higher values for the entire coastline compared to the previous case. The Canary Islands also exhibit new accumulation areas, as some emission sources were located in this region. However, accumulations in the Alboran Sea and the Mediterranean Sea, in general, are slightly reduced. In the open ocean, concentrations between 0.1% and 0.5% are recorded, indicating that the range of the simulated particles is mainly local.

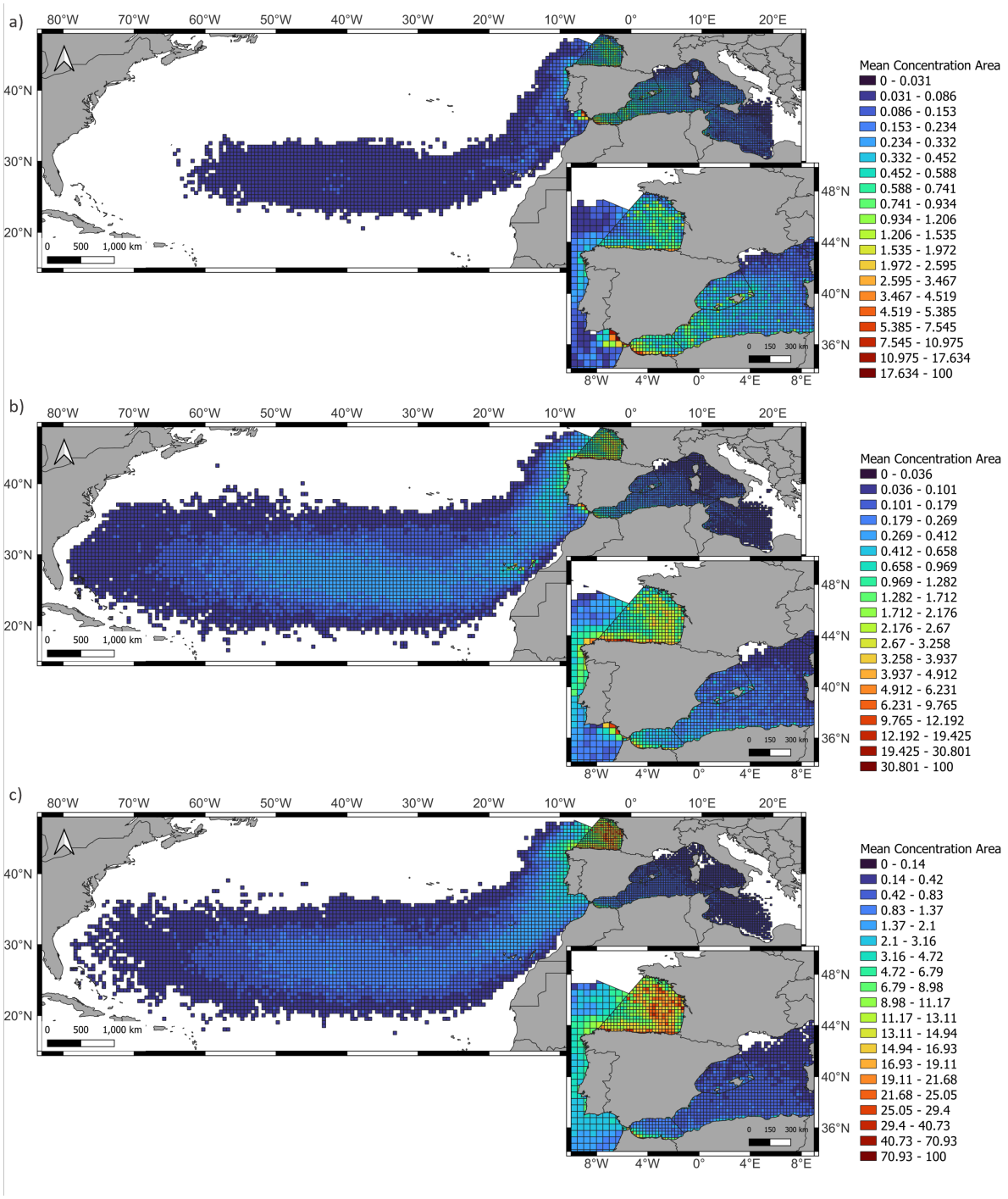

Figure 5.4: Global relative accumulation in the North Atlantic Ocean for each of the emission types considered: a) rivers, b) on land, c) marine traffic.

Finally, we consider emissions from maritime traffic and simulate a continuous emission within a polygon positioned parallel to the coast at a distance of approximately 10 *km*. The results show a high concentration in the Bay of Biscay, with a stronger concentration appearing around the French coast. However, the concentrations near the Cantabrian coast, which were observed in previous cases, are attenuated in this scenario. This finding suggests that the high concentrations in cells close to the coastline may be due to an inaccurate estimation of the

hydrodynamic fields in these areas. In this case, we consider a larger number of emission points with a higher emission frequency, which may result in more pronounced accumulation regions. However, the concentrations in the Gulf of Cadiz decrease. Floating particle concentrations in the Alboran Sea are maintained in terms of location near the coast of Morocco, consistent with the circulation in the area, but with less intensity than for other type of emissions.

These concentration values for the North Atlantic area provide a good first approximation. But they do not provide information on the dispersive tendency of the particles according to the region of emission. Therefore, in the following section, we analyze the dispersion patterns.

5.4.2 Dispersion

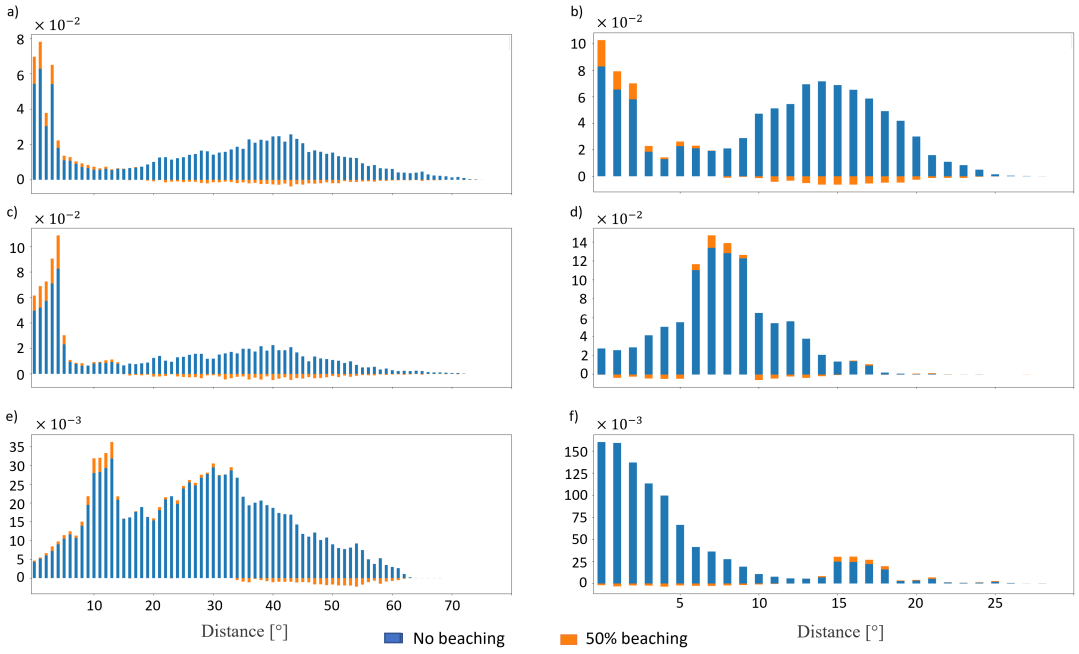

Figure 5.5: Relative dispersion in latitudes and longitudes for point sources (rivers and on-land) grouped by regions. a) Dispersion in longitudes and b) in latitudes for R1 (emissions in northern Spain). c) Dispersion in longitudes and d) in latitudes for R2 (emissions in southern Spain). e) Dispersion in longitudes and f) in latitudes for R3 (emissions in the Canary Islands).The blue bars correspond to the results without beaching, and the orange bars correspond to the variation when introducing this factor.

The dispersion of simulated particles in latitude and longitude was studied grouping the point sources (rivers and on-land emissions) into zones, resulting in three regions as shown in Figure 5.2: R1, covering the north coast of the peninsula; R2, covering the Gulf of Cadiz; and R3, covering the Canary Islands. For each individual source, the relative dispersion of particles related to the emitter location was determined by recording the position of the particles emitted from point sources at their final state after 7 years of simulation. The relative dispersion was calculated as the difference between the final and initial position. The results of the study for longitudes (left column) and latitudes (right column) for the three considered regions are presented in Figure 5.5 as a normalized histogram to show the distribution of particle

dispersion. The dispersion of R1 emissions is represented in Figure 5.5a) and b), that of R2 emissions in Figure 5.5c) and d), and that of R3 emissions in Figure 5.5e) and f). The orange bars show the differences in dispersion when assuming 50% beaching, with an orange bar added above the blue one for longitudes and latitudes where the concentration increases and below the blue one for cases where it decreases.

R1 includes all sources located in the northern region of the Iberian Peninsula. The highest concentration of Lagrangian particles is observed at short distances in both latitude and longitude. The dynamics of the Bay of Biscay vary between the winter and summer seasons, and the semi-enclosed nature of the region leads to particle retention. When particles are emitted near the eastern inner bay, a larger distribution of particles is observed in nearby longitudes and latitudes compared to sources located further west. In warm seasons, emissions closer to the Atlantic Ocean experience greater dispersion towards middle distances, likely due to the westward flow during this time of year. This seasonal effect is confirmed in the subsequent section of this study. Additionally, the effect of beaching intensifies the accumulation of particles in both latitude and longitude, while reducing the accumulation at middle distances.

In the case of the Gulf of Cadiz (R2), the highest concentration of particles is observed at longitudes below 5 degrees, whereas a large concentration of particles is found at medium distances in the 5-10 degree range from the emission points in terms of latitudes, while the near and far distances show less significant concentrations. The beaching process reinforces this behavior, indicating that particles tend to accumulate in this region. The semi-enclosed nature of the Gulf of Cadiz promotes particle retention in the region, which is consistent with the circulation patterns in the area. During winter, the circulation flows around the coast towards the south (Moroccan coast) while in summer, it flows towards the north (Spanish coast). This circulation pattern is also reflected in the dispersion of particles in latitudes.

In the case of the Canary Islands (R3), greater dispersion is observed at medium and remote longitudes, while the opposite is observed in terms of latitude dispersion, as the region is affected by the Canary Current. This dynamic drives the transportation of water masses from the west of the peninsula to tropical and subtropical latitudes.

The presented results provide insights into dispersive patterns based on the region of particle emissions. However, the above-described particle distribution does not offer information about the average time particles spend in specific areas. To determine the retention time of Lagrangian particles in semi-enclosed regions like the Bay of Biscay, the Gulf of Cadiz, and the Alboran Sea, the following subsection will analyze the temporal variation of these particles. Open areas will not be considered since the focus is on understanding the time retention of particles in these regions.

5.4.3 Seasonality and Transboundary Pollution

To evaluate seasonality, only emissions from maritime traffic are considered as they are emitted continuously and not influenced by variable emission rates. Additionally, maritime

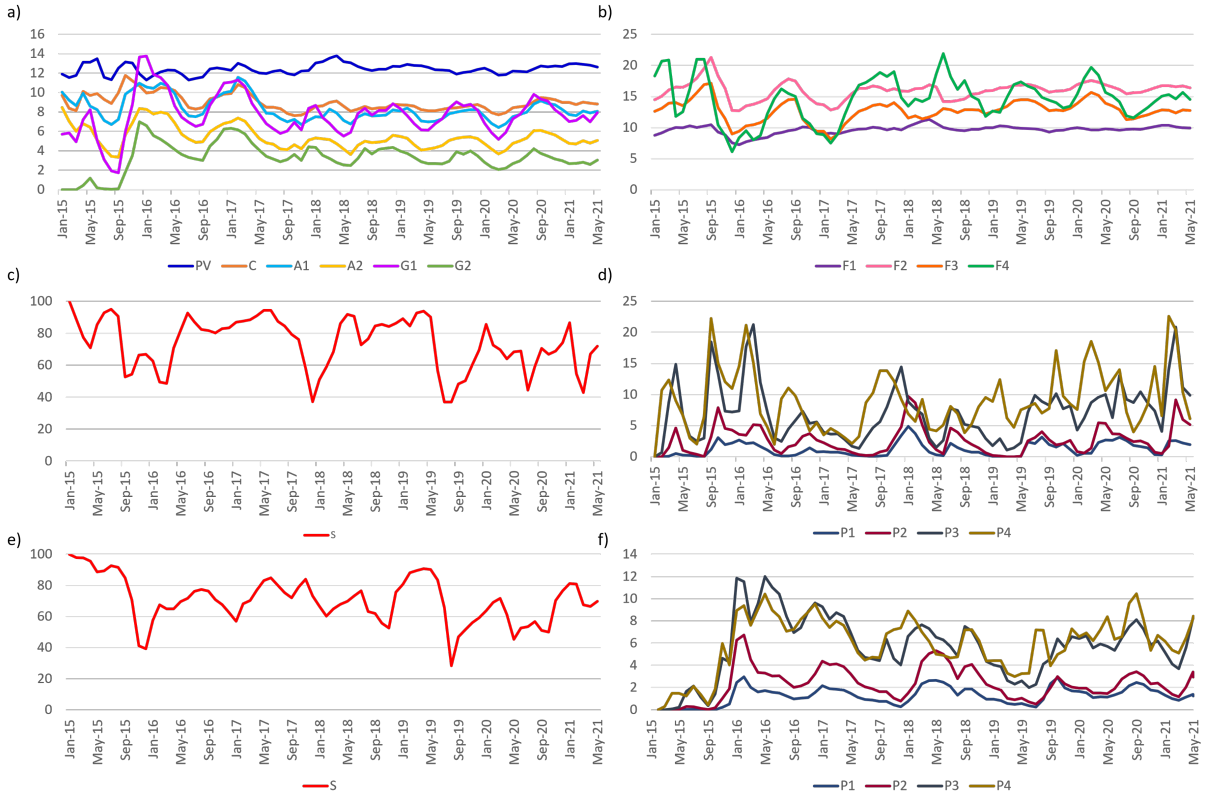

Figure 5.6: Relative contribution of each of the maritime sources in three semi enclaved regions around the peninsula: a) PV, C, A1, A2, G1, G2 and b) F1, F2, F3 and F4 contributions over the Bay of Biscay; c) S and d) P1, P2, P3 and P4 contributions over the Gulf of Cadiz; e) S and f) P1, P2, P3 and P4 contributions over the Alboran Sea.

traffic emissions are not weighted sources and emit a higher number of particles per emission segment, which helps minimize errors due to spatiotemporal variations. To evaluate the relative significance of transboundary pollution in the regions of interest, sources located off the coasts of France and Portugal are also considered. The total number of particles emitted by each maritime traffic source is calculated and grouped by month to study seasonality. The relative contribution of each marine source is obtained as the ratio of its emission to the total sum of all sources. The results are presented in Figure 5.6. The left graphs show the most significant Spanish contributions for each region, while the right graphs show the foreign contributions. Contributions that were below 1.5% for the entire seven-year period are excluded.

The results for the Bay of Biscay are presented in Figure 5.6a) and b). The contribution of Spanish emissions (Figure 5.6a)) shows a periodic growth trend between September and April, corresponding to the autumn and winter seasons. This is followed by a decrease during the spring and summer seasons until September. The pattern is less pronounced for the PV segment, which has the highest contribution due to its location in an intermediate zone of the R1 area. As a result, its contribution does not undergo significant temporal variation during the year, acting as a local source unaffected by regional hydrodynamics. The contributions of segments C and A1, which are close to the intermediate region, also show small variations. However, westernmost regions such as A2, G1, and G2 have more noticeable seasonal variability. French sources show stable contributions with F1 having the highest average contribution of 9.65%

(Figure 5.6b)). F4 has the most significant seasonal variability due to its location in the northern region, and its contribution increases during warm months. Segments P1 and P2 have a small contribution (below 1%), and P3, P4, and S show negligible contributions (below 0.001%). The Bay of Biscay's circulation demarcation and the predominant west-to-east current during winter and opposite movement during summer months contribute to this pattern.

Figures 5.6b), c), d), and e) depict the contributions in the Gulf of Cádiz and the Alboran Sea. Since both areas are connected via the Strait of Gibraltar, their trends are closely linked. The dominant contribution in both regions is from southern Spain's emission segment (S), followed by sources along the Portuguese coastline. The sources in the north of the Iberian Peninsula have negligible contributions, averaging below 1.5%. In the Gulf of Cadiz, the particle concentration peaks during the spring and summer months, coinciding with the surface currents' eastward flow towards the Strait of Gibraltar. During late autumn and early winter, a sharp decline is observed due to the Atlantic current's weakness entering the region. Similarly, in the Alboran Sea, the highest contribution occurs in the spring and summer months. The increased inflow of water via the strait strengthens the Western Alboran Gyre (WAG), resulting in higher particle input. A decrease in contributions (both for the south and Portugal) is observed during the autumn and winter months due to the WAG's weakening or destabilization, caused by a reduction in the Atlantic jet flow. Thus, seasonality plays a crucial role in the accumulation of plastic marine debris.

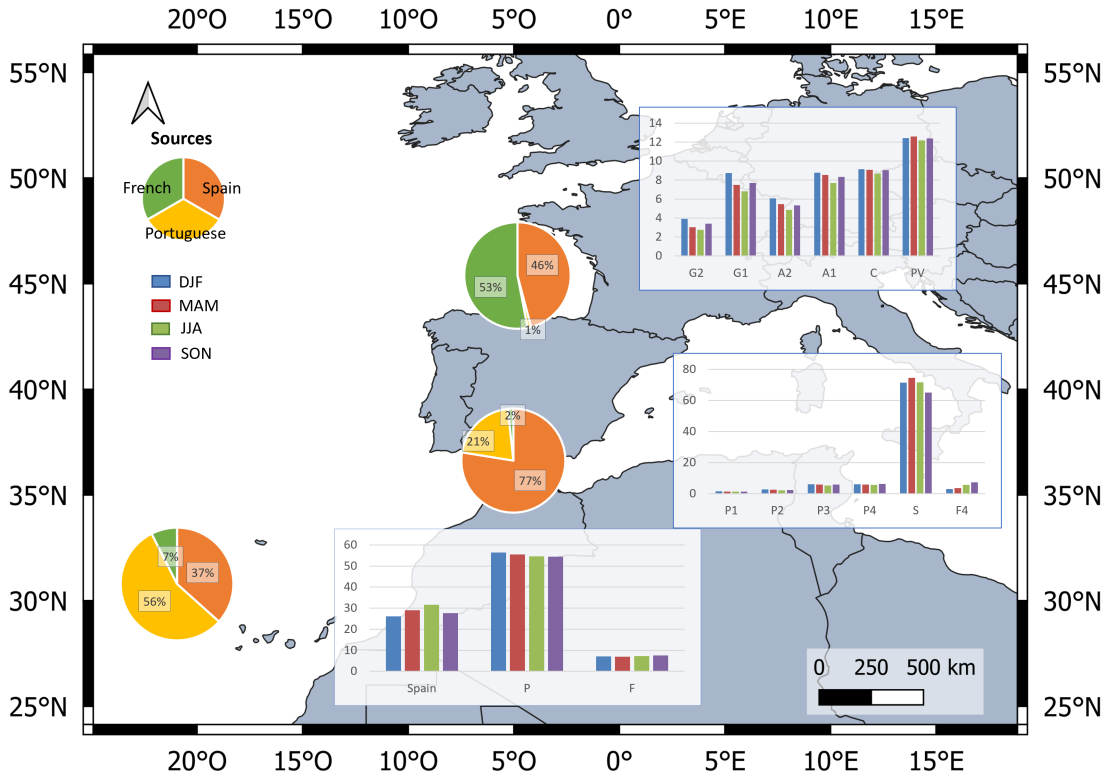

Figure 5.7: Contribution of transboundary pollution in pie charts and the seasonal evolution of the most significant sources in bar charts. Spanish sources are presented in orange, Portuguese sources are presented in yellow and French sources are presented in green. Blue bars correspond to winter, red bars correspond to spring, green bars correspond to summer, and purple bars correspond to fall.

Figure 5.7 presents the transboundary contribution throughout the entire simulation period. Pie charts demonstrate the relative contributions for three regions: the Bay of Biscay, the Strait of Gibraltar/Alboran Sea, and the Canary Islands. The corresponding bar charts on the right-hand side display the seasonal variation of the major contributing sources for each area based on the marine sources analysis. In the Bay of Biscay, French sources contribute the most (53%), followed by Spanish sources (46%), with Portuguese sources representing only 1%. This is expected due to the shape of the bay and the location of the French sources in the corner zone. The westernmost Spanish sources (G2, G1, A1) have higher contributions during the colder seasons and a decrease during the warmer seasons. Seasonal effects tend to decrease for sources located farther east, as observed in the case of A1, C, and PV.

In the Gulf of Cadiz and the Alboran Sea regions, the dominant contribution comes from Spanish sources, accounting for 77%, mainly from the southern part of the Iberian Peninsula (S), followed by Portuguese sources (21%) and French sources (2%). Portuguese sources remain relatively constant throughout the entire simulation period, while the contribution from S is higher during the warmer months, and there is a significant increase from F4 during the second half of the year. In the Canary Islands region, Portuguese sources constitute the largest contribution (56%), followed by Spanish sources (37%) and French sources (7%). Both French and Portuguese sources exhibit a stable contribution throughout the year, while the contribution from Spanish sources shows a marked increase during the warmer months.

5.5 Discussion

Marine plastic pollution is a pressing environmental issue that requires immediate attention as it transcends national borders. This study utilizes the MOHID-Lagrangian tool to conduct a Lagrangian statistical analysis and identify potential areas of floating plastic debris accumulation in the North Atlantic Ocean. The model provides control over three types of emitters in the Atlantic coast of Spain: (1) rivers, (2) on-land, and (3) maritime traffic. There have been also included France and Portugal contributions as marine traffic types. Rivers and on-land sources were modeled as point sources, with a time-varying emission rate considered for rivers due to their expected flow contribution. On-land sources were set up with continuous emissions, and source importance was determined based on values provided by CEDEX. Offshore sources were modeled to have a continuous emission parallel to the peninsular coastline, coinciding with the area of greatest vessel presence provided by EMODnet.

Although we made rigorous and cautious efforts to address emissions, it remains the primary source of error in this type of study. Due to a lack of knowledge about emission rates and the exact locations of plastic debris in the ocean, modeling its transport and distribution is a significant challenge. For instance, river flooding, estuary residence time, or possible retention zones can influence river emission rates. Similarly, in the case of marine environments, determining when and where ALDFG and other waste has been released is difficult.

Initially, simulations spanning seven years were conducted for each source of plastic pollution. To determine the concentrations in the North Atlantic domain, only the effect of surface currents on particle transport were considered, without taking into account any

beaching processes. The highest concentrations for the three considered sources were identified near the peninsular coast, with three specific regions of particular interest: the Bay of Biscay, the Gulf of Cadiz, and the southern coast of the Alboran Sea. Concentrations of plastic debris were observed in the Canary Islands region for on-land sources, whereas high concentration cells were detected near the coastline for point sources. Nonetheless, these accumulations were less prominent when sources not immediately above the shoreline were taken into account, indicating that the estimated hydrodynamic field values near the coastline may have errors owing to grid resolution. Thus, it can be concluded that:

- Relative accumulation maps provide a good initial approximation, but they do not provide detailed information on the dispersion of Lagrangian particles in the open ocean.
- Modeling plastic concentrations in the ocean requires considering multiple factors, such as the spatial and temporal resolution of the model, the precision of the forcing data, and the complexity of the particle transport process. The balance between computational cost and high spatial and temporal resolution is crucial when modeling at large scales. While high-resolution models are better equipped to capture the transport and dispersion of plastic particles, they come with higher computational costs and can introduce numerical instability. Therefore, a balance is necessary to achieve the required accuracy. Additionally, high-resolution models are recommended for accumulations near shore locations.

The study calculated the relative dispersion of particles for point sources, including rivers and on-land sources, in three regions: sources from the northern peninsula (R1), sources from the Gulf of Cadiz (R2), and sources from the Canary Islands region (R3). The results demonstrated that particle dispersion varied depending on the emission zone. A beaching factor of 50% was considered, indicating that particles tend to accumulate near emission points in the first region (R1) and disperse significantly in mid-latitudes in the second region (R2). In the Canary Islands region (R3), particle dispersion followed the circulation in the area, transported towards tropical and subtropical latitudes and the east coast of the Americas via the Canary Current. Then, dispersion patterns are consistent with the dynamics of the area.

To examine the seasonal behavior of particles and their temporal evolution, we focused on semi-enclosed regions (Bay of Biscay, Gulf of Cadiz, and Alboran Sea) and considered only emissions from marine sources. Accumulation patterns were consistent with the seasonal dynamics of each region, with the highest contributions coming from the closest sources in the Bay of Biscay. During the autumn and winter months, west-to-east movement resulted in greater contributions from westerly sources in that area, while the opposite occurred during spring and summer. In the southern regions (Gulf of Cadiz and Alboran Sea), the highest contributions came from the southernmost regions of Spain and Portugal, with the Atlantic jet driving particles towards these regions in spring and summer. This approach could be expanded to include variable ratio emissions such as rivers, allowing us to link seasonality with emission variation.

The study estimated the relative transboundary contribution in four regions: the Bay of Biscay, the Strait of Gibraltar/Alboran Sea, the Gulf of Cadiz, and the Canary Islands. The

results showed that French sources were the largest contributors in the Bay of Biscay (53%), followed by Spanish sources (46%), and Portuguese sources (1%). In the Gulf of Cadiz and Alboran Sea regions, Spanish sources had the highest contribution (77%), followed by Portuguese sources (21%) and French sources (2%). Portuguese sources were found to have the highest contribution in the Canary Islands region (56%), followed by Spanish sources (37%) and French sources (7%). The contribution from different sources varied across seasons and regions, with French sources making a significant contribution in the Bay of Biscay and Spanish sources in the Gulf of Cadiz and Alboran Sea.

Chapter 6

Atmospheric Lagrangian Tracking of the Moisture Participating in HPEs

*The results from this chapter have already been published as S. Cloux[1], D. Garaboa-Paz[1], D. Insua-Costa[1], G. Miguez-Macho[1], & V. Pérez-Muñuzuri[1], "Extreme precipitation events in the Mediterranean area: contrasting two different models for moisture source identification." Hydrology and Earth System Sciences, 25(12), 6465-6477. 2021
DOI: https://doi.org/10.5194/hess-25-6465-2021

[1] CRETUS Research Center, Nonlinear Physics Group, Faculty of Physics, University of Santiago de Compostela, Spain.

6.1 Introduction

A major concern of climate change is the increase in extreme weather events. Many analyzed areas have experienced changes in total precipitation and temperature extremes, indicating this rise. Climate change is causing heavy precipitation events to become more frequent and intense [166]. As temperatures rise, more water evaporates into the atmosphere, leading to heavier rain and snowfall. This can result in severe flooding, landslides, and other types of damage. Heavy precipitation events have significant social and economic consequences, as they can disrupt transportation systems, damage homes and businesses, and contaminate water sources. Additionally, they can lead to food and water shortages, as well as public health crises [167]. To prepare for these events, it is essential to have accurate and reliable weather forecasts. Achieving this requires ongoing research and development of weather prediction models, as well as the use of advanced technology such as radar and satellite imagery. It is also crucial for communities to have emergency response plans in place, and for individuals to take measures to protect themselves and their property. This may include building or retrofitting homes to be more flood-resistant and creating early warning systems to alert people to potential hazards. Overall, heavy precipitation events are a serious concern that will likely become more pressing as the climate continues to change. It is crucial for governments, organizations, and individuals to take action to prepare for and respond to these events in order to mitigate their impact.

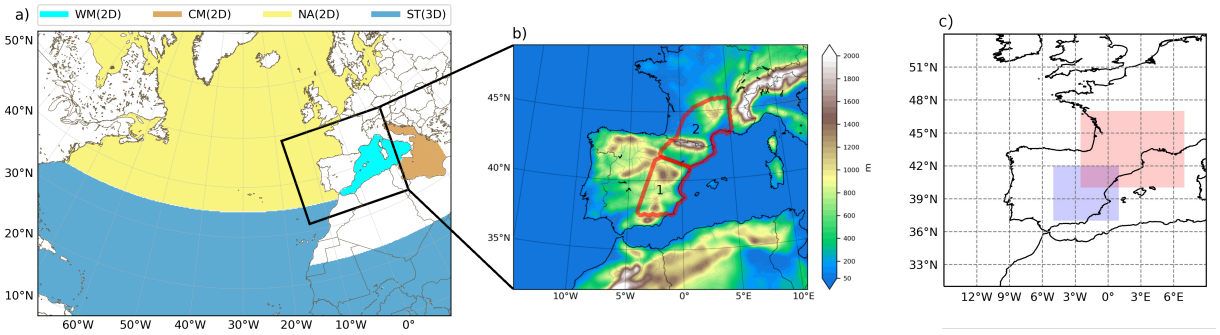

Figure 6.1: (a) Moisture sources considered: western Mediterranean (cyan), central Mediterranean (brown) and North Atlantic (yellow) 2D sources; and tropical and subtropical 3D source(blue). (b) Regions most affected by the October (1) and November (2) events (original figure from Insua-Costa et al., 2019). (c) FLEXPART-WRF particle selection areas for the October (blue) and November (red) events.

As introduced in Chapter 3, the Western Mediterranean Region is exposed to heavy precipitation and flooding due to several characteristics, such as the large body of warm water in the Mediterranean, complex orography, and northern latitude [72, 73, 74]. Most of the extreme events occur in the autumn when Atlantic lows or cut-off lows interact with the warm waters of the Mediterranean Sea, leading to strong convection. In addition, atmospheric rivers (ARs) act as moisture channels, rapidly transporting moisture from one location to another, which can significantly contribute to high precipitation values during these episodes [168, 91, 110]. Different studies have suggested that other ocean basins, particularly the Atlantic, may also contribute to these extreme events. Various methodologies have been used to determine the origin of moisture, as discussed in Chapter 3. Lagrangian models are the most commonly used. This methodology analyzes changes in moisture content in air parcels tracked backward or forward in time. They are generally offline and very efficient from a computational point of view. On the other hand, online Eulerian-type methods are much more computationally expensive and therefore have been used less frequently. However, they are considered to be the most accurate tool for studying moisture sources (see [84] for a classification of the different models used for moisture tracking).

6.2 Methodology

In this study, we examine the sources of moisture during two catastrophic flooding events in the WMR using both the Lagrangian and Eulerian methods. The online Eulerian moisture tracking model employed is the Weather Research and Forecasting (WRF) Model with water vapor tracer diagnostics (WRF-WVT [114]). The results obtained using this tool were already presented in a previous article [83]. The objective of our study is to conduct a similar analysis using the offline Lagrangian FLEXPART-WRF model [115] and, complementarily, the U-Track-atmospheric-moisture model [108] to compare the results with the previous ones. The particulars of the mentioned models are expounded upon in Chapter 2. Table 6.1 delineates the principal characteristics that could potentially result in disparities among the results of the model.

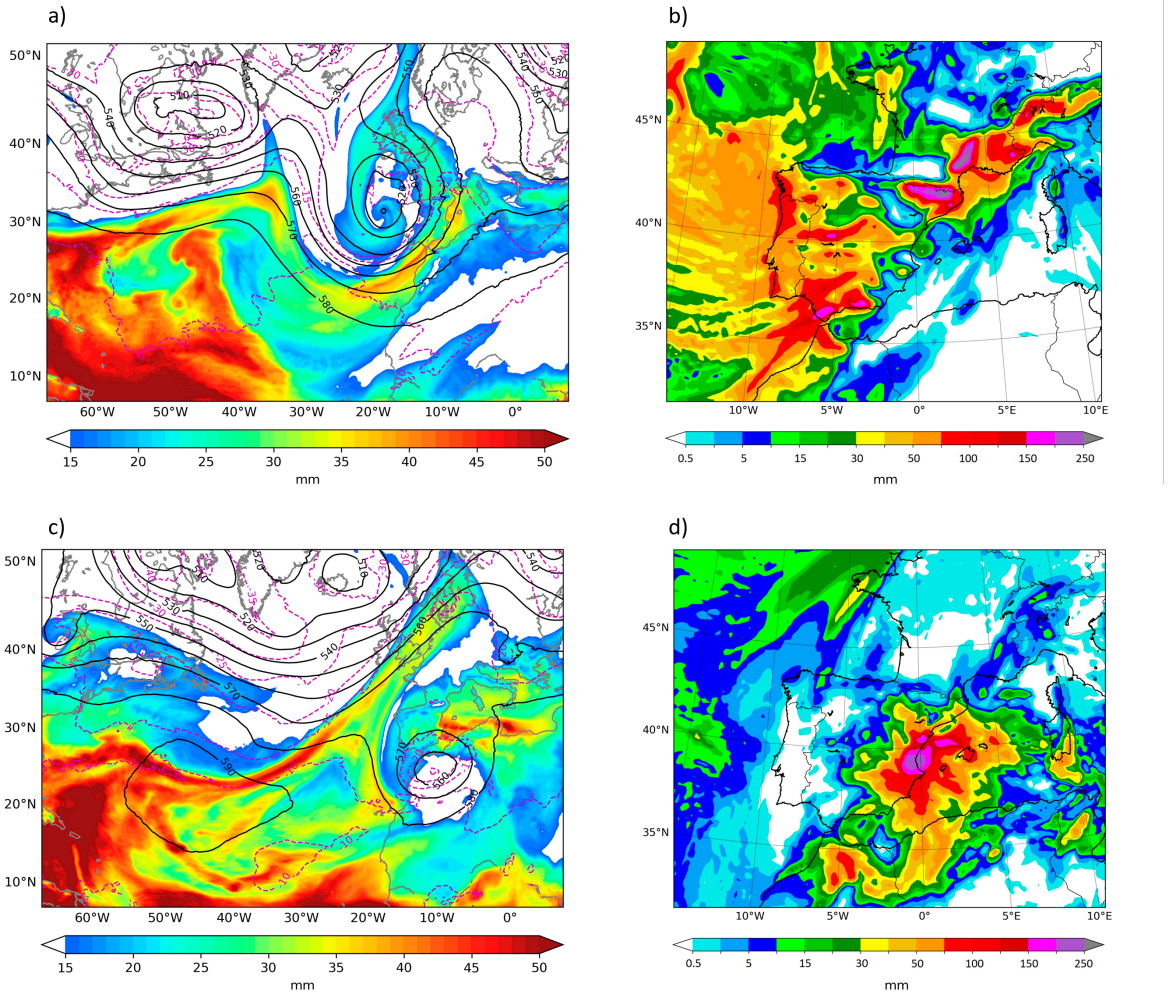

Figure 6.2: (a) Synoptic situation (from WRF simulation) on 20 October 1982 at 12:00 UTC. Geopotential height (solid black contours, dam) and temperature at 500 hPa and total precipitable water (shades, mm). (b) Simulated total precipitation (mm) from 19 October at 06:00 UTC to 22 October at 06:00 UTC. (c) Similar to (a) but for 7 November 1982 at 12:00 UTC. (d) Simulated to (b) but from 6 November at 06:00 UTC to 9 November at 06:00 UTC.

6.2.1 Analysis of Atmospheric Events

October Event

On October 20th, 1982, an event known as ”the Tous case” caused a catastrophic flood due to anomalous precipitation in the Spanish Levante. The Valencian Community was severely impacted by the heavy rainfall, as shown in Figure 6.2b). This event was the first mesoscale convective complex identified in Europe (as discussed in detail by [169]). The synoptic conditions that led to this exceptional precipitation event were typical of the setup that frequently affects the region, as illustrated in Figure 6.2a). These conditions involved a cutoff low near the Iberian Peninsula that increased thermal and dynamic instability. At the same time, low pressures originating from North Africa at lower levels produced a warm and humid

flow that sustained convection continuously.

November Event

A few days after the Tous case flooding event on 20 October, another devastating flood occurred in the WMR on 7 November. This time, the heavy rainfall primarily affected the northeast of Spain, southeast France, and Andorra (as seen in Figure 6.2d)). Unlike the October flooding, the atmospheric conditions that led to the excessive rainfall in November were greatly different (as shown in Figure 6.2c). A deep low-pressure system located off the Atlantic coast of Galicia caused a very humid and relatively warm southwesterly flow to hit the Pyrenees and the southern face of the French Massif Central. This caused an orographic lift in these areas, leading to the formation of convective cores embedded in a broader area of stratiform rainfall, which then resulted in persistent and at times extremely intense precipitation (for a more in-depth discussion, see [170]).

6.2.2 Eulerian Approach

The results of the WRF-WVT for the two precipitation events analyzed here in 1982 were previously presented in [83]. The authors analyzed moisture from sea surface evaporation and atmospheric water transport from tropical and subtropical regions, using three 2D sources and one 3D source, respectively. Figure 6.1 depicts the simulation domain and source regions used by [83]. The simulations were performed using the WRF model with a horizontal resolution of 20 *km* and 35 vertical levels, and ERA-Interim reanalysis [171] was used as the initial and boundary conditions. The results of the WRF-WVT simulations will be used as input for the FLEXPART-WRF model and for comparison with the results obtained from the offline Lagrangian tool. This approach is particularly appropriate for validating the Lagrangian model results, as both models are driven by the same WRF meteorological model.

6.2.3 Lagrangian Approach

E-P Balance

The simulation domain, which covers the area from 90°W to 60°E and from 3°S to 65°N, is divided into 4 million air parcels based on the distribution of atmospheric mass. These particles are then advected backward in time for 11 days using the atmospheric fields from WRF simulations as the driving force. To trace the origin of moisture, the change in specific humidity (q) along the trajectory of each particle is calculated every 3 hours. Then, for each trajectory, the water vapor budget ($e - p$) is obtained using equation 3.7. Based on this, the net water flux over a model grid cell of area A ($1^\circ \times 1^\circ$) is estimated by summing the variation rate in specific humidity for all the air parcels (K) contained in the atmospheric column over that area, as described by equation 3.8. To estimate the moisture source regions that contributed to the catastrophic precipitation event in 1982 WMR, we calculate the E–P balance for only those air parcels involved in the event. Using the precipitation fields from the WRF simulations (Figure 6.2), we consider particles within the affected region (blue in Figure 6.1c) during the October 1982 episode, which took place from 19 October at 06:00 UTC to 21 October at 21:00

	WRF-WVTs	FLEXPART-WRF	U-Tack
Moisture pathways	Eulerian	Lagrangian	Lagrangian
Simulation	Online	Offline	Offline
Track direction	Forward	Backward	Forward
Phase changes	Yes	No	No
Moisture Attribution	Evaporation	E-P balance	Moisture allocation
BLH parameterization	Hong et al. (2006) [172]	Hanna (1982) [118]	–
Convection Scheme	Kain et al. (1990) [173]	Emanuel et al. (1999) [117]	Dirmeyer et al. (2007) [98]

Table 6.1: Differences between the WRF-WVTs, FLEXPART-WRF and U-Track models.

UTC. Similarly, for the November 1982 event, we focus on particles within the red area in Figure 6.1c), which occurred from 6 November at 06:00 UTC to 8 November at 21:00 UTC. To ensure that we are only considering air parcels that contribute to precipitation, we will select those with $\frac{dq}{dt} < -0.06\ g\ \left(kg \cdot 3\ h^{-1}\right)$ over an area with significant accumulated rainfall rates $E-P < -2\ mm\ (3\ h)^{-1}$. These thresholds were chosen according to Stohl et al. [110]. Since we are analyzing only a portion of the air parcels, the *E–P* balance should not be interpreted as the net surface water flux, but rather as an indication of whether the particles contributing to extreme rainfall gained or lost moisture. The *E–P* field is calculated every 3 hours and accumulated over periods of 1, 4, 7, and 11 days prior to the precipitation events under investigation. This method of identifying moisture sources is based on the *E–P* field, as described by [112].

Quantifying the Contribution of the Moisture Sources

Tracking an air parcel backwards in time over an 11-day period can reveal different gains and losses of water vapor. For instance, consider an air parcel involved in the 1982 Mediterranean rains that had positive values of dq/dt 8 days prior to the event when it was located over the tropical Atlantic. The fact that the parcel gained moisture in that area does not guarantee that it contributed to the phenomenon. It is likely that moisture precipitated before the parcel reached the target region. Thus, regions with positive $E-P$ values should not be considered as actual sources of moisture, but rather as areas with the potential to contribute moisture. Sodemann et al. [111] presents a solution to quantify the relative contribution of moisture sources by avoiding the issue of precipitation before arrival. The method tracks all subsequent gains and losses of a given moisture uptake to determine if it reaches the study area or precipitates beforehand, following equation 3.11. By determining the uptakes that actually contribute to the rain event being analyzed, we can calculate the relative contribution (*RC*) as equations 3.14 and 3.15.

In addition, the U-Track atmospheric-moisture model is used to estimate the relative

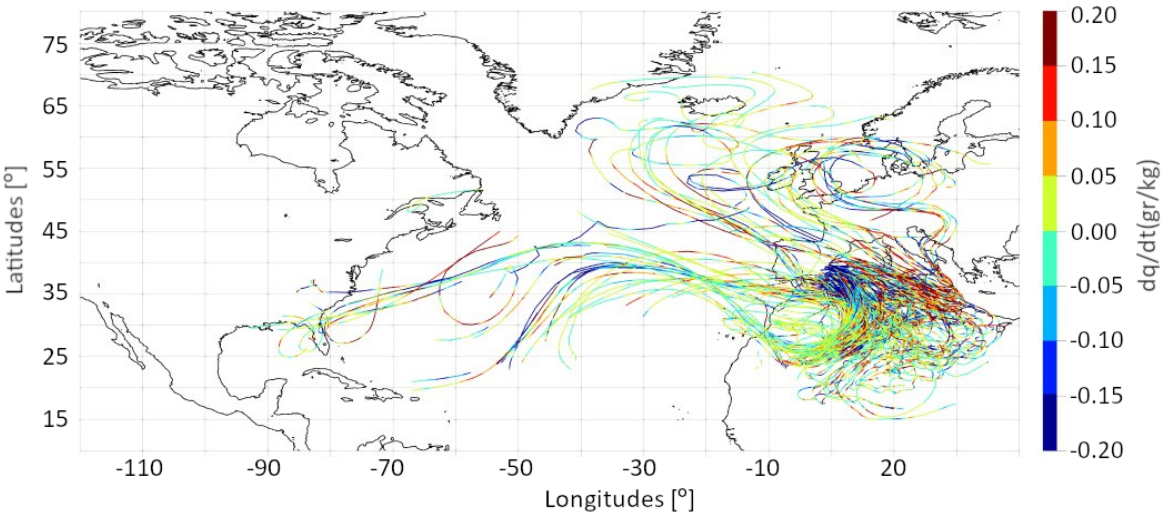

Figure 6.3: A period of 11 days backtracking for a reduced subset of selected particles precipitating over the target area (blue in Figure 1c) between 18:00–21:00 UTC on 20 October. Moisture exchanges are represented along the particle path.

contributions of the same sources. For this purpose, input data from the ERA5 model with daily resolution is used. Moisture is released over the defined areas as shown in the Figure 6.1 (a) and tracked for each source for a period of 26 and 30 days. Thus, the subtraction of both simulation results leaves only the moisture that has been released during the days corresponding to the event. By summing the moisture precipitated over the region where the event took place, we can obtain the relative contribution from a given event according to the equation 3.16. After conducting our own sensitivity analysis on the integration time and vertical mixing parameters (see more information in A.1), we have estimated the proportional impacts of each source considering the vertical mixing occurring every 24 hours, without considering the vertical flow component (ω), and using a integration time step of 3 hours.

6.3 Results

6.3.1 FLEXPART-WRF Moisture Source Diagnosis

October Event

Figure 6.3 shows humidity exchanges for a small group of previously selected particles. We only consider particles that have experienced a significant decrease in moisture during the time period of 18:00–21:00 UTC on October 20. The high concentration of trajectories in the western and central Mediterranean suggests that much of the moisture could be from evaporation in this region. The dq/dt values of air particles traveling through the Mediterranean are usually positive, indicating that they acquire moisture as they pass through this region. Moreover, some of the trajectories suggest a remote origin of the moisture, with some particles originating from the tropical Atlantic and reaching the affected area after passing over the Atlantic and North Africa. The counterclockwise turn of the trajectories over Morocco is a

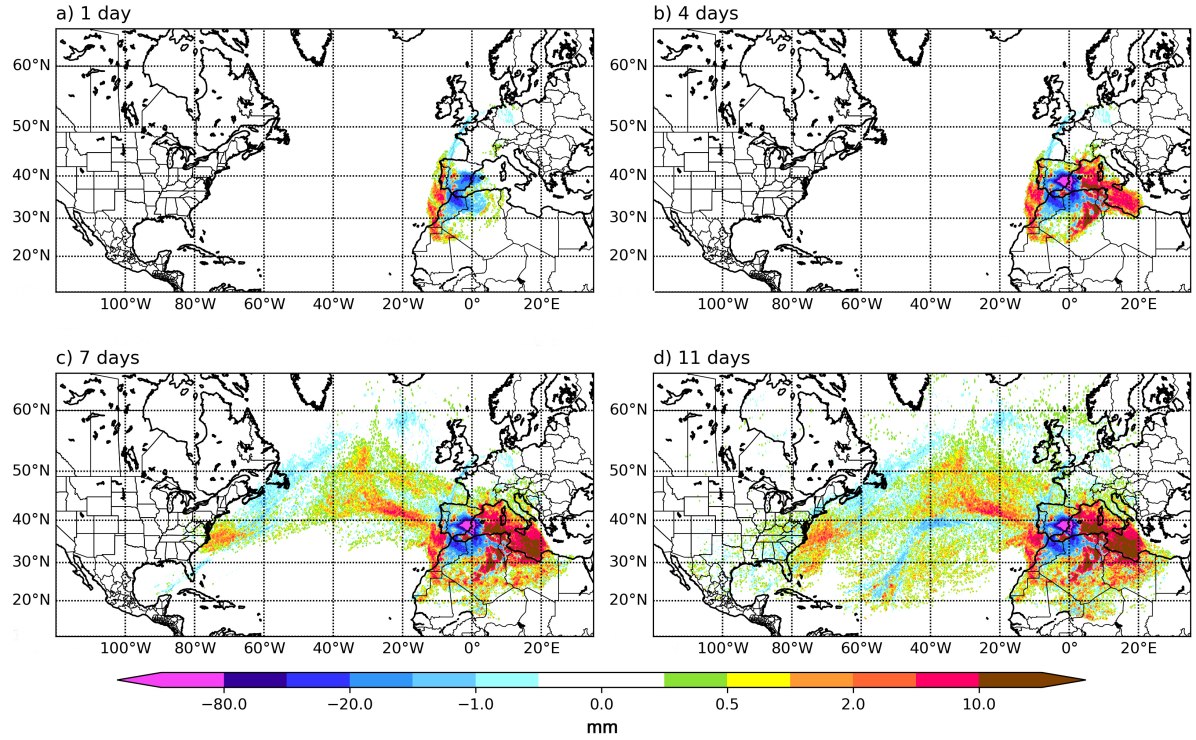

Figure 6.4: *E–P* balance evolution back in time for 1 (a), 4 (b), 7 (c) and 11 d (d). Particles were selected from 5°W-1°E and $37-42$°N for 19 October from 06:00 UTC to 21 October at 21:00 UTC.

result of the position of the cutoff low that caused the heavy rains (as shown in Figure 6.2). Additionally, other air parcels have origins in the North Atlantic, suggesting that multiple sources of moisture may contribute to the event.

The $E-P$ balance represented in Figure 6.4 highlights the regions in which the air particles that are contributing to the current precipitation event are gaining or losing moisture. Specifically, we present the evolution of the $E-P$ balance for the time periods of 1, 4, 7, and 11 days prior to the event (at 06:00 UTC on the current day). As expected, the lowest $E-P$ values are observed over the target region during the first three days, which demonstrates the discharge of moisture during the extreme precipitation event. Hence, negative values in the initial days indicate the area that was most affected by the intense rainfall. In the first 24 hours, the highest positive $E-P$ values are found at the eastern end of the Atlantic. As we move back in time, up to four days before the end of the event, the areas with positive $E-P$ values expand and cover much of the western and central Mediterranean. Therefore, these surrounding regions must have supplied the air particles that contributed to the event hours before they reached the target region. For the Mediterranean Sea, $E-P$ values continue to increase up to seven days before the event, indicating that not only was the contribution of evaporation significant in the hours leading up to the event, but the evaporation in the preceding days was also important. Moreover, there is a clear difference between days four and seven: positive (and negative) $E-P$ values appear in remote regions, primarily over the North Atlantic. These positive values extend into the tropical and subtropical Atlantic when we calculate the accumulated $E-P$ of the previous 11 days. This suggests that the contribution of humidity from the Atlantic might have

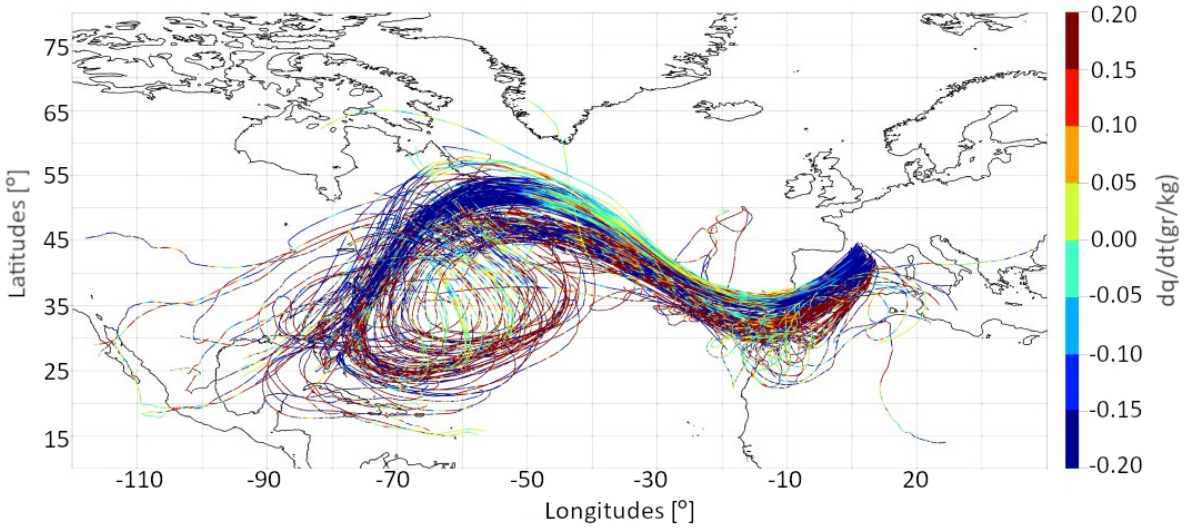

Figure 6.5: A period of 11 days backtracking for a subset of particles precipitating over the region of interest between 12:00–15:00 UTC on 7 November. Color corresponds to moisture exchanges along the paths followed by particles.

been significant, and this humidity would have had a longer residence time. One last region with positive $E - P$ values is North Africa. Although the values on the northern coast of the continent might be realistic, the values inland are not consistent since evaporation in that area of the Sahara is virtually nonexistent throughout the year. Therefore, these values must be due to the limitations of the method.

November Event

Figure 6.5 shows the change in specific humidity for a subset of particles that lost significant moisture between 12:00 to 15:00 UTC on November 7th. In contrast to the October event, the trajectories of the particles are relatively uniform, with a predominant path evident. Most of the particles come from the western tropical Atlantic and are transported northward across the Atlantic by the deep low-pressure system responsible for the intense rainfall event (Figure 6.2). Before arriving at the northeast of the Iberian Peninsula, the air masses were driven northward once again in the final phase, entering the region through northern Africa and southern Spain. A few air masses crossed over the western tip of the Mediterranean on their way to the target area. These findings suggest that the primary source of moisture in this case must have been the Atlantic, and the contribution from the Mediterranean was probably limited, as the air masses spent only a short time over this possible moisture source.

Figure 6.6 is similar to Figure 6.4, but focuses on the November event. In the first 24 hours of the event, a wide area of negative $E - P$ values was observed due to the large low-pressure system off the coast of Galicia (Figure 6.2). Only the western Mediterranean showed positive $E - P$ values during this time, indicating that it provided a final source of humidity before the precipitation reached the affected region. The $E - P$ field accumulated over the four days prior to the end of the event highlights the areas most impacted by extreme rainfall: northeast and southwest Spain, southern France, and Andorra. The positive $E - P$ values extend towards the

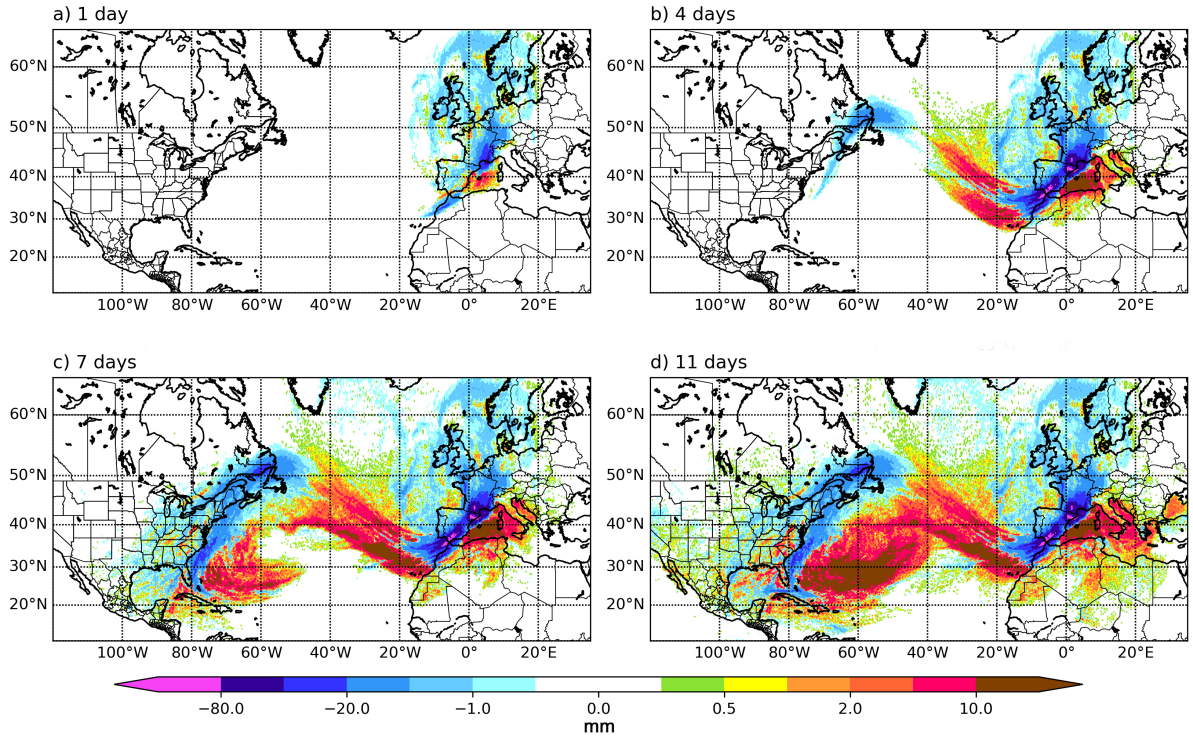

Figure 6.6: Similar to Figure 6.4. Balance E–P evolution back in time for 1 (a), 4 (b), 7 (c) and 11 days (d). Particles were selected from 2.5°W - 7°E and $40-47$°N for 6 November from 06:00 UTC to 8 November at 21:00 UTC.

Atlantic and become stronger in the Mediterranean. The highest $E-P$ values can be found in the tropical and subtropical western Atlantic between days 7 and 11. The distribution of $E-P$ values aligns with the particle trajectories (Figure 6.5) and the precipitable water field (Figure 6.2c). Thus, the air mass responsible for the event originated from the tropical and subtropical regions and replenished its moisture levels as it traveled through the Atlantic and the western Mediterranean.

6.3.2 Comparison of WRF-WVT, FLEXPART-WRF and U-Tack Methodologies

The previous analysis provides a qualitative understanding of the moisture sources, but it cannot provide a quantitative measurement. In contrast, the WRF-WVT method, developed by [114] calculates the exact contribution of precipitation from the four source regions (shown in Figure 6.1a) for the two autumn 1982 events. To compare these results with those obtained using the FLEXPART-WRF technique, the same contributions have been calculated using the methodology introduced by [111]. Figure 6.7 displays the fraction of total precipitation accumulated during the October 1982 event that came from each of the four sources, calculated using the WRF-WVT (blue bars) and the FLEXPART-WRF (purple bars) methods. Both methods give similar contributions from the western Mediterranean Sea (16.81% vs 19.14%) and North Atlantic Ocean (13.25% vs 14.89%). However, the central

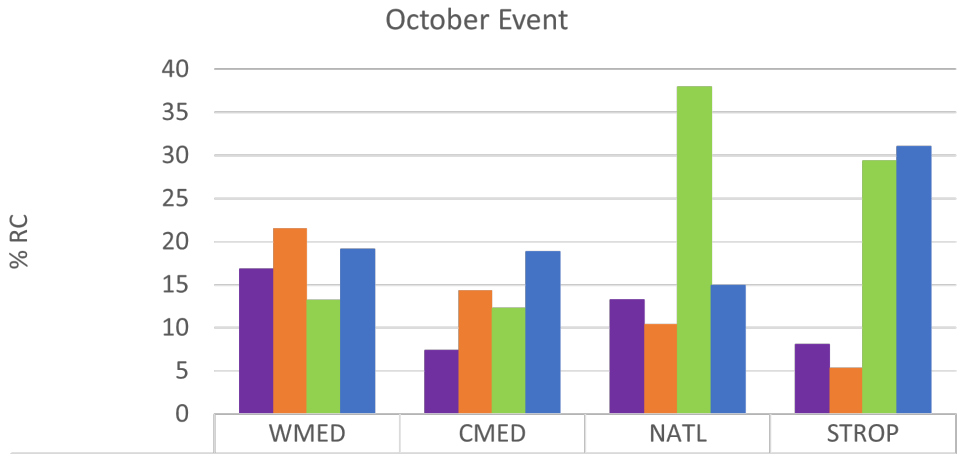

	WMED	CMED	NATL	STROP
FLEXPART	16,81	7,38	13,25	8,05
FLEXPART_BLH	21,56	14,38	10,43	5,39
U-TRACK	13,17	12,25	37,97	29,36
WRF-WVT	19,14	18,82	14,89	31,02

Figure 6.7: Comparison between the relative contributions provided by the FLEXPART-WRF, U-Track and the WRF-WVT models for the October event. WMED, CMED, NATL and STROP correspond to the western Mediterranean, central Mediterranean, North Atlantic and tropical/subtropical areas, respectively.

Mediterranean contribution, as determined by the FLEXPART-WRF, is half of that calculated by the WRF-WVT (7.38% vs 18.28%). The most noticeable difference between the results from both methods is seen in the tropics and subtropics. While for the WRF-WVT, this is the primary source (31.02%), the contribution from this area is only 5.39% according to the FLEXPART-WRF. This major difference results in the WRF-WVT attributing 83% of the relative contribution to the combination of the four sources, while the FLEXPART-WRF reports a much smaller contribution of 45.49%.

When considering the relative contributions below BLH (orange bars), the results become more similar between the new methodology and the WRF-WVT. This new method provides better results for the western (21.56% vs 16.81%) and central (14.38% vs 7.38%) Mediterranean Sea. However, for remote sources such as the North Atlantic (10.43% vs 13.25%) and Tropical regions (5.39% vs 8.05%), the new estimations are lower than those calculated for the entire column. The overall humidity allocation is slightly higher, around 51.76%. The relative contribution for each source is also estimated using the UTrack method (green bars). For the October event, the relative contribution of the local sources is lower than that estimated by the WRF-WVT (13.17% vs 19.14% for the WMED and 12.25% vs 18.28% for the CMED). The contribution of the North Atlantic is highly overestimated (37.97% vs 14.89%), in relation to the Eulerian model, while for the tropics, this model is the closest to the expected result (29.36% vs 31.02%). However, as a whole, this model is able to assign a higher percentage of humidity (93%) in relation to FLEXPART (52%), much closer to that detected by WRF (83%).

For the November event (Figure 6.8), both the WRF-WVT and FLEXPART-WRF methods show similar joint relative contributions from the four analyzed sources. Specifically,

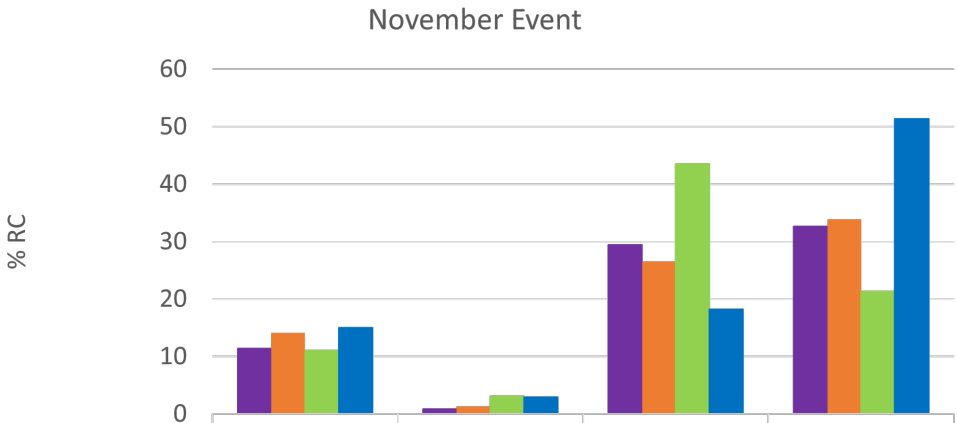

	WMED	CMED	NATL	STROP
FLEXPART	11,4	0,83	29,41	32,69
FLEXPART_BLH	14,14	1,35	26,58	33,94
U-TRACK	11,04	3,11	43,54	21,31
WRF-WVT	15,06	2,96	18,2	51,39

Figure 6.8: Comparison between the relative contributions provided by the FLEXPART-WRF, U-Track and the WRF-WVT models for the November event. WMED, CMED, NATL and STROP correspond to the western Mediterranean, central Mediterranean, North Atlantic and tropical/subtropical areas, respectively.

the WRF-WVT estimates a joint contribution of 88.15%, while the FLEXPART-WRF estimates a slightly lower joint contribution of 74.37%. The two methods also produce comparable contributions for the central Mediterranean Sea (2.96% for WRF-WVT and 0.83% for FLEXPART-WRF). Additionally, both methods provide similar estimates for the contribution of the western Mediterranean Sea, with the WRF-WVT estimating 15.60% and the FLEXPART-WRF estimating 11.44%. However, there are some differences between the two methods when it comes to the contribution of moisture from the North Atlantic and tropics/subtropics. Specifically, the FLEXPART-WRF overestimates the contribution of moisture from the North Atlantic (29.41%) compared to the WRF-WVT estimate of 18.20%. On the other hand, the FLEXPART-WRF underestimates the contribution of moisture from the tropics and subtropics (32.69%) compared to the WRF-WVT estimate of 51.39%.

When reviewing contributions under BLH (orange bars), the results become more similar across all sources for this event. We obtained improvements for the western region (WMED) of 14.14% compared to FLEXPART-WRF and 11.44% for WRF-WVT and for the central region (CMED) of 1.35% compared to FLEXPART-WRF and 0.83% for WRF-WVT. The percentage for the North Atlantic Ocean decreased to 26.58% compared to FLEXPART-WRF's 29.41%, which is closer to WRF-WVT's estimate. For tropical regions, the contribution slightly increased to 33.94% compared to FLEXPART-WRF's 32.69%. Overall, the assigned humidity is 76%. Regarding the U-Track model (green bars), we found a slightly smaller contribution in the WMED of 11.04% compared to WRF-WVT's 15.6%, but a more similar contribution in the CMED of 3.11% compared to WRF-WVT's 2.69%. However, for medium or remote sources, the percentages are not as similar with 43.54% for FLEXPART-WRF and 18.2% for WRF-WVT in the WMED, and 21.31% for FLEXPART-WRF and 51.39% for WRF-WVT in

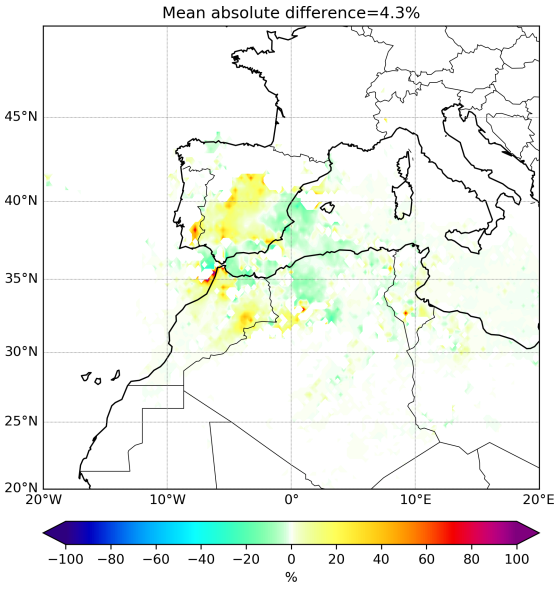

Figure 6.9: Relative difference (%) between E–P field values calculated considering humidity phase changes and without considering them. The domain has been cropped with respect to Figs. 6.4 and 6.6 because the values outside the shown area are very small.

the CMED. In terms of global humidity, UTrack allocates 79% of the moisture.

6.4 Discussion

There are two primary methods for investigating the origin of moisture: Lagrangian-offline and Eulerian-online models. While the choice between the two can be a point of debate, Lagrangian models are generally more computationally efficient, making them more practical to implement and thus, widely used in the field. However, it is crucial to recognize the limitations of these techniques in order to conduct a comprehensive analysis.

The aim of this study was to assess the effectiveness of the Lagrangian FLEXPART-WRF model by comparing its results with those obtained from the Eulerian WRF-WVT model. The study also utilized the U-Track model. Specifically, the performance of the models during two severe rainfall events that occurred in the western Mediterranean region during October and November of 1982 was evaluated. In order to establish a benchmark for comparison, the WRF-WVT model results were considered as the virtual truth. A novelty of this study is the analysis of moisture sources from a nonlocal point of view, meaning a large-scale domain was employed to cover sources of remote origin. The aim was to assess whether the FLEXPART-WRF has the same capacity to detect short-distance sources as well as long-distance ones.

The results indicate a significant difference in the relative contributions obtained using the FLEXPART-WRF and WRF-WVT methods. The largest discrepancy is observed in the contributions from subtropical and tropical sources. In October, FLEXPART-WRF underestimates this source by 74%, while in November, the underestimation is 36%. For

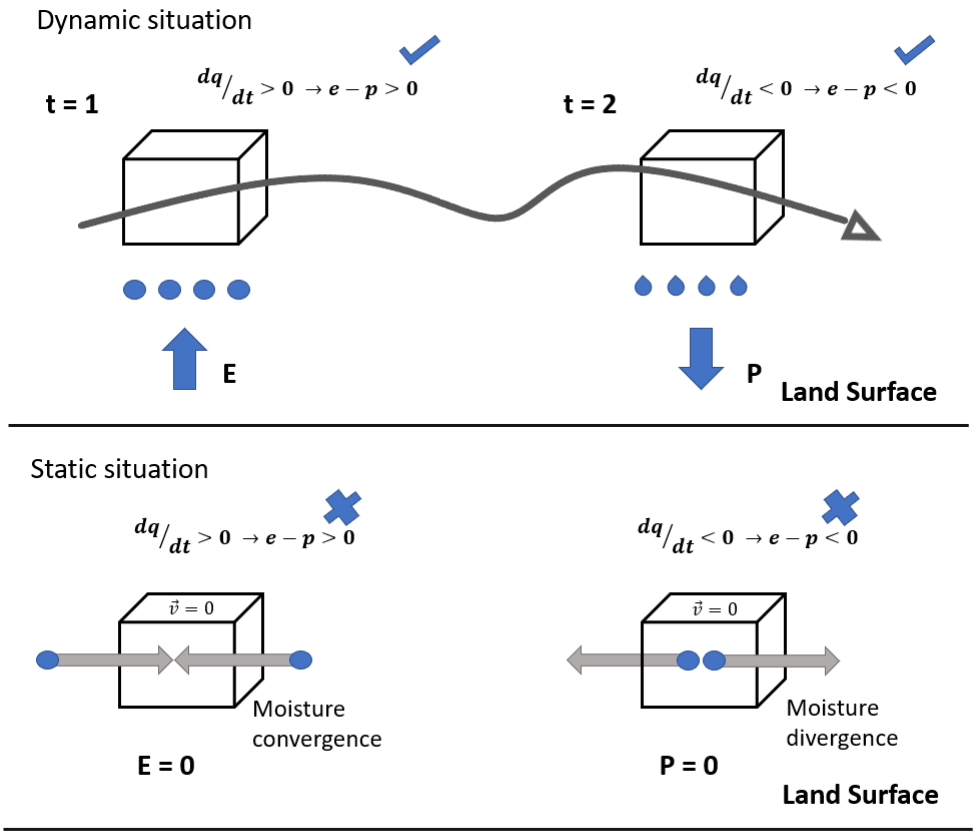

Figure 6.10: Schematic representation of the problem with convergence and divergence of moisture undergone by the FLEXPART-WRF.

local moisture sources, such as the Mediterranean Sea, there is generally a better match, but significant biases still exist.

Based on our experiments, we found that the FLEXPART-WRF model has limitations for quantitative moisture source analysis in certain case studies, particularly for estimating moisture contributions from remote sources like the tropics and subtropics in our case. However, in November, the underestimation for tropical and subtropical moisture was significantly less than in October due to higher winds that allowed air parcels to travel faster along a narrower pathway. In contrast, slower particle movement and diverse paths in October led to more backward dispersion in time and more time spent in regions with weak winds, which made calculations more challenging. Another inherent problem associated with re-estimating moisture values is that the more distant a source and the more precipitation that occurs in the intermediate steps, the more devalued the contribution of that source will be. This could explain why the Lagrangian models always estimate tropical sources' contributions lower than the Eulerian model. The U-Track model results, however, did not show significant enhancement. Although not central to the study, these findings contribute to our overall understanding of moisture estimates. Therefore, determining moisture presents a challenge in numerical terms and requires numerous refinements in estimation and calculation, which can significantly influence the results.

Another important consideration is related to the unrealistic values that the FLEXPART-WRF yields in some parts of the study region, especially for the October case over the Sahara. The $E-P$ values suggest a significant moisture gain, but it is not possible for that gain to come from a surface evaporation flux because evaporation over that area is essentially zero. We initially hypothesized that these unrealistic values might be due to phase changes, which are not taken into account by the FLEXPART-WRF. To measure this impact, we utilized the six moisture species (vapor, cloud water, rainwater, snow, ice, and graupel) present in the WRF model, which enabled us to incorporate the combined total of these species in the FLEXPART-WRF. In other words, we conducted a calculation similar to Eq. (1), but this time with q representing the sum of all moisture species within an air parcel instead of only water vapor. The results indicate that the influence of including liquid and solid water in the model is negligible, with an average relative difference of only 4% in $E-P$ field values (as shown in Figure 6.9).

Finally, another issue that could have contributed the most to the errors encountered is the fact that the FLEXPART-WRF neglects the convergence and divergence of moisture, as shown in Figure 6.10. This issue requires further investigation, specifically focused on situations involving moisture convergence and divergence, to establish a more robust and definitive conclusion.

GENERAL CONCLUSIONS

The aim of this thesis was to study the Lagrangian transport of moisture and plastic debris in the atmosphere and ocean, respectively. For the latter case, a particle tracking approach was developed, where no transported quantities were considered, but only the evolution of the particle position on the ocean surface. Initially, a validation study of the numerical model was carried out, and subsequently, it was applied to a large-scale problem. For the atmosphere, two Lagrangian models were used to study the transport of moisture, and their results were compared with those of an Eulerian model. Lagrangian models have the advantage that we can identify particle trajectories, as well as the evolution of quantities associated with them. Therefore, we studied the sources of moisture using a backtracking method in the atmosphere, while using a forward integration, we studied the accumulation areas for plastic debris in the ocean.

However, when studying complex physical problems, such as those presented here, certain phenomena are not solved adequately in terms of a Lagrangian description. For example, the dependence of model mismatch (Eulerian vs. Lagrangian) on the spatial resolution of the models, the different use of flow and turbulence information used by both methods on the same flow field, or the differences in computation time between Eulerian and Lagrangian methods (the Eulerian method usually requires less computing time than the Lagrangian method because the latter needs to track the development of each particle. Also, the particle number needs to be sufficiently large to ensure statistical stability) show the various issues among both methods that need to be adequately addressed. Other problems arising with the Lagrangian modeling of plastic debris are the influence of several factors on the transport of plastics, such as wind, waves, degradation, beaching, biofouling, or their size, among others, on the transport of plastics. These issues need to be incorporated into future developments for a better description of the phenomenon.

Taking everything mentioned above into account, the primary findings of this study are as follows.

- **Is the MOHID-Lagrangian model a good tool for marine litter tracking?** Yes, in the oceanographic field, the applicability of the MOHID-Lagrangian tool has been confirmed. Surface surveys have yielded satisfactory results when compared with data collected on beaches.

- **Is this model versatile for studying coastal accumulations?** Yes, the model allows for the configuration of beaching by modifying the depth parameter and probability of retention parameter. During the validation study utilizing coastal data, we assessed three different beaching probabilities to model high, medium, and low retention scenarios.

However, accurate characterization of retention requires high-resolution models of the coast as well as knowledge of the retention of the targeted coastal segment.

- **Can specific accumulation values be determined?** No, specific concentrations cannot be determined because the actual emission values of potential sources of discharges to the sea are unknown. However, concentrations can be determined in relative terms.

- **Can this model be used in regional and global studies?** Yes, in the second study presented in this thesis, the MOHID-Lagrangian tool was used to perform a regional statistical study to determine the accumulations in a domain covering the entire North Atlantic Ocean. However, as the size of the domain increases, the resolution of the models becomes lower and the concentrations determined become less reliable. Additionally, the reproduction of smaller-scale phenomena begins to be lost, resulting in less accurate results.

- **Do onshore emissions have a long range?** Our results indicate that the majority of accumulations occur at points close to the coast over a period of 7 years. However, particles have been observed to reach the Sargasso Sea within 7 years, implying that there is a likelihood of these particles reaching remote regions.

- **Is the dispersion of plastics a deterministic phenomenon?** The dispersion of plastics is primarily governed by ocean circulation phenomena, particularly surface currents in our particular case. This was confirmed by analyzing the results of dispersion and seasonal variation of the accumulations.

- **Is the use of Lagrangian methods a good approach for moisture allocation?** Yes, Lagrangian models are a good tool for moisture allocation as they are computationally efficient. This methodology allows us to determine the trajectory of moisture and identify potential sources of moisture. However, as they are offline methods, they require reliable input data.

- **Is the $E-P$ method a good indicator of sources and sinks?** No, the values associated with the $E-P$ map can serve as a first approximation to indicate moisture sources, but it is not a definitive indicator of sources and sinks. Since it is a single representation for a large period of time, some positive contributions may mask other negative ones. In addition, the E and P fields can be evaluated separately, considering this representation.

- **Therefore, is the recalculation of humidity related to all losses and gains along its path a good correction?** Yes, because in this way we can associate the gains or losses of each path separately to each area. However, this method also presents errors associated with the calculation itself. In the case of the most remote sources, the longer the trajectory, the more likely it is that an intermediate precipitation has occurred. Therefore, the higher the number of reestimates, the lower the weight of the source.

- **Can similar relative contributions be estimated by WRF-WVT and FLEXPART-WRF?** The results show that local sources can be determined similarly by both methods. However, when considering middle and remote regions, large disparities appear between the results. This may be due to calculation errors or attribution errors.

Appendix A

Supplementary Results

A.1 Results for Chapter 6

A.1.1 Sensitivity Analysis of the U-Track model

As a complement to the study presented in Chapter 6, a minor sensitivity analysis was conducted on the U-Track model to examine the effects of different configurations. Figure A.1 depicts the outcomes of modifying the vertical mixing parameter while considering the ω field from ERA5 for the October event. Similar to this, A.2 presents the results for the November event. A.3 shows the influence of the integration time step for both events.

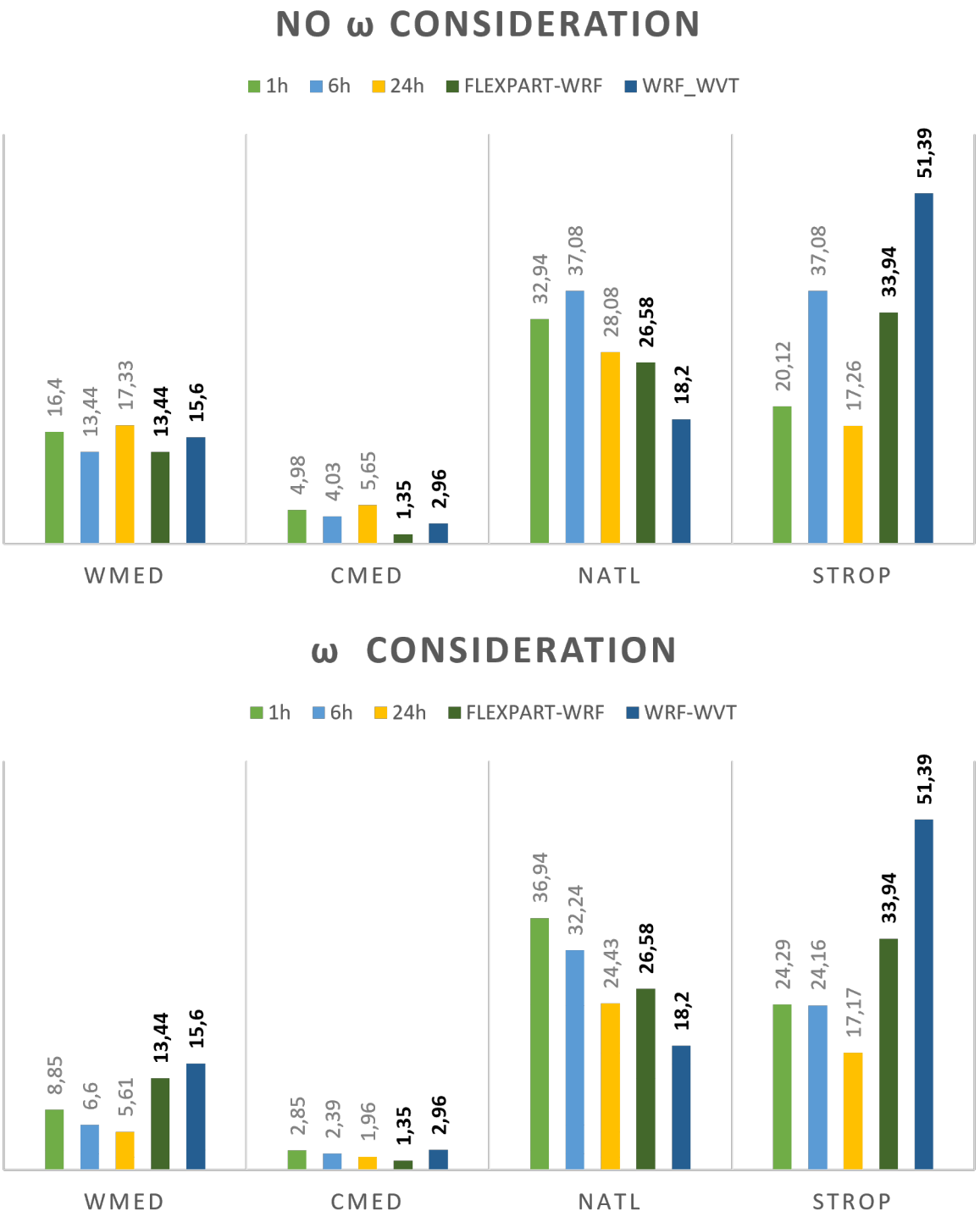

Figure A.1: U-Track sensitivity analysis for the vertical mixing parametrization for the October event.

Figure A.2: U-Track sensitivity analysis for the vertical mixing parametrization for the November event.

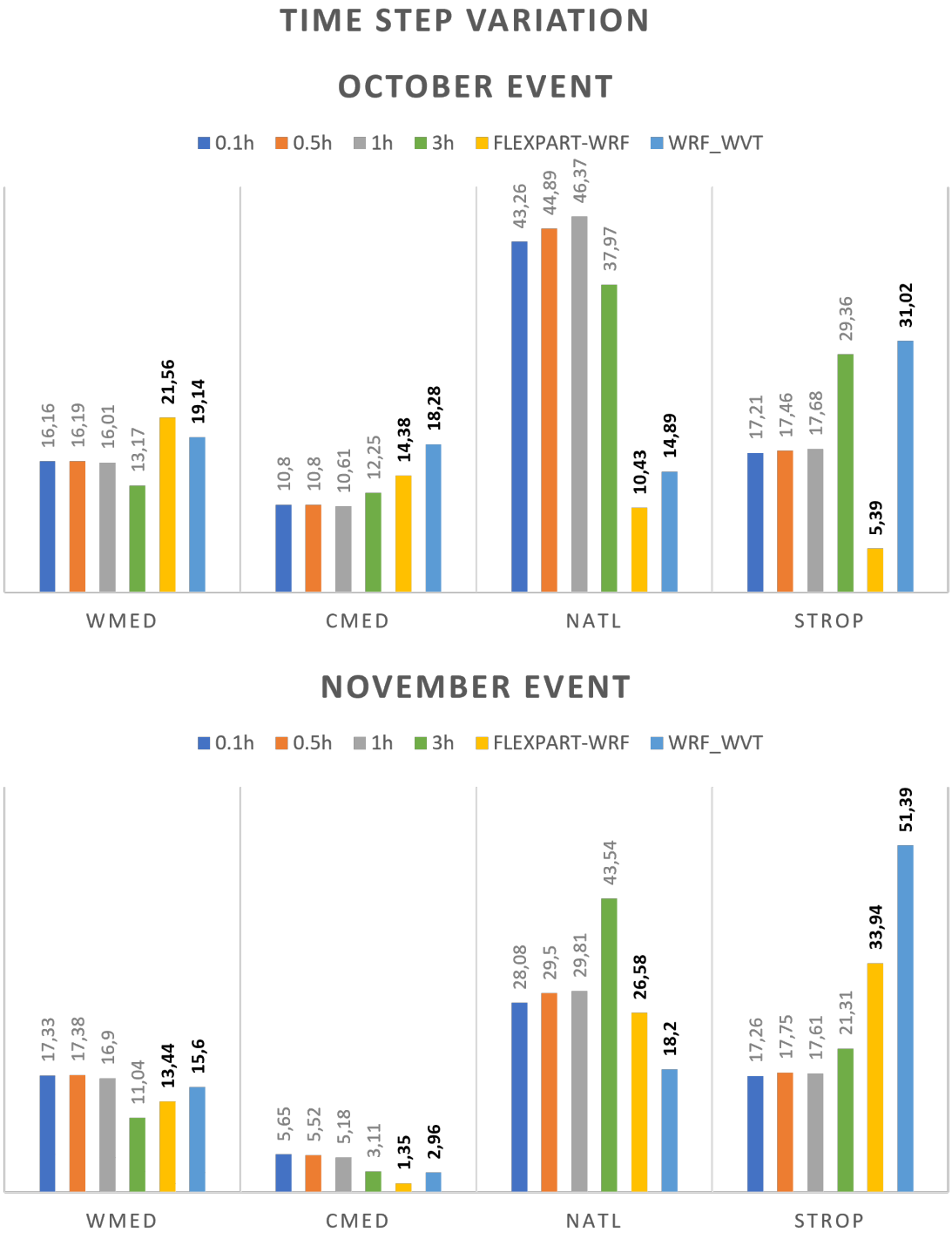

Figure A.3: U-Track sensitivity analysis for the integration time step for both events.

Appendix

Copyright Permissions

Figure 2.1

This figure is published in an article by IOP Publishing. All articles from this publisher are licenced under the Creative Commons Attribution 4.0 licence `https://creativecommons.org/licenses/by/4.0/` and therefore permission is not required. For further information, please refer to `https://ioppublishing.org/copyright/`

Figure 3.2

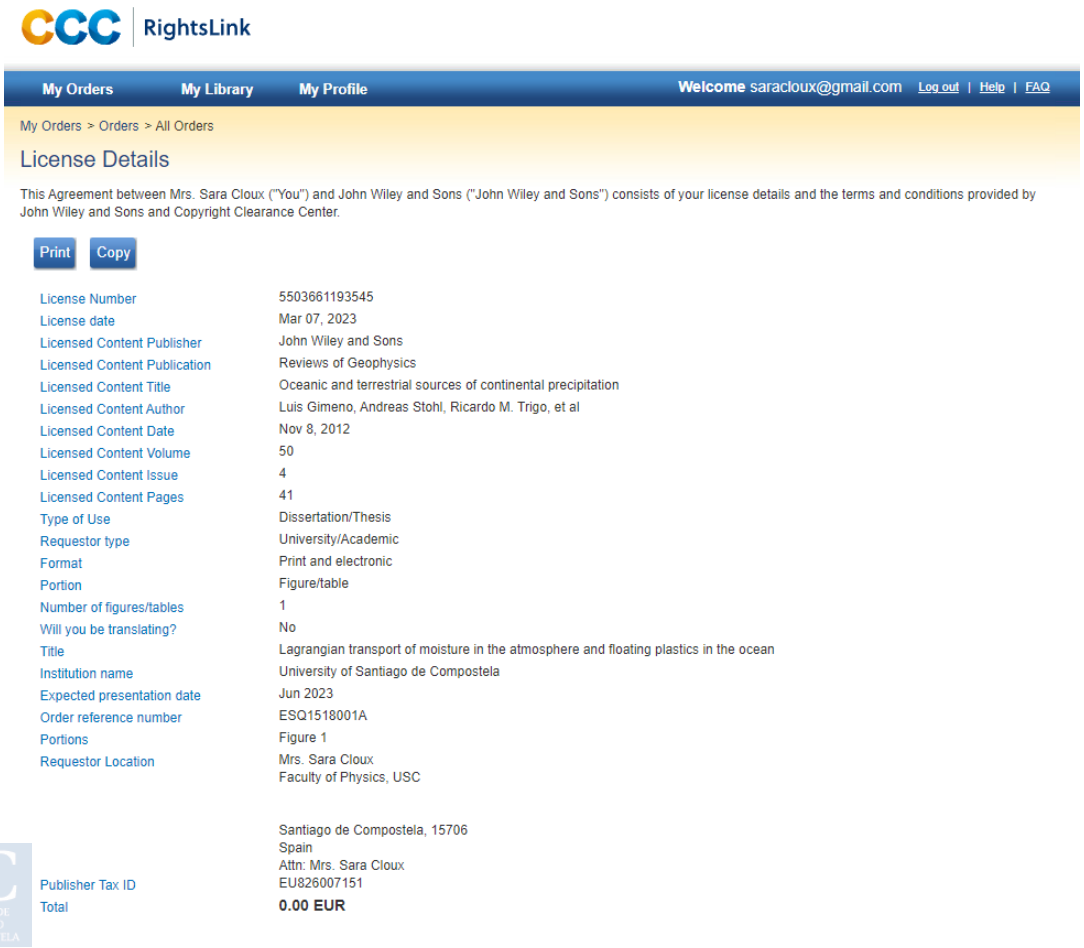

CCC RightsLink

My Orders | My Library | My Profile — Welcome saracloux@gmail.com Log out | Help | FAQ

My Orders > Orders > All Orders

License Details

This Agreement between Mrs. Sara Cloux ("You") and John Wiley and Sons ("John Wiley and Sons") consists of your license details and the terms and conditions provided by John Wiley and Sons and Copyright Clearance Center.

Print Copy

License Number	5503661193545
License date	Mar 07, 2023
Licensed Content Publisher	John Wiley and Sons
Licensed Content Publication	Reviews of Geophysics
Licensed Content Title	Oceanic and terrestrial sources of continental precipitation
Licensed Content Author	Luis Gimeno, Andreas Stohl, Ricardo M. Trigo, et al
Licensed Content Date	Nov 8, 2012
Licensed Content Volume	50
Licensed Content Issue	4
Licensed Content Pages	41
Type of Use	Dissertation/Thesis
Requestor type	University/Academic
Format	Print and electronic
Portion	Figure/table
Number of figures/tables	1
Will you be translating?	No
Title	Lagrangian transport of moisture in the atmosphere and floating plastics in the ocean
Institution name	University of Santiago de Compostela
Expected presentation date	Jun 2023
Order reference number	ESQ1518001A
Portions	Figure 1
Requestor Location	Mrs. Sara Cloux Faculty of Physics, USC Santiago de Compostela, 15706 Spain Attn: Mrs. Sara Cloux
Publisher Tax ID	EU826007151
Total	**0.00 EUR**

Figure 3.3

This figure is published in an article by Copernicus Publications. All articles from this publisher are licenced under the Creative Commons Attribution 4.0 licence https://creativecommons.org/licenses/by/4.0/ and therefore permission is not required. For further information, please refer to https://www.hydrology-and-earth-system-sciences.net/policies/licence_and_copyright.html

Figure 3.4

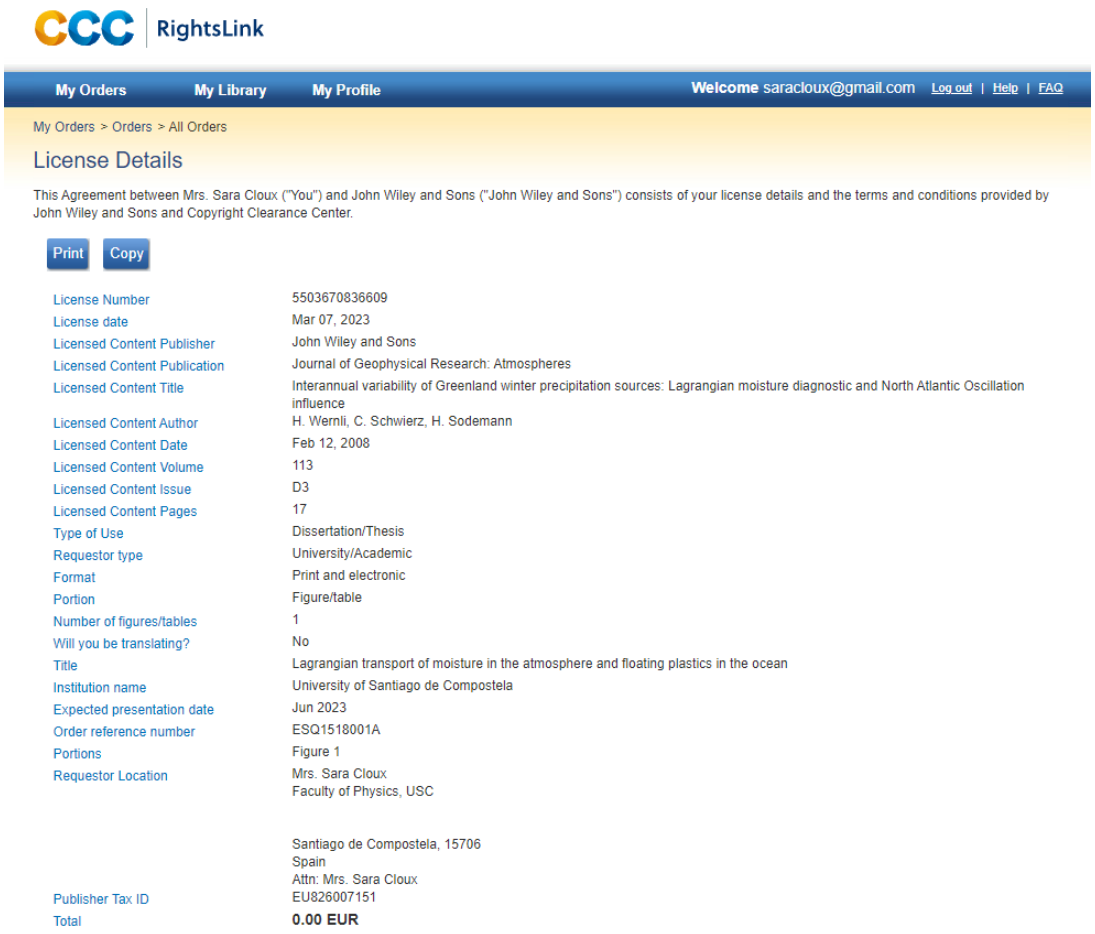

RightsLink

My Orders | My Library | My Profile | Welcome saracloux@gmail.com | Log out | Help | FAQ

My Orders > Orders > All Orders

License Details

This Agreement between Mrs. Sara Cloux ("You") and John Wiley and Sons ("John Wiley and Sons") consists of your license details and the terms and conditions provided by John Wiley and Sons and Copyright Clearance Center.

Print Copy

License Number	5503670836609
License date	Mar 07, 2023
Licensed Content Publisher	John Wiley and Sons
Licensed Content Publication	Journal of Geophysical Research: Atmospheres
Licensed Content Title	Interannual variability of Greenland winter precipitation sources: Lagrangian moisture diagnostic and North Atlantic Oscillation influence
Licensed Content Author	H. Wernli, C. Schwierz, H. Sodemann
Licensed Content Date	Feb 12, 2008
Licensed Content Volume	113
Licensed Content Issue	D3
Licensed Content Pages	17
Type of Use	Dissertation/Thesis
Requestor type	University/Academic
Format	Print and electronic
Portion	Figure/table
Number of figures/tables	1
Will you be translating?	No
Title	Lagrangian transport of moisture in the atmosphere and floating plastics in the ocean
Institution name	University of Santiago de Compostela
Expected presentation date	Jun 2023
Order reference number	ESQ1518001A
Portions	Figure 1
Requestor Location	Mrs. Sara Cloux Faculty of Physics, USC Santiago de Compostela, 15706 Spain Attn: Mrs. Sara Cloux
Publisher Tax ID	EU826007151
Total	**0.00 EUR**

Figure 3.1

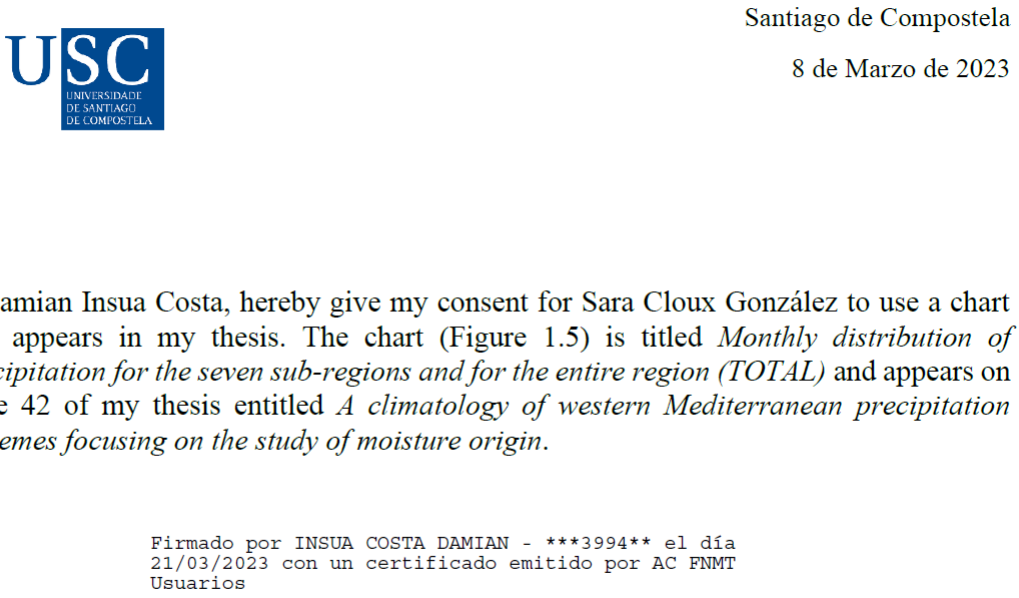

Santiago de Compostela

8 de Marzo de 2023

I, Damian Insua Costa, hereby give my consent for Sara Cloux González to use a chart that appears in my thesis. The chart (Figure 1.5) is titled *Monthly distribution of precipitation for the seven sub-regions and for the entire region (TOTAL)* and appears on page 42 of my thesis entitled *A climatology of western Mediterranean precipitation extremes focusing on the study of moisture origin*.

Firmado por INSUA COSTA DAMIAN - ***3994** el día 21/03/2023 con un certificado emitido por AC FNMT Usuarios

Figure 3.5 This figure is published in an article by Copernicus Publications. All articles from this publisher are licenced under the Creative Commons Attribution 4.0 licence https://creativecommons.org/licenses/by/4.0/ and therefore permission is not required. For further information, please refer to https://www.hydrology-and-earth-system-sciences.net/policies/licence_and_copyright.html

Article 1 S. Cloux, D. Garaboa-Paz, D. Insua-Costa, G. Miguez-Macho, & V. Pérez-Muñuzuri, "Extreme precipitation events in the Mediterranean area: contrasting two different models for moisture source identification." Hydrology and Earth System Sciences, 25(12), 6465-6477. 2021. DOI: https://doi.org/10.5194/hess-25-6465-2021

This is an open access article distributed under the terms of the Creative Commons CC-BY license https://creativecommons.org/licenses/by/4.0/ and therefore permission is not required. For further information, please refer to https://service.elsevier.com/app/contact/supporthub/permissions-helpdesk/

Article 2 S. Cloux, P. Pérez, H. de Pablo and V. Pérez Muñuzuri, "A regional Lagrangian model to evaluate the dispersion of floating macroplastics in the North Atlantic Ocean from different types of sources in the Iberian Peninsula." 2023.

This article, when published, will also be licenced under the Creative Commons CC-BY license https://creativecommons.org/licenses/by/4.0/. For further

information, please refer to https://service.elsevier.com/app/contact/supporthub/permissions-helpdesk/

Article 3 S. Cloux, D. Garaboa-Paz, D. Insua-Costa, G. Miguez-Macho, & V. Pérez-Muñuzuri, "Extreme precipitation events in the Mediterranean area: contrasting two different models for moisture source identification." Hydrology and Earth System Sciences, 25(12), 6465-6477. 2021. DOI: https://doi.org/10.5194/hess-25-6465-2021

Bibliography

[1] H. Schamel, "Lagrangian fluid description with simple applications in compressible plasma and gas dynamics," 2004.

[2] G. Haller, "Lagrangian coherent structures," 2015.

[3] R. Samulyak, X. Wang, and H. C. Chen, "Lagrangian particle method for compressible fluid dynamics," *Journal of Computational Physics*, 2018.

[4] T. Murashima and T. Taniguchi, "Multiscale Lagrangian fluid dynamics simulation for polymeric fluid," *Journal of Polymer Science, Part B: Polymer Physics*, 2010.

[5] P. B. Ryzhakov, R. Rossi, S. R. Idelsohn, and E. Oñate, "A monolithic Lagrangian approach for fluid-structure interaction problems," *Computational Mechanics*, 2010.

[6] K. Takabatake, X. Sun, M. Sakai, D. Pavlidis, J. Xiang, and C. C. Pain, "Numerical study on a heat transfer model in a Lagrangian fluid dynamics simulation," *International Journal of Heat and Mass Transfer*, 2016.

[7] A. Darwish, G. Di Labbio, W. Saleh, and L. Kadem, "In vitro characterization of Lagrangian fluid transport downstream of a dysfunctional bileaflet mechanical aortic valve," *AIP Advances*, 2020.

[8] A. Darwish, S. Norouzi, G. Di Labbio, and L. Kadem, "Extracting Lagrangian coherent structures in cardiovascular flows using Lagrangian descriptors," *Physics of Fluids*, 2021.

[9] R. Duran, F. J. Beron-Vera, and M. J. Olascoaga, "Extracting quasi-steady Lagrangian transport patterns from the ocean circulation: An application to the Gulf of Mexico," *Scientific Reports*, 2018.

[10] A. Bower, S. Lozier, A. Biastoch, K. Drouin, N. Foukal, H. Furey, M. Lankhorst, S. Rühs, and S. Zou, "Lagrangian Views of the Pathways of the Atlantic Meridional Overturning Circulation," 2019.

[11] L. Rousselet, P. Cessi, and G. Forget, "Routes of the Upper Branch of the Atlantic Meridional Overturning Circulation according to an Ocean State Estimate," *Geophysical Research Letters*, 2020.

[12] T. Kukulka and F. Veron, "Lagrangian investigation of wave-driven turbulence in the ocean surface boundary layer," *Journal of Physical Oceanography*, 2019.

[13] S. Berti and G. Lapeyre, "Lagrangian pair dispersion in upper-ocean turbulence in the presence of mixed-layer instabilities," *Physics of Fluids*, 2021.

[14] S. Kelly, E. Popova, Y. Aksenov, R. Marsh, and A. Yool, "Lagrangian Modeling of Arctic Ocean Circulation Pathways: Impact of Advection on Spread of Pollutants," *Journal of Geophysical Research: Oceans*, 2018.

[15] N. Schmidt, V. Fauvelle, A. Ody, J. Castro-Jiménez, J. Jouanno, T. Changeux, T. Thibaut, and R. Sempéré, "The Amazon River: A Major Source of Organic Plastic Additives to the Tropical North Atlantic?" *Environmental Science and Technology*, 2019.

[16] M. K. Gough, F. J. Beron-Vera, M. J. Olascoaga, J. Sheinbaum, J. Jouanno, and R. Duran, "Persistent Lagrangian transport patterns in the northwestern Gulf of Mexico," *Journal of Physical Oceanography*, 2019.

[17] D. Lindo-Atichati, P. Montero, R. Rodil, J. B. Quintana, and M. Miró, "Modeling Dispersal of UV Filters in Estuaries," *Environmental Science and Technology*, 2019.

[18] J. Staneva, M. Ricker, R. C. Alvarez, Ø. Breivik, and C. Schrum, "Effects of wave-induced processes in a coupled wave-ocean model on particle transport simulations," *Water (Switzerland)*, 2021.

[19] T. S. M. Amelia, W. M. A. W. M. Khalik, M. C. Ong, Y. T. Shao, H. J. Pan, and K. Bhubalan, "Marine microplastics as vectors of major ocean pollutants and its hazards to the marine ecosystem and humans," 2021.

[20] S. Krause, M. Molari, E. V. Gorb, S. N. Gorb, E. Kossel, and M. Haeckel, "Persistence of plastic debris and its colonization by bacterial communities after two decades on the abyssal seafloor," *Scientific Reports*, 2020.

[21] N. Rangel-Buitrago, A. Williams, M. F. Costa, and V. de Jonge, "Curbing the inexorable rising in marine litter: An overview," *Ocean and Coastal Management*, 2020.

[22] K. Min, J. D. Cuiffi, and R. T. Mathers, "Ranking environmental degradation trends of plastic marine debris based on physical properties and molecular structure," *Nature Communications*, 2020.

[23] C. Wayman and H. Niemann, "The fate of plastic in the ocean environment-a minireview," *Environmental Science: Processes and Impacts*, vol. 23, no. 2, pp. 198–212, 2021.

[24] A. Alfaro-Núñez, D. Astorga, L. Cáceres-Farías, L. Bastidas, C. Soto Villegas, K. Macay, and J. H. Christensen, "Microplastic pollution in seawater and marine organisms across the Tropical Eastern Pacific and Galápagos," *Scientific Reports*, vol. 11, no. 1, dec 2021.

[25] M. E. Miller, M. Hamann, and F. J. Kroon, "Bioaccumulation and biomagnification of microplastics in marine organisms: A review and meta-analysis of current data," oct 2020.

[26] E. Guzzetti, A. Sureda, S. Tejada, and C. Faggio, "Microplastic in marine organism: Environmental and toxicological effects," pp. 164–171, dec 2018.

[27] D. Yang, H. Shi, L. Li, J. Li, K. Jabeen, and P. Kolandhasamy, "Microplastic Pollution in Table Salts from China," *Environmental Science and Technology*, vol. 49, no. 22, 2015.

[28] M. Chalbot, M. Lianou, I. Vei, A. Kotronarou, and I. G. Kavouras, "Spatial attribution of sulfate and dust aerosol sources in an urban area using receptor modeling coupled with Lagrangian trajectories," *Atmospheric Pollution Research*, vol. 4, no. 3, pp. 346–353, 2013.

[29] Y. Yan, X. Li, Y. Shang, and J. Tu, "Evaluation of airborne disease infection risks in an airliner cabin using the Lagrangian-based Wells-Riley approach," *Building and environment*, vol. 121, pp. 79–92, 2017.

[30] A. D. Urlea, N. Barbu, S. Andrei, and S. Ştefan, "Simulation of Vesuvius volcanic ash hazards within Romanian airspace using the Hybrid Single-Particle Lagrangian Integrated Trajectory Volcanic Ash numerical model," *Meteorological Applications*, vol. 28, no. 3, p. e2001, 2021.

[31] D. Insua-Costa, M. Lemus-Cánovas, G. Miguez-Macho, and M. C. Llasat, "Climatology and ranking of hazardous precipitation events in the western Mediterranean area," *Atmospheric Research*, 2021.

[32] J. I. Barredo, "Major flood disasters in Europe: 1950-2005," *Natural Hazards*, 2007.

[33] R. Nieto, L. Gimeno, A. Drumond, and E. Hernandez, "A Lagrangian identification of the main moisture sources and sinks affecting the Mediterranean area," *WSEAS Transactions on Environment and Development*, 2010.

[34] J. I. Steinfeld, "Atmospheric Chemistry and Physics: From Air Pollution to Climate Change," *Environment: Science and Policy for Sustainable Development*, 1998.

[35] Z. Neufeld and E. Hernández-García, *Chemical and Biological Processes in Fluid Flows: A Dynamical Systems Approach*, 2009.

[36] G. Haller and T. Sapsis, "Where do inertial particles go in fluid flows?" *Physica D: Nonlinear Phenomena*, vol. 237, no. 5, pp. 573–583, 2008.

[37] F. J. Beron-Vera, M. J. Olascoaga, and R. Lumpkin, "Inertia-induced accumulation of flotsam in the subtropical gyres," *Geophysical Research Letters*, vol. 43, no. 23, pp. 12,228–12,233, 2016.

[38] F. J. Beron-Vera, M. J. Olascoaga, and P. Miron, "Building a Maxey-Riley framework for surface ocean inertial particle dynamics," *Physics of Fluids*, 2019.

[39] P. Miron, M. J. Olascoaga, F. J. Beron-Vera, N. F. Putman, J. Triñanes, R. Lumpkin, and G. J. Goni, "Clustering of Marine-Debris- and Sargassum-Like Drifters Explained by Inertial Particle Dynamics," *Geophysical Research Letters*, 2020.

[40] R. Geyer, J. R. Jambeck, and K. L. Law, "Production, use, and fate of all plastics ever made," *Science Advances*, 2017.

[41] ——, "Supplementary Materials for: Production, use, and fate of all plastics ever made," *Science Advances*, 2017.

[42] L. Lebreton, M. Egger, and B. Slat, "A global mass budget for positively buoyant macroplastic debris in the ocean," *Scientific Reports*, 2019.

[43] P. G. Ryan, "Does size and buoyancy affect the long-distance transport of floating debris?" *Environmental Research Letters*, 2015.

[44] E. Van Sebille, S. Aliani, K. L. Law, N. Maximenko, J. M. Alsina, A. Bagaev, M. Bergmann, B. Chapron, I. Chubarenko, A. Cózar, P. Delandmeter, M. Egger, B. Fox-Kemper, S. P. Garaba, L. Goddijn-Murphy, B. D. Hardesty, M. J. Hoffman, A. Isobe, C. E. Jongedijk, M. L. Kaandorp, L. Khatmullina, A. A. Koelmans, T. Kukulka, C. Laufkötter, L. Lebreton, D. Lobelle, C. Maes, V. Martinez-Vicente, M. A. Morales Maqueda, M. Poulain-Zarcos, E. Rodríguez, P. G. Ryan, A. L. Shanks, W. J. Shim, G. Suaria, M. Thiel, T. S. Van Den Bremer, and D. Wichmann, "The physical oceanography of the transport of floating marine debris," p. 2, 2020.

[45] N. Maximenko, J. Hafner, and P. Niiler, "Pathways of marine debris derived from trajectories of Lagrangian drifters," *Marine Pollution Bulletin*, 2012.

[46] A. Cozar, F. Echevarria, J. I. Gonzalez-Gordillo, X. Irigoien, B. Ubeda, S. Hernandez-Leon, A. T. Palma, S. Navarro, J. Garcia-de Lomas, A. Ruiz, M. L. Fernandez-de Puelles, and C. M. Duarte, "Plastic debris in the open ocean," *Proceedings of the National Academy of Sciences*, vol. 111, no. 28, pp. 10 239–10 244, 2014. [Online]. Available: http://www.pnas.org/cgi/doi/10.1073/pnas.1314705111

[47] V. Onink, D. Wichmann, P. Delandmeter, and E. van Sebille, "The Role of Ekman Currents, Geostrophy, and Stokes Drift in the Accumulation of Floating Microplastic," *Journal of Geophysical Research: Oceans*, 2019.

[48] L. Lebreton, B. Slat, F. Ferrari, B. Sainte-Rose, J. Aitken, R. Marthouse, S. Hajbane, S. Cunsolo, A. Schwarz, A. Levivier, K. Noble, P. Debeljak, H. Maral, R. Schoeneich-Argent, R. Brambini, and J. Reisser, "Evidence that the Great Pacific Garbage Patch is rapidly accumulating plastic," *Scientific Reports*, 2018.

[49] C. Maes, B. Blanke, and E. Martinez, "Origin and fate of surface drift in the oceanic convergence zones of the eastern Pacific," *Geophysical Research Letters*, 2016.

[50] L. Brach, P. Deixonne, M. F. Bernard, E. Durand, M. C. Desjean, E. Perez, E. van Sebille, and A. ter Halle, "Anticyclonic eddies increase accumulation of microplastic in the North Atlantic subtropical gyre," *Marine Pollution Bulletin*, 2018.

[51] C. Dong, Y. Liu, R. Lumpkin, M. Lankhorst, D. Chen, J. C. Mcwilliams, and Y. Guan, "A Scheme to identify loops from trajectories of oceanic surface drifters: An application in the kuroshio extension region," *Journal of Atmospheric and Oceanic Technology*, 2011.

[52] G. G. Stokes, "On the theory of oscillatory waves," *Trans. Cam. Philos. Soc.*, vol. 8, pp. 441–455, 1847.

[53] F. J. Tapia, J. Pineda, F. J. Ocampo-Torres, H. L. Fuchs, P. E. Parnell, P. Montero, and S. Ramos, "High-frequency observations of wind-forced onshore transport at a coastal site in Baja California," *Continental Shelf Research*, 2004.

[54] G. S. Enrico Zambianchi Ilaria Iermano and S. Aliani, "Marine litter in the Mediterranean Sea: an oceanographic perspective," *Marine litter in the Mediterranean and Black Sea*, 2014.

[55] I. Langmuir, "Surface motion of water induced by wind," *Science*, 1938.

[56] E. M. Acha, A. Piola, O. Iribarne, and H. Mianzan, *Ecological processes at marine fronts: oases in the ocean*. Springer, 2015.

[57] E. C. Atwood, F. M. Falcieri, S. Piehl, M. Bochow, M. Matthies, J. Franke, S. Carniel, M. Sclavo, C. Laforsch, and F. Siegert, "Coastal accumulation of microplastic particles emitted from the Po River, Northern Italy: Comparing remote sensing and hydrodynamic modelling with in situ sample collections," *Marine Pollution Bulletin*, 2019.

[58] I. Peeken, S. Primpke, B. Beyer, J. Gütermann, C. Katlein, T. Krumpen, M. Bergmann, L. Hehemann, and G. Gerdts, "Arctic sea ice is an important temporal sink and means of transport for microplastic," *Nature Communications*, 2018.

[59] J. H. Trowbridge and S. J. Lentz, "The bottom boundary layer," 2018.

[60] R. T. Buxton, C. A. Currey, P. O. Lyver, and C. J. Jones, "Incidence of plastic fragments among burrow-nesting seabird colonies on offshore islands in northern New Zealand," *Marine Pollution Bulletin*, 2013.

[61] M. Kooi, E. H. Van Nes, M. Scheffer, and A. A. Koelmans, "Ups and Downs in the Ocean: Effects of Biofouling on Vertical Transport of Microplastics," *Environmental Science and Technology*, 2017.

[62] A. Gallagher, P. Randall, D. Sivyer, U. Binetti, G. Lokuge, and M. Munas, "Abandoned, lost or otherwise discarded fishing gear (ALDFG) in Sri Lanka – A pilot study collecting baseline data," *Marine Policy*, vol. 148, no. January, p. 105386, 2023. [Online]. Available: https://doi.org/10.1016/j.marpol.2022.105386

[63] D. A. Lavers and G. Villarini, "The nexus between atmospheric rivers and extreme precipitation across Europe," *Geophysical Research Letters*, 2013.

[64] D. Stuparu, M. van der Meulen, F. Kleissen, D. Vethaak, and G. El Serafy, "Developing a transport model for plastic distribution in the North Sea," in *E-proceedings of the 36th IAHR World Congress*, vol. 28, 2015.

[65] M. W. Lammerts, "Marine litter in port areas-developing a propagation model," 2016.

[66] M. C. Sousa, M. DeCastro, J. Gago, A. S. Ribeiro, M. Des, J. L. Gómez-Gesteira, J. M. Dias, and M. Gomez-Gesteira, "Modelling the distribution of microplastics released by wastewater treatment plants in Ria de Vigo (NW Iberian Peninsula)," *Marine Pollution Bulletin*, 2021.

[67] D. F. Carlson, G. Suaria, S. Aliani, E. Fredj, T. Fortibuoni, A. Griffa, A. Russo, and V. Melli, "Combining litter observations with a regional ocean model to identify sources and sinks of floating debris in a semi-enclosed basin: The Adriatic Sea," *Frontiers in Marine Science*, 2017.

[68] W. R. Turrell, "How litter moves along a macro tidal mid-latitude coast exposed to a coastal current," *Marine Pollution Bulletin*, 2020.

[69] F. Campuzano, D. Brito, M. Juliano, R. Fernandes, H. de Pablo, and R. Neves, "Coupling watersheds, estuaries and regional ocean through numerical modelling for Western Iberia: a novel methodology," *Ocean Dynamics*, 2016.

[70] "EMDAT.database." [Online]. Available: http://www.emdat.be/database

[71] M. C. Llasat, M. Llasat-Botija, M. A. Prat, F. Porcú, C. Price, A. Mugnai, K. Lagouvardos, V. Kotroni, D. Katsanos, S. Michaelides, Y. Yair, K. Savvidou, and K. Nicolaides, "High-impact floods and flash floods in Mediterranean countries: The FLASH preliminary database," *Advances in Geosciences*, 2010.

[72] A. Buzzi, N. Tartaglione, and P. Malguzzi, "Numerical simulations of the 1994 piedmont flood: Role of orography and moist processes," *Monthly Weather Review*, 1998.

[73] M. C. Llasat, "High magnitude storms and floods," *The Physical Geography of the Mediterranean, edited by: Woodward, JC, Oxford University Press, Oxford*, pp. 513–540, 2009.

[74] U. Dayan, K. Nissen, and U. Ulbrich, "Review Article: Atmospheric conditions inducing extreme precipitation over the eastern and western Mediterranean," 2015.

[75] A. Mariotti, M. V. Struglia, N. Zeng, and K. M. Lau, "The hydrological cycle in the Mediterranean region and implications for the water budget of the Mediterranean sea," *Journal of Climate*, 2002.

[76] R. Nieto, L. Gimeno, L. de la Torre, P. Ribera, D. Gallego, R. García-Herrera, J. A. García, M. Nuñez, A. Redaño, and J. Lorente, "Climatological features of cutoff low systems in the Northern Hemisphere," *Journal of Climate*, 2005.

[77] C. Soci, E. Bazile, F. O. Besson, and T. Landelius, "High-resolution precipitation re-analysis system for climatological purposes," *Tellus, Series A: Dynamic Meteorology and Oceanography*, 2016.

[78] D. Insua-Costa, "A climatology of western Mediterranean precipitation extremes focusing on the study of moisture origin," Ph.D. dissertation, Santiago de Compostela, 2021.

[79] M. C. Llasat, M. Llasat-Botija, O. Petrucci, A. A. Pasqua, J. Rosselló, F. Vinet, and L. Boissier, "Towards a database on societal impact of Mediterranean floods within the framework of the HYMEX project," *Natural Hazards and Earth System Science*, 2013.

[80] A. Winschall, S. Pfahl, H. Sodemann, and H. Wernli, "Impact of North Atlantic evaporation hot spots on southern Alpine heavy precipitation events," *Quarterly Journal of the Royal Meteorological Society*, 2012.

[81] J. G. Pinto, S. Ulbrich, A. Parodi, R. Rudari, G. Boni, and U. Ulbrich, "Identification and ranking of extraordinary rainfall events over Northwest Italy: The role of Atlantic moisture," *Journal of Geophysical Research Atmospheres*, 2013.

[82] S. O. Krichak, J. Barkan, J. S. Breitgand, S. Gualdi, and S. B. Feldstein, "The role of the export of tropical moisture into midlatitudes for extreme precipitation events in the Mediterranean region," *Theoretical and Applied Climatology*, 2015.

[83] D. Insua-Costa, G. Miguez-Macho, and C. Llasat, "Local and remote moisture sources for extreme precipitation: A study of the two catastrophic 1982 western Mediterranean episodes," *Hydrology and Earth System Sciences*, vol. 23, no. 9, pp. 3885–3900, 2019.

[84] F. Dominguez, H. Hu, and J. A. Martinez, "Two-layer dynamic recycling model (2L-DRM): learning from moisture tracking models of different complexity," *Journal of Hydrometeorology*, vol. 21, no. 1, pp. 3–16, 2020.

[85] O. Reale, L. Feudale, and B. Turato, "Evaporative moisture sources during a sequence of floods in the Mediterranean region," *Geophysical Research Letters*, 2001.

[86] B. Turato, O. Reale, and F. Siccardi, "Water vapor sources of the October 2000 Piedmont flood," *Journal of Hydrometeorology*, 2004.

[87] F. Duffourg and V. Ducrocq, "Origin of the moisture feeding the heavy precipitating systems over southeastern France," *Natural Hazards and Earth System Science*, 2011.

[88] L. Gimeno, A. Stohl, R. M. Trigo, F. Dominguez, K. Yoshimura, L. Yu, A. Drumond, A. M. Durn-Quesada, and R. Nieto, "Oceanic and terrestrial sources of continental precipitation," *Reviews of Geophysics*, 2012.

[89] K. E. Trenberth, L. Smith, T. Qian, A. Dai, and J. Fasullo, "Estimates of the global water budget and its annual cycle using observational and model Data," 2007.

[90] A. Numaguti, "Origin and recycling processes of precipitating water over the Eurasian continent: Experiments using an atmospheric general circulation model," *Journal of Geophysical Research Atmospheres*, 1999.

[91] H. Sodemann and A. Stohl, "Moisture origin and meridional transport in atmospheric rivers and their association with multiple cyclones," *Monthly Weather Review*, 2013.

[92] R. A. Houze, "Cloud dynamics," *Cloud dynamics*, 1993.

[93] K. L. Brubaker, D. Entekhabi, and P. S. Eagleson, "Estimation of continental precipitation recycling," *Journal of Climate*, 1993.

[94] A. Rios-Entenza and G. Miguez-Macho, "Moisture recycling and the maximum of precipitation in spring in the Iberian Peninsula," *Climate Dynamics*, 2014.

[95] G. I. Burde and A. Zangvil, "The estimation of regional precipitation recycling. Part I: Review of recycling models," *Journal of Climate*, 2001.

[96] G. I. Burde, "Bulk recycling models with incomplete vertical mixing. Part I: Conceptual framework and models," *Journal of Climate*, 2006.

[97] F. Dominguez, P. Kumar, X. Z. Liang, and M. Ting, "Impact of atmospheric moisture storage on precipitation recycling," *Journal of Climate*, 2006.

[98] P. A. Dirmeyer and K. L. Brubaker, "Characterization of the global hydrologic cycle from a back-trajectory analysis of atmospheric water vapor," *Journal of Hydrometeorology*, 2007.

[99] E. Salati, A. Dall'Olio, E. Matsui, and J. R. Gat, "Recycling of water in the Amazon Basin: An isotopic study," *Water Resources Research*, 1979.

[100] A. Henderson-Sellers, K. McGuffie, and H. Zhang, "Stable isotopes as validation tools for global climate model predictions of the impact of Amazonian deforestation," *Journal of Climate*, 2002.

[101] K. Yoshimura, T. Oki, and K. Ichiyanagi, "Evaluation of two-dimensional atmospheric water circulation fields in reanalyses by using precipitation isotopes databases," *Journal of Geophysical Research D: Atmospheres*, 2004.

[102] P. N. Blossey, Z. Kuang, and D. M. Romps, "Isotopic composition of water in the tropical tropopause layer in cloud-resolving simulations of an idealized tropical circulation," *Journal of Geophysical Research Atmospheres*, 2010.

[103] S. Joussaume, R. Sadourny, and J. Jouzel, "A general circulation model of water isotope cycles in the atmosphere," *Nature*, 1984.

[104] R. Koster, J. Jouzel, R. Suozzo, G. Russell, W. Broecker, D. Rind, and P. Eagleson, "Global sources of local precipitation as determined by the Nasa/Giss GCM," *Geophysical Research Letters*, 1986.

[105] M. G. Bosilovich and S. D. Schubert, "Water vapor tracers as diagnostics of the regional hydrologic cycle," *Journal of Hydrometeorology*, 2002.

[106] R. J. Van Der Ent, H. H. Savenije, B. Schaefli, and S. C. Steele-Dunne, "Origin and fate of atmospheric moisture over continents," *Water Resources Research*, 2010.

[107] R. J. van der Ent, O. A. Tuinenburg, H.-R. Knoche, H. Kunstmann, and H. H. G. Savenije, "Should we use a simple or complex model for moisture recycling and atmospheric moisture tracking?" *Hydrology and Earth System Sciences Discussions*, 2013.

[108] O. A. Tuinenburg and A. Staal, "Tracking the global flows of atmospheric moisture and associated uncertainties," *Hydrology and Earth System Sciences*, 2020.

[109] P. A. Dirmeyer and K. L. Brubaker, "Contrasting evaporative moisture sources during the drought of 1988 and the flood of 1993," *Journal of Geophysical Research: Atmospheres*, vol. 104, no. D16, pp. 19 383–19 397, 1999.

[110] A. Stohl, C. Forster, and H. Sodemann, "Remote sources of water vapor forming precipitation on the Norwegian west coast at 60°N - A tale of hurricanes and an atmospheric river," *Journal of Geophysical Research Atmospheres*, 2008.

[111] H. Sodemann, C. Schwierz, and H. Wernli, "Interannual variability of Greenland winter precipitation sources: Lagrangian moisture diagnostic and North Atlantic Oscillation influence," *Journal of Geophysical Research Atmospheres*, 2008.

[112] A. Stohl and P. James, "A Lagrangian analysis of the atmospheric branch of the global water cycle: Part 1: Method description, validation, and demonstration for the August 2002 flooding in central Europe," *Journal of Hydrometeorology*, 2004.

[113] ——, "A Lagrangian analysis of the atmospheric branch of the global water cycle. Part II: Moisture transports between earth's ocean basins and river catchments," *Journal of Hydrometeorology*, 2005.

[114] D. Insua-Costa and G. Miguez-Macho, "A new moisture tagging capability in the Weather Research and Forecasting model: Formulation, validation and application to the 2014 Great Lake-effect snowstorm," *Earth System Dynamics*, 2018.

[115] J. Brioude, D. Arnold, A. Stohl, M. Cassiani, D. Morton, P. Seibert, W. Angevine, S. Evan, A. Dingwell, J. D. Fast, R. C. Easter, I. Pisso, J. Burkhart, and G. Wotawa, "The Lagrangian particle dispersion model FLEXPART-WRF version 3.1," *Geoscientific Model Development*, 2013.

[116] et al. Skamarock WC, "A description of the advanced research WRF version 3, NCAR Tech. Note, NCAR/TN-468+STR," *Natl. Cent. for Atmos. Res. Boulder, Colorado*, 2008.

[117] K. A. Emanuel and M. Živković-Rothman, "Development and evaluation of a convection scheme for use in climate models," *Journal of the Atmospheric Sciences*, 1999.

[118] S. R. Hanna, "Atmospheric turbulence and air pollution modelling," *Atmospheric Turbulence and Air Pollution Modelling*, pp. 275–310, 1982.

[119] A. Herrera, A. Acosta-Dacal, O. Pérez Luzardo, I. Martínez, J. Rapp, S. Reinold, S. Montesdeoca-Esponda, D. Montero, and M. Gómez, "Bioaccumulation of additives and chemical contaminants from environmental microplastics in European seabass (Dicentrarchus labrax)," *Science of the Total Environment*, vol. 822, may 2022.

[120] J. Bhagat, L. Zang, N. Nishimura, and Y. Shimada, "Zebrafish: An emerging model to study microplastic and nanoplastic toxicity," aug 2020.

[121] J. Hwang, D. Choi, S. Han, S. Y. Jung, J. Choi, and J. Hong, "Potential toxicity of polystyrene microplastic particles," *Scientific Reports*, 2020.

[122] Z. Akdogan and B. Guven, "Microplastics in the environment: A critical review of current understanding and identification of future research needs," 2019.

[123] L. Lv, X. Yan, L. Feng, S. Jiang, Z. Lu, H. Xie, S. Sun, J. Chen, and C. Li, "Challenge for the detection of microplastics in the environment," pp. 5–15, jan 2021.

[124] W. J. Shim, S. H. Hong, and S. E. Eo, "Identification methods in microplastic analysis: a review," *Analytical Methods*, vol. 9, no. 9, pp. 1384–1391, 2017.

[125] J. Gago, A. Filgueiras, M. L. Pedrotti, M. Caetano, and J. Frias, "Standardised protocol for monitoring microplastics in seawater. Deliverable 4.1." 2019.

[126] R. Andrades, R. A. dos Santos, A. S. Martins, D. Teles, and R. G. Santos, "Scavenging as a pathway for plastic ingestion by marine animals," *Environmental Pollution*, 2019.

[127] N. Davaasuren, A. Marino, C. Boardman, M. Alparone, F. Nunziata, N. Ackermann, and I. Hajnsek, "Detecting microplastics pollution in world oceans using SAR remote sensing," in *International Geoscience and Remote Sensing Symposium (IGARSS)*, 2018.

[128] L. Goddijn-Murphy and B. Williamson, "On thermal infrared remote sensing of plastic pollution in natural waters," 2019.

[129] E. P. Chassignet, X. Xu, and O. Zavala-Romero, "Tracking Marine Litter With a Global Ocean Model: Where Does It Go? Where Does It Come From?" *Frontiers in Marine Science*, 2021.

[130] D. V. Politikos, C. Ioakeimidis, G. Papatheodorou, and K. Tsiaras, "Modeling the fate and distribution of floating litter particles in the Aegean Sea (E. Mediterranean)," *Frontiers in Marine Science*, 2017.

[131] INE, "Instituto Nacional de Estadística."

[132] V. Onink, C. E. Jongedijk, M. J. Hoffman, E. van Sebille, and C. Laufkötter, "Global simulations of marine plastic transport show plastic trapping in coastal zones," *Environmental Research Letters*, 2021.

[133] A. Williams and N. Rangel-Buitrago, "Marine Litter: Solutions for a Major Environmental Problem," *Journal of Coastal Research*, vol. 35, no. 3, p. 648, jan 2019.

[134] S. Karbalaei, P. Hanachi, T. R. Walker, and M. Cole, "Occurrence, sources, human health impacts and mitigation of microplastic pollution," 2018.

[135] B. Liu, L. Hou, Y. Wang, W. Ma, B. Yan, X. Li, and G. Chen, "Emission Estimate and Countermeasures of Marine Plastic Debris and Microplastics in China," *Research of Environmental Sciences*, 2020.

[136] C. J. van Calcar and T. H. M. van Emmerik, "Abundance of plastic debris across European and Asian rivers," *Environmental Research Letters*, 2019.

[137] T. van Emmerik, T. C. Kieu-Le, M. Loozen, K. van Oeveren, E. Strady, X. T. Bui, M. Egger, J. Gasperi, L. Lebreton, P. D. Nguyen, A. Schwarz, B. Slat, and B. Tassin, "A methodology to characterize riverine macroplastic emission into the ocean," *Frontiers in Marine Science*, 2018.

[138] D. González-Fernández, A. Cózar, G. Hanke, J. Viejo, C. Morales-Caselles, R. Bakiu, D. Barceló, F. Bessa, A. Bruge, M. Cabrera, J. Castro-Jiménez, M. Constant, R. Crosti, Y. Galletti, A. E. Kideys, N. Machitadze, J. Pereira de Brito, M. Pogojeva, N. Ratola,

J. Rigueira, E. Rojo-Nieto, O. Savenko, R. I. Schöneich-Argent, G. Siedlewicz, G. Suaria, and M. Tourgeli, "Floating macrolitter leaked from Europe into the ocean," *Nature Sustainability*, vol. 4, no. 6, pp. 474–483, 2021. [Online]. Available: http://dx.doi.org/10.1038/s41893-021-00722-6

[139] H. de Pablo, J. Sobrinho, D. Garaboa-Paz, C. Fonteles, R. Neves, and M. B. Gaspar, "The Influence of the River Discharge on Residence Time, Exposure Time and Integrated Water Fractions for the Tagus Estuary (Portugal)," *Frontiers in Marine Science*, vol. 8, no. January, pp. 1–16, 2022.

[140] A. Bauer-Civiello, K. Critchell, M. Hoogenboom, and M. Hamann, "Input of plastic debris in an urban tropical river system," *Marine Pollution Bulletin*, vol. 144, pp. 235–242, jul 2019.

[141] J. R. Jambeck, R. Geyer, C. Wilcox, T. R. Siegler, M. Perryman, A. Andrady, R. Narayan, and K. L. Law, "Plastic waste inputs from land into the ocean," *Science*, 2015.

[142] P. Masiá, A. Ardura, M. Gaitán, S. Gerber, F. Rayon-Viña, and E. Garcia-Vazquez, "Maritime ports and beach management as sources of coastal macro-, meso-, and microplastic pollution," *Environmental Science and Pollution Research*, 2021. [Online]. Available: https://consorcioaa.com/saneamiento/,

[143] W. Krauss, "The North Atlantic Current," *Journal of Geophysical Research*, vol. 91, no. C4, p. 5061, 1986.

[144] G. Dietrich and K. Kalle, "General oceanography; an introduction," 1957.

[145] C. O. D. ISELIN, "Papers in Physical Oceanography and Meteorology," *Mass. Inst. Tech. and Woods Hole Ocean. Inst. In preparation*, 1940.

[146] C. R. Mann, "The termination of the Gulf Stream and the beginning of the North Atlantic Current," in *Deep Sea Research and Oceanographic Abstracts*, vol. 14, no. 3, 1967, pp. 337–359.

[147] ——, "33.—A Review of the Branching of the Gulf Stream System," *Proceedings of the Royal Society of Edinburgh, Section B: Biological Sciences*, vol. 72, no. 1, pp. 341–349, 1972.

[148] Y. Friocourt, B. Levier, S. Speich, B. Blanke, and S. S. Drijfhout, "A regional numerical ocean model of the circulation in the Bay of Biscay," *Journal of Geophysical Research: Oceans*, 2007.

[149] L. Solabarrieta, A. Rubio, S. Castanedo, R. Medina, G. Charria, and C. Hernandez, "Surface water circulation patterns in the southeastern Bay of Biscay: New evidences from HF radar data," 2014.

[150] H. M. Van Aken, "The hydrography of the mid-latitude Northeast Atlantic Ocean - Part III: The subducted thermocline water mass," *Deep-Sea Research Part I: Oceanographic Research Papers*, 2001.

[151] ——, "Surface currents in the Bay of Biscay as observed with drifters between 1995 and 1999," *Deep-Sea Research Part I: Oceanographic Research Papers*, vol. 49, no. 6, pp. 1071–1086, 2002.

[152] C. Millot, "Circulation in the Western Mediterranean Sea," *Journal of Marine Systems*, 1999.

[153] K. Tsiaras, Y. Hatzonikolakis, S. Kalaroni, A. Pollani, and G. Triantafyllou, "Modeling the Pathways and Accumulation Patterns of Micro- and Macro-Plastics in the Mediterranean," *Frontiers in Marine Science*, vol. 8, no. October, 2021.

[154] A. Peliz, J. Dubert, P. Marchesiello, and A. Teles-machado, "Surface circulation in the Gulf of Cadiz : Model and mean flow structure," vol. 112, no. February, pp. 1–20, 2007.

[155] H. Perkins, T. Kinder, and P. la Violette, "The Atlantic inflow in the western Alboran Sea," *J. PHYSICAL OCEANOGRAPHY*, 1990.

[156] M. M. Flexas, D. Gomis, S. Ruiz, A. Pascual, and P. León, "In situ and satellite observations of the eastward migration of the Western Alboran Sea Gyre," *Progress in Oceanography*, 2006.

[157] A. Peliz, D. Boutov, and A. Teles-Machado, "The Alboran Sea mesoscale in a long term high resolution simulation: Statistical analysis," *Ocean Modelling*, 2013.

[158] M. Vargas-Yáez, F. Plaza, J. García-Lafuente, T. Sarhan, J. M. Vargas, and P. Vélez-Belchi, "About the seasonal variability of the Alboran Sea circulation," *Journal of Marine Systems*, 2002.

[159] G. André, P. Garreau, V. Garnier, and P. Fraunié, "Modelled variability of the sea surface circulation in the North-western Mediterranean Sea and in the Gulf of Lions," *Ocean Dynamics*, 2005.

[160] C. Alberola, C. Millot, and J. Font, "On the seasonal and mesoscale variabilities of the Northern Current during the PRIMO-0 experiment in the western Mediterranean Sea," *Oceanologica Acta*, 1995.

[161] F. Criado-Aldeanueva, J. Garcia-Lafuente, G. Navarro, and J. Ruiz, "Seasonal and interannual variability of the surface circulation in the eastern Gulf of Cadiz (SW Iberia)," *Journal of Geophysical Research: Oceans*, vol. 114, no. 1, jan 2009.

[162] P. Vélez-Belchí, M. Pérez-Hernández, M. Casanova-Masjoan, L. Cana, and A. Hernández-Guerra, "On the seasonal catiability of the Canary Current and the Atlantic Meridional Overturning Circulation," *Journal of Geophysical Research: Oceans*, vol. 122, pp. 4518–4538, 2017.

[163] A. y. M. A. MAPAMA (Ministerio de Agricultura y Pesca and C. C. d. E. y. E. d. O. Públicas), "Acumulación de presiones que pueden causar la entrada de basuras al mar desde tierra en la Demarcación Noratlántica (EM NOR PRE Basura Terrestre)," 2012. [Online]. Available: http://infomar.cedex.es:8080/geonetwork/srv/spa/catalog.search;jsessionid=node01ozdfxabk663h1tw377hxbz5hp5184.node0#/metadata/03d74c07-d5a0-4242-8217-95463efff062

[164] ——, "Acumulación de presiones que pueden provocar la entrada de basuras en el mar desde tierra en la Demarcación Sudatlántica (EM SUD PRE Basura Terrestre)." 2012. [Online]. Available: http://infomar.cedex.es:8080/geonetwork/srv/spa/catalog.search;jsessionid=node01ozdfxabk663h1tw377hxbz5hp5184.node0#/metadata/88f254fb-67ea-49a7-9138-e7eeaeb9050f

[165] ——, "Acumulación de presiones que pueden causar la entrada de basuras al mar desde tierra en la Demarcación Canaria (EM CAN PRE Basura Terrestre)," 2012. [Online]. Available: http://infomar.cedex.es:8080/geonetwork/srv/spa/catalog.search#/metadata/ff945929-0918-46b9-a8e8-42069b6aa20d

[166] D. R. Easterling, G. A. Meehl, C. Parmesan, S. A. Changnon, T. R. Karl, and L. O. Mearns, "Climate extremes: Observations, modeling, and impacts," 2000.

[167] P. Adhikari, Y. Hong, K. R. Douglas, D. B. Kirschbaum, J. Gourley, R. Adler, and G. R. Brakenridge, "A digitized global flood inventory (1998-2008): Compilation and preliminary results," *Natural Hazards*, 2010.

[168] J. Eiras-Barca, F. Dominguez, H. Hu, D. Garaboa-Paz, and G. Miguez-Macho, "Evaluation of the moisture sources in two extreme landfalling atmospheric river events using an Eulerian WRF tracers tool," *Earth System Dynamics*, 2017.

[169] R. Romero, C. A. Doswell, and C. Ramis, "Mesoscale numerical study of two cases of long-lived quasi-stationary convective systems over eastern Spain," *Monthly Weather Review*, 2000.

[170] L. Trapero, J. Bech, F. Duffourg, P. Esteban, and J. Lorente, "Mesoscale numerical analysis of the historical November 1982 heavy precipitation event over Andorra (Eastern Pyrenees)," *Natural Hazards and Earth System Sciences*, 2013.

[171] D. P. Dee, S. M. Uppala, A. J. Simmons, P. Berrisford, P. Poli, S. Kobayashi, U. Andrae, M. A. Balmaseda, G. Balsamo, P. Bauer, P. Bechtold, A. C. M. Beljaars, L. van de Berg, J. Bidlot, N. Bormann, C. Delsol, R. Dragani, M. Fuentes, A. J. Geer, L. Haimberger, S. B. Healy, H. Hersbach, E. V. Hólm, L. Isaksen, P. Kållberg, M. Köhler, M. Matricardi, A. P. Mcnally, B. M. Monge-Sanz, J. J. Morcrette, B. K. Park, C. Peubey, P. de Rosnay, C. Tavolato, J. N. Thépaut, and F. Vitart, "The ERA-Interim reanalysis: Configuration and performance of the data assimilation system," *Quarterly Journal of the Royal Meteorological Society*, 2011.

[172] S. Y. Hong, Y. Noh, and J. Dudhia, "A new vertical diffusion package with an explicit treatment of entrainment processes," *Monthly Weather Review*, 2006.

[173] J. S. Kain and J. M. Fritsch, "A one-dimensional entraining/detraining plume model and its application in convective parameterization," *Journal of the Atmospheric Sciences*, 1990.

This thesis focuses on the study of Lagrangian transport in different types of fluids. The aim of this work is to explore interactions between particles and fluids in two different areas of science; oceanography and meteorology. Different practical applications, such as the movement of plastics in the ocean and the transport of moisture in the atmosphere, will be examined in both study areas. To do this, we will explore the use of numerical Lagrangian models to validate results and test new hypotheses.